University of Nevada, Reno

Evaluation of Cracking Behavior of Cold In-Place Recycling Asphalt Mixtures

A thesis submitted in partial fulfillment of the
Requirements for the degree of Master of Science in
Civil and Environmental Engineering

by

Mateo Eduardo Carvajal

Dr. Peter E. Sebaaly/Thesis Advisor

December 2018

UNIVERSITY OF NEVADA RENO

THE GRADUATE SCHOOL

We recommend that the thesis
prepared under our supervision by

MATEO EDUARDO CARVAJAL

entitled

Evaluation of Cracking Behavior of Cold In-Place Recycling Asphalt Mixtures

be accepted in partial fulfillment of the
requirements for the degree of

MASTER OF SCIENCE

Peter E. Sebaaly, Ph.D., Advisor

Elie Y. Hajj, Ph.D., Committee Member

Adam Hand, Ph.D., Committee Member

Jennifer Lowman, Ph.D., Graduate School Representative

David W. Zeh, Ph.D., Dean, Graduate School

December, 2018

ABSTRACT

During the last decades, the asphalt pavement industry has been looking for innovative ways to make its products more environmentally friendly, and recycling methodologies have become widely accepted. According to the National Asphalt Pavement Association, during 2017 construction season, more than 76.2 million tons of RAP were put to use in new pavements in the United States, saving taxpayers more than $2.2 billion. [1]

Recycling of the existing deteriorated asphalt pavement offers an attractive approach from the economic and structural standpoint. However, a severely cracked asphalt pavement presents a challenge for the design engineer due to the uncertainty in its cracking behavior and its potential of reflecting the cracks through the new overlay. The Cold In-place Recycling technique has demonstrated effectiveness in delaying the problem of reflective cracking and providing strong base layer, resulting in the requirement of a thinner overlay [2] [3] [4].

This study evaluated the cracking properties of CIR by means of the Overlay Tester (OT) and the Flexural Beam Fatigue Test. The results indicated that CIR materials have good (low) crack propagation rates but the required energy to initiate a crack is low as well. In addition, some flexibility was observed in the Beam Fatigue Test but a stiff-brittle behavior was predominant. The performance characteristics of the CIR materials were used in a mechanistic analysis to recommend a structural layer coefficient for CIR layer in a flexible pavement structure.

TABLE OF CONTENTS

LIST OF TABLES

LIST OF FIGURES

Chapter 1. Introduction

Because of economic, energy, and environmental conservation reasons, the worldwide interest in using recycled materials in flexible pavements has increased significantly over the last few decades. Cold In-place Recycling (CIR) of asphalt pavements has become popular over the past years, as a result of its extensive economic and environmental benefits, coupled with satisfactory field performance results. However, regardless of the acceptable performance of CIR pavements, some engineering properties of this material have not been deeply scrutinized. This study focuses on evaluating the cracking behavior of CIR mixtures manufactured with a wide range of asphalt emulsions.

- CIR is a major pavement rehabilitation treatment, consisting of milling the top 2 – 5 inches of the asphalt concrete (AC) layer followed by in-place cold mixing with asphalt emulsion and stabilizing agents (i.e. Portland cement or hydrated lime) and compacted using traditional methods.

Some advantages of CIR technology of asphalt pavements are listed as follows ([2]; [5]; [6]; [7]; [8]):

- Conservation of energy and resources: No heating and hauling is needed, thus, air pollution and energy consumption is significantly reduced.
- Environmentally friendly technique: Disposal of old materials is reduced to minimal.
- Better quality layer: When used as a base layer, the structural capacity of CIR is considerably better that any unbound material.

- Demonstrated effectiveness in mitigating reflective cracking: Due to the good crack propagation properties, CIR has demonstrated remarkable performance when attenuating cracking in field study sections.
- Geometry of pavement is maintained: Cross slope can be maintained and problems with fixed clearance are avoided.
- Relatively quick rehabilitation process: Technology is playing a big role in pavement industry and nowadays, the rates of machines production keep increasing, shorten construction times and improving efficiency.
- Long-term cost effective treatment and maintenance costs reduced.

Some disadvantages of CIR technology of asphalt pavements are listed as follows ([3]; [9]; [10]; [11]; [12])

- CIR requires an overlay or surface treatment as a wearing course.
- Must be constructed in warm, dry weather and thus construction is limited to the summer season.
- Cold recycling materials without additives may be susceptible to moisture damage (stripping and raveling). Several studies performed by Ayala, [9]; Castro, [10]; Niazi and Jalili [11], etc., demonstrated that the addition of hydrated lime and/or Portland may improve resistance to moisture damage.
- In-place density during construction is not practical to measure and some projects have reported lower densities and higher air voids than expected.
- When mixed with Portland cement, CIR has exhibited problems of shrinkage cracking.

1.1. Objective and Scope

The objective of this study is to evaluate the cracking characteristics of CIR mixtures in terms of their ability to resist reflective cracking into the new AC overlay and to resistance fatigue cracking under repeated loads. Four types of CIR mixtures were manufactured from a single source of reclaimed asphalt pavement (RAP) mixed with four types of asphalt emulsions. Two types of lime slurry (6.0% and 4.5%) were used with each type of CIR mix leading to a total of eight evaluated CIR mixtures.

1.2. Thesis Outline

This thesis is organized into eight chapters. Chapter 1 presents an introduction, giving the general background of the CIR and stating objectives and scope of this research.

Chapter 2 reviews the literature concerning CIR pavements, particularly the efforts conducted to characterize the cracking behavior of this type of pavement rehabilitation.

Chapter 3 presents the materials used in this investigation, namely RAP, asphalt emulsion, and hydrated lime. A complete characterization of the emulsified asphalt binder residue was conducted according to the Superpave Performance Grading System (PG).

Chapter 4 presents the Reflective cracking behavior of the CIR mixtures according to the results obtained with the Texas Overlay testing machine.

Chapter 5 assess the fatigue behavior of CIR mixtures by means of the flexural beam fatigue test.

A mechanistic analysis of fatigue performance and a verification of rutting performance of CIR mixtures are summarized in Chapter 6.

Finally, the findings, conclusions and recommendations are presented in Chapter 7, as well as the References in Chapter 8.

Chapter 2. Literature review

The increased use of CIR as a rehabilitation technique has generated a particular interest to properly characterize the behavior of this type of mixtures. Such investigations have been focused into three major areas; (1) Mix design (2) performance of CIR pavements, and (3) engineering and performance properties of CIR mixtures. This chapter reviews relevant literature concerning the structural behavior of CIR mainly those efforts that assessed the cracking behavior of this particular material.

The cracking behavior of CIR mixtures has been approached from different perspectives. Lin et al, [13] investigated the dynamic characteristics of a CIR mixture using asphalt emulsion (CRME) and cement. Dynamic modulus and phase angle were studied at different curing times. Creep and relaxation tests were performed to determine service conditions at higher temperatures. Fatigue life was evaluated with the four-point bending test at 59°F (15°C). Three levels of microstrain were considered (300, 400 and 500). The fatigue life was defined as the number of cycles N_f at which the initial stiffness of the mixture was reduced to 50%. Additional evaluation of cracking characteristics was conducted by analyzing the fracture interface microstructure with a Scanning Electron Microscopy (SEM). The results of this study indicated that CRME is a viscoelastic material evidencing time-temperature dependence effect during its early and fully cured stage. According to the Burgers model, this material has excellent ability to resist permanent deformation at 140°F (60°C), however, fatigue life of CRME was observed to be only 1/5 to 1/10 of ordinary asphalt mixture at high strain, still meeting the

requirements for heavy traffic in China's road structures specifications (>25,000,000 cycle/track).

Gao et al [14], evaluated the laboratory fatigue behavior of CIR mixtures with the application of digital image correlation (DIC) technique. The semicircular bending (SCB) and indirect tensile test (IDT) were utilized to compare the resistance of CIR and hot mix asphalt (HMA) mixtures to crack propagation in the stress-controlled mode of loading. The results indicated that the addition of 1.5% of cement to the CIR mixtures improves their overall fatigue performance life. The SCB and IDT tests indicated that the AC mixtures shows much better fatigue performance under the same stress amplitude. However, under the same stress level, the difference between the two regression lines of fatigue for CIR and AC mixtures was not significant. In addition, the SCB test demonstrated that the initial stiffness for AC mixtures is about 1.8 times the stiffness of CIR mixtures.

An experimental study on fatigue properties of CIR mixtures manufactured with asphalt emulsion and foamed asphalt was conducted by Yan et al in 2010 [15]. The Nottingham Asphalt Tester (NAT) was used to assess the fatigue behavior of the mixtures. Fatigue life was analyzed at 59°F (15°C) and four stress levels. In addition, the law of displacement and crack development was determined during the fatigue testing. The results indicated that foam CIR mixtures displayed a higher fatigue life at low stress levels, while emulsion CIR mixtures displayed a higher fatigue life at high stress levels. Qualitative analysis indicated that emulsion CIR mixtures showed a plastic fatigue failure due to its visco-elastic characteristics, while fatigue damage of foam CIR mixtures

showed a brittle fracture. The law of vertical displacement (deformation) and crack development indicated that emulsion CIR mixtures included three states of displacement development before cracking, while foam CIR mixtures included two stages of displacement development before cracking.

Kavussi and Modarres, [16] studied the influence of asphalt cement on the fatigue life of CIR mixtures, given the crystalline nature of the pozzolanic bonds, cemented materials tend to be brittle which can reduce flexibility and fatigue life of CIR mixtures. In this study, extensive indirect tensile strength (IDT) and resilient modulus tests were performed at different temperatures (varying from -50 to 77°F (10 to 25°C)) and curing times (varying from 7 to 120 days). Test results showed that the effect of cement depends on the initial strain level. At 300 microstrain level and above, the addition of cement caused a reduction in fatigue life, while below 300 microstrain the opposite trend was observed.

An assessment of fracture parameters to predict field cracking performance of CIR mixtures was conducted by Charmot and Romero in 2010 [4]. The ability of fracture parameters to predict field cracking performance of CIR pavements was assessed based on the performance of nine projects, located in three states. These projects consisted of past rehabilitation projects, 2 to 5 years old, involving CIR and new AC overlay mixtures. The performance evaluation of the sites was based on transverse and longitudinal cracking. Fracture energy was found to be an appropriate indicator to differentiate between satisfactory and poor performance of CIR pavements. The

recommendation of this effort was to include fracture energy in specifications to optimize the cracking resistance of CIR mixtures.

Ruenkrairergsa et al. [17], conducted several laboratory tests to determine the fatigue resistance of CIR mixtures manufactured with foamed asphalt. Three sources of RAP and virgin crushed stone at various ratios were mixed with foamed asphalt binder. The mixtures were tested in the IDT at a tensile stress of 3.6 psi(25 kPa) at 77°F(25°C) until failure. The results shown in Figure 1 indicate that the increasing the RAP content from 50 to 80% recued the fatigue resistance of the CIR mix while increasing the RAP content from 0 to 50% did not have an impact. These findings indicate that RAP can replace virgin aggregates up to 50% without affecting fatigue properties.

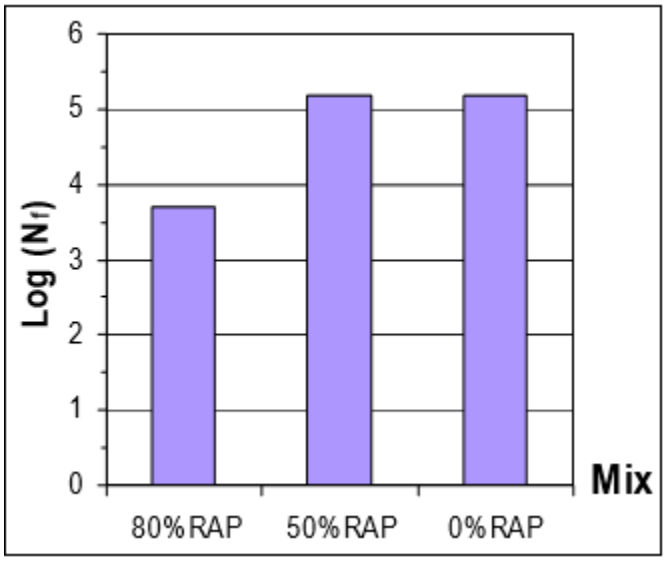

Figure 1. Fatigue resistance of foam CIR mixtures [17].

In addition to the laboratory evaluations, several studies have focused on determining the effectiveness of Cold in-place recycling as a reflective cracking control technique in the field. Sebaaly et al, [2] evaluated the long-term performance of several CIR pavements in

Nevada. The projects were constructed during 1997-1998 on US-50, US-95 and NV-396. The research concluded that CIR is an effective rehabilitation technique for roads with low and medium volume traffic levels. The results proved that CIR produces a more flexible and stable base course with a greater tendency to reduce the development of reflective and thermal cracking, as well as rutting. A structural layer coefficient of 0.26 was recommended for the structural pavement design based on the AASHTO 1993 Guide.

Morian et al. [18] evaluated the performance of 13 CIR projects in Pennsylvania with service life periods from one to 20 years. The effectiveness of the CIR layer in resisting reflective cracking from underlying concrete pavements was evaluated. The research showed that CIR provided resistance against reflective cracking between two and three times better when compared with conventionally resurfaced control sections. In addition, CIR demonstrated to be a stress-sensitive material, providing increased stiffness in response to increased load. This property becomes an important factor in delaying the development of reflective cracking.

Chapter 3. Materials Characterization

This chapter presents the main characteristics of the materials used in this research, including; RAP materials, asphalt emulsions, and additives.

3.1. Reclaimed Asphalt Pavement

A single source of RAP from the Granite Construction Co. plant at Lockwood was used in this study. The experimental plan evaluated non-graded RAP materials. The only specification in terms of gradation was a maximum size of 1.0 inch.

Based on the recommendations of previous research conducted with the same RAP source [9] [10], the following process was used to prepare RAP materials:

- Non-Graded RAP
    - Empty a 55-gallon barrel containing RAP sampled from the stockpile.
    - Crush the RAP twice through a 1.0 inch opening crusher to obtain approximately 100% passing 1.0 inch sieve.
    - Split the RAP into smaller representative samples (~55 lbs. (25 kg) using the quartering method.
    - Dry the RAP at 140°F (60°C) until constant mass.
    - Use the mechanical splitter to obtain representative samples depending on the purpose of the CIR specimens.
    - Conduct sieve analysis to verify gradation (Results are shown in section3.1.1)

3.1.1. Sieve Analysis of Non-graded RAP

After emptying the 55-galon barrels and following the process abovementioned, a sieve analysis according to AASHTO T-27 [19] was conducted to verify the actual gradation of the RAP and compare with materials used in previous research efforts [10]. The purpose of this exercise is to ensure uniform gradation is used throughout the research. Figure 2 shows the average, minimum, and maximum percentages obtained from the historical records of the RAP materials, as well as the gradation used by Castro, [10] for developing the Superpave mix design for CIR.

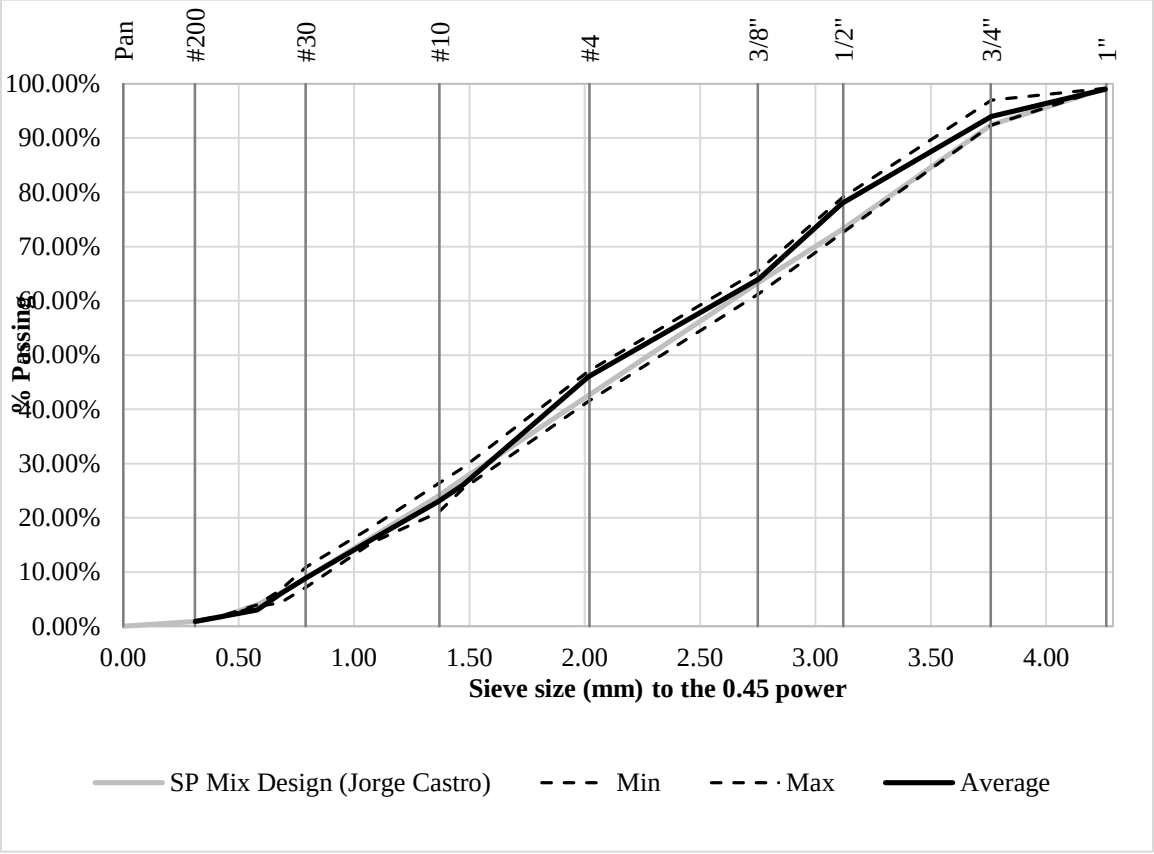

Figure 2. Historical records of RAP gradation of non-graded materials.

It can be seen that the average gradation for the non-graded RAP materials obtained in this research is slightly finer than the gradation obtained by Castro, [10]; however, the difference between these values is not significant and comparisons between the obtained results can be made.

3.2. Asphalt Emulsion Testing

The performance of the CIR is highly controlled by the characteristics of the binding agent used in this process. In this research asphalt emulsions were used as the binding agents of the CIR mixtures. In order to determine the impact of the asphalt emulsion type on the cracking behavior of CIR mixtures, four different types of emulsions were included in this study. The properties of the asphalt emulsions are described as follows.

3.2.1. Characteristics of Asphalt Emulsions

Table 1 summarizes the information provided by the respective supplier regarding modifier or additives used during the manufacturing of the asphalt emulsion.

Table 1. Asphalt Emulsion Modifier/Additive Information.

Emulsion Type	Modifier/Additive
A	None (Standard)
B	Latex
C	Polymer
D	Rubber

3.2.2. Percentage Residue of Asphalt Emulsions

Properties of the asphalt binder residue in the emulsion have a significant impact of the performance of the CIR mixture [20]. The relative proportion of asphalt binder to water in the emulsion was determined according to ASTM D7497: "Standard Practice for Recovering Residue from Emulsified Asphalt Using Low Temperature Evaporative Technique" [21]. This method was adopted based on the recommendations provided by the NCHRP 09-50 study entitled: "Performance-Related Specifications for Asphaltic Binders Used in Preservation Surface Treatments" [22].

The D7497 method consists of recovering the asphalt binder residue using a low temperature evaporative technique, which most closely resembles the conditions that the pavement experiences in the field. The procedure includes pouring the required amount of asphalt emulsion onto a silicone mat and spread it evenly with a spatula, to give a spread rate of 1.5 to 2.0 kg/m^2. The silicone mat with the asphalt emulsion is placed into a 77 ± 3°F (25 ± 2°C) forced draft oven for 24 ± 1 h. After that, the silicone mat with the asphalt emulsion is transferred to a 140± 3°F (60-± 2°C) forced draft oven for 24 ± 1 h. Once the period of evaporation is completed, the percentage of residue is determined by difference of weights.

In this study, PAV pans of 2 inches (50mm) diameter were used instead of silicone mats. Figure 3 to Figure 6 show the samples of asphalt emulsion after the recovery process. It can be seen that asphalt emulsion type B showed some type of cracking after the recovery process. This behavior may be attributed to the properties of the latex additive used. Nonetheless, other rest of the emulsions that also contain additives such as polymer and

rubber did not show this pattern of cracking. The results of the percentage residue for the four emulsions are shown in Table 2. The data showed that emulsions B and C have significantly higher percentage residue than emulsions A and D. The evaluations will further examine the impact of the difference in percentage residue on the cracking characteristics of the CIR mixtures

Figure 3. Type A asphalt emulsion residue.

Figure 4. Type B asphalt emulsion residue.

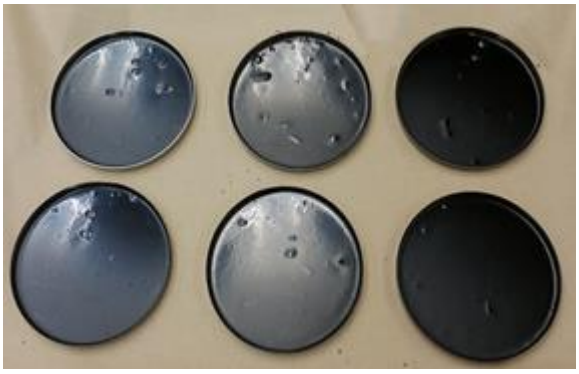

Figure 5. Type C asphalt emulsion residue.

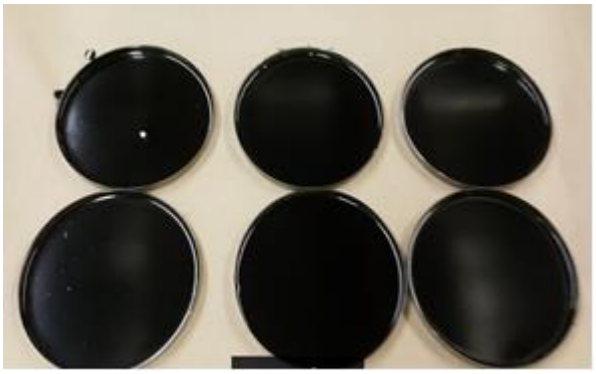

Figure 6. Type D asphalt emulsion residue.

Table 2. Results of Percentage Residue for the Emulsions Evaluated in this Study.

Emulsion Type	Percentage Residue (%)
Type A	64.72
Type B	72.43
Type C	76.28
Type D	63.02

3.2.3. Evaluation of Performance Grade of Asphalt Binder Residue

In order to fully understand the behavior of the CIR mixtures, the performance grade (PG) of the asphalt binder residue from each emulsions were determined. The asphalt binder residue from each emulsion was obtained following ASTM D7497 as described earlier. After extraction, the asphalt binder residues were graded using the Superpave PG method as presented in AASHTO M320 -Table 1 [23]. A summary of the test results is presented in Table 3 to

Emulsion Type C					
Test	**Test method**	**Specification**	**Testing Temperature**		
Dynamic Shear on Original, °C			**58**	**64**	**70**
G*/sinδ, kPa	**AASHTO M332**	**1.00 Min.**	3.51	1.64	0.78
Pass/Fail Temperature, °C			68.3		
Dynamic Shear on PAV residue °C	**AASHTO R28**		**19**	**22**	**25**
G*sinδ, kPa	**AASHTO M332**	**5000 Max.**	---	5227	3196
Pass/Fail Temperature, °C			22.3		
Bending Beam Rheometer, °C	**AASHTO T313**			-18	-24
Creep stiffness (S) on PAV residue at 60 sec, MPa		**300 Max.**		230	477
Creep stiffness (m-value) on PAV residue at 60 sec		**0.300 Min.**		0.309	0.251
Pass/Fail Temperature-Stiffness, °C			-30.2		
Pass/Fail Temperature- m-value, °C			-28.9		
Pass/Fail Lower Temperature, °C			-28.9		
ΔTc		Ts - Tm	-1.3		
True grade			**PG 68.3-28.9**		
PG grade	**AASHTO M320**		**PG 64-28**		

Table 6 and Figure 7 to Figure 11.The detailed test results including the respective precision and bias are presented in Appendix 9.1.

Table 3. Properties and PG for Asphalt Binder Residue of Emulsion Type A.

Emulsion Type A					
Test	**Test method**	**Specification**	**Testing Temperature**		
Dynamic Shear on Original, °C			**46**	**52**	**58**
G*/sinδ, kPa	**AASHTO M332**	**1.00 Min.**	3.39	1.55	0.73
Pass/Fail Temperature, °C			55.2		
Dynamic Shear on PAV residue °C	**AASHTO R28**		**13**	**16**	**19**
G*sinδ, kPa	**AASHTO M332**	**5000 Max.**	5186	3140	1910
Pass/Fail Temperature, °C			13.2		
Bending Beam Rheometer, °C	**AASHTO T313**			-18	-24
Creep stiffness (S) on PAV residue at 60 sec, MPa		**300 Max.**		109	270
Creep stiffness (m-value) on PAV residue at 60 sec		**0.300 Min.**		0.401	0.33
Pass/Fail Temperature-Stiffness, °C			-34.6		
Pass/Fail Temperature- m-value, °C			-35.9		
Pass/Fail Lower Temperature, °C			-34.6		
ΔTc		Ts - Tm	1.3		
True grade			**PG 55.2-34.6**		
PG grade	**AASHTO M320**		**PG 52-34**		

Table 4. Properties and PG for Asphalt Binder Residue of Emulsion Type B.

Emulsion Type B					
Test	**Test method**	**Specification**	**Testing Temperature**		
Dynamic Shear on Original, °C			**58**	**64**	**70**
G*/sinδ, kPa	**AASHTO M332**	**1.00 Min.**	3.81	1.77	0.86
Pass/Fail Temperature, °C			68.1		
Dynamic Shear on PAV residue °C	**AASHTO R28**		**19**	**22**	**25**
G*sinδ, kPa	**AASHTO M332**	**5000 Max.**	5810	3890	2676
Pass/Fail Temperature, °C			20.1		
Bending Beam Rheometer, °C	**AASHTO T313**			-18	-24
Creep stiffness (S) on PAV residue at 60 sec, MPa		**300 Max.**		292	413
Creep stiffness (m-value) on PAV residue at 60 sec		**0.300 Min.**		0.307	0.249
Pass/Fail Temperature-Stiffness, °C			-28.5		
Pass/Fail Temperature- m-value, °C			-28.7		
Pass/Fail Lower Temperature, °C			-28.5		
ΔTc		Ts - Tm	0.2		
True grade			**PG 68.1-28.5**		
PG grade	**AASHTO M320**		**PG 64-28**		

Table 5. Properties and PG for Asphalt Binder Residue of Emulsion Type C.

Emulsion Type C					
Test	**Test method**	**Specification**	**Testing Temperature**		
Dynamic Shear on Original, °C			**58**	**64**	**70**
G*/sinδ, kPa	**AASHTO M332**	**1.00 Min.**	3.51	1.64	0.78
Pass/Fail Temperature, °C			68.3		
Dynamic Shear on PAV residue °C	**AASHTO R28**		**19**	**22**	**25**
G*sinδ, kPa	**AASHTO M332**	**5000 Max.**	---	5227	3196
Pass/Fail Temperature, °C			22.3		
Bending Beam Rheometer, °C	**AASHTO T313**			-18	-24
Creep stiffness (S) on PAV residue at 60 sec, MPa		**300 Max.**		230	477
Creep stiffness (m-value) on PAV residue at 60 sec		**0.300 Min.**		0.309	0.251
Pass/Fail Temperature-Stiffness, °C			-30.2		
Pass/Fail Temperature- m-value, °C			-28.9		
Pass/Fail Lower Temperature, °C			-28.9		
ΔTc		Ts - Tm	-1.3		
True grade			**PG 68.3-28.9**		
PG grade	**AASHTO M320**		**PG 64-28**		

Table 6. Properties and PG for Asphalt Binder Residue of Emulsion Type D.

Emulsion Type D					
Test	**Test method**	**Specification**	**Testing Temperature**		
Dynamic Shear on Original, °C			**52**	**58**	**64**
G*/sinδ, kPa	**AASHTO M332**	**1.00 Min.**	2.78	1.23	0.59
Pass/Fail Temperature, °C			59.4		
Dynamic Shear on PAV residue °C	**AASHTO R28**		**13**	**16**	**19**
G*sinδ, kPa	**AASHTO M332**	**5000 Max.**	6963	4840	3379
Pass/Fail Temperature, °C			15.8		
Bending Beam Rheometer, °C	**AASHTO T313**			-18	-24
Creep stiffness (S) on PAV residue at 60 sec, MPa		**300 Max.**		164	399
Creep stiffness (m-value) on PAV residue at 60 sec		**0.300 Min.**		0.342	0.262
Pass/Fail Temperature-Stiffness, °C			-32.1		
Pass/Fail Temperature- m-value, °C			-31.1		
Pass/Fail Lower Temperature, °C			-31.1		
ΔTc		Ts - Tm	-1.0		
True grade			**PG 59.4-31.1**		
PG grade	**AASHTO M320**		**PG 58-28**		

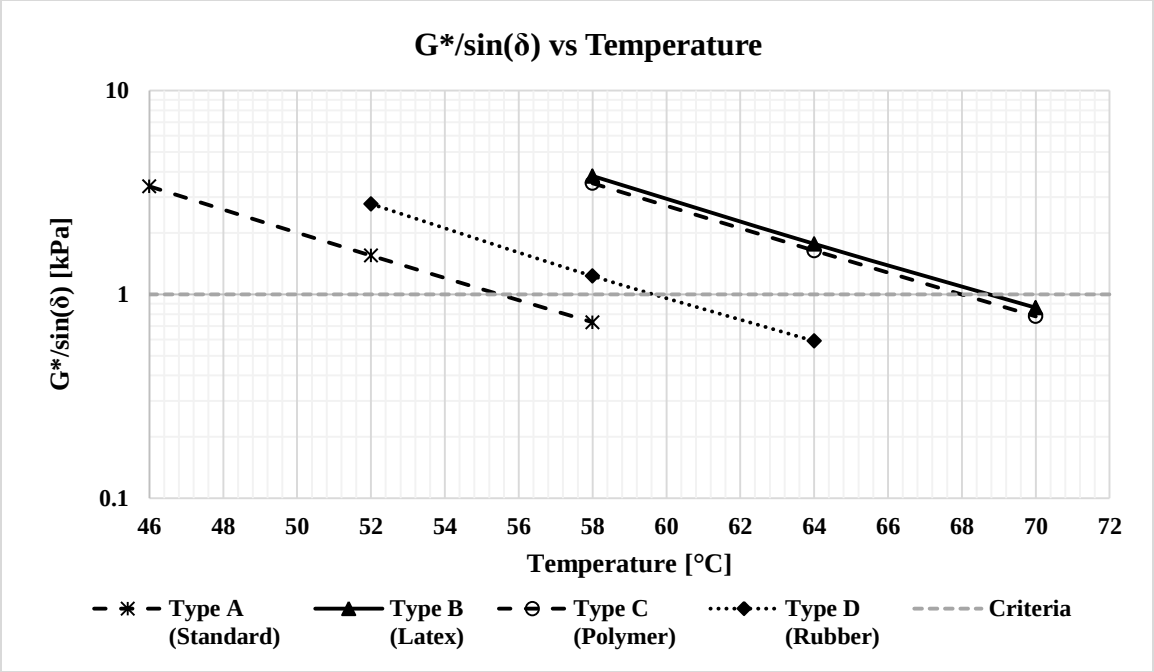

Figure 7. DSR original test results (G*/sin (δ) vs temperature).

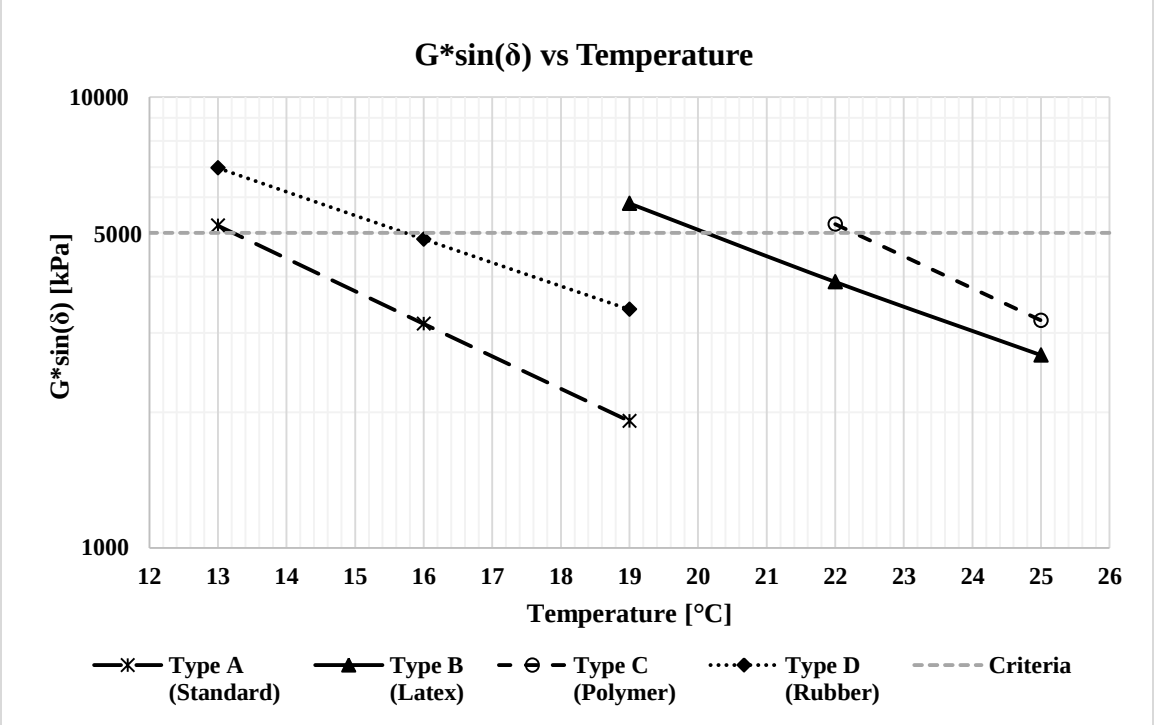

Figure 8. PAV test results (G*sin (δ) vs temperature).

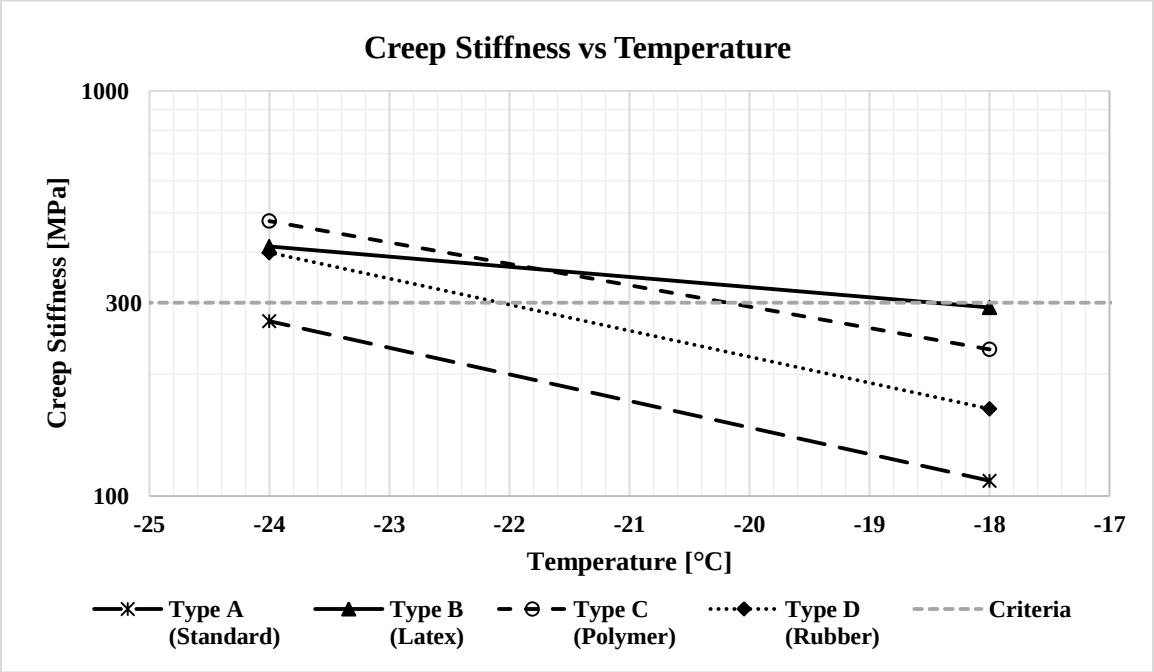

Figure 9. BBR test results (Creep stiffness vs temperature).

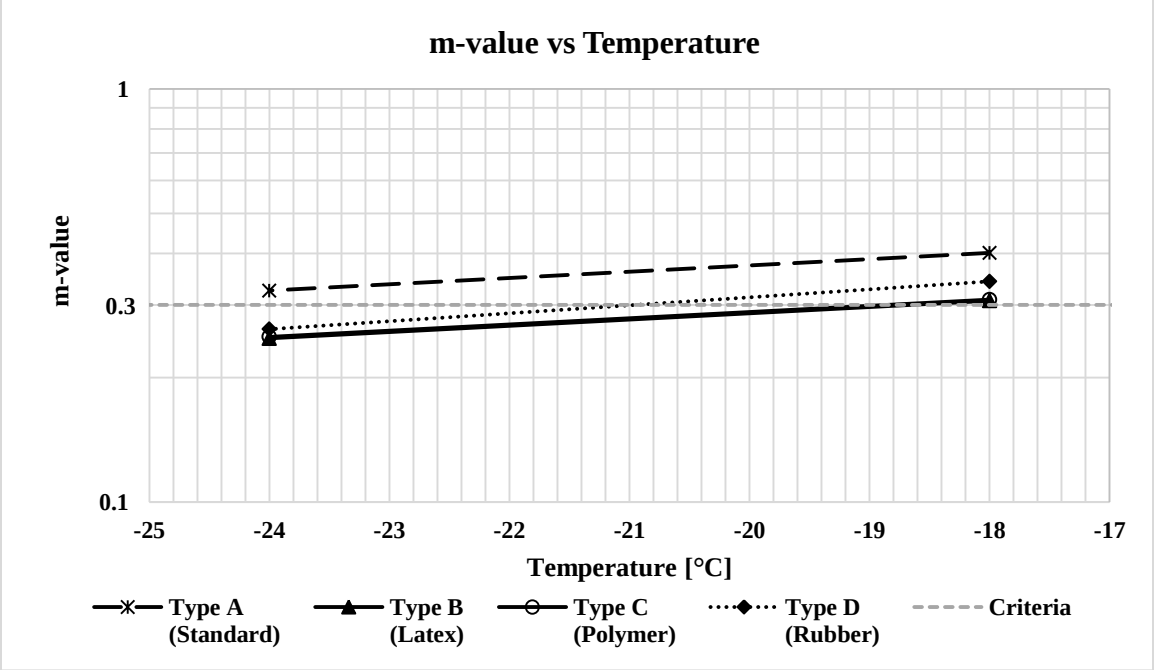

Figure 10. BBR test results (m-value vs Temperature).

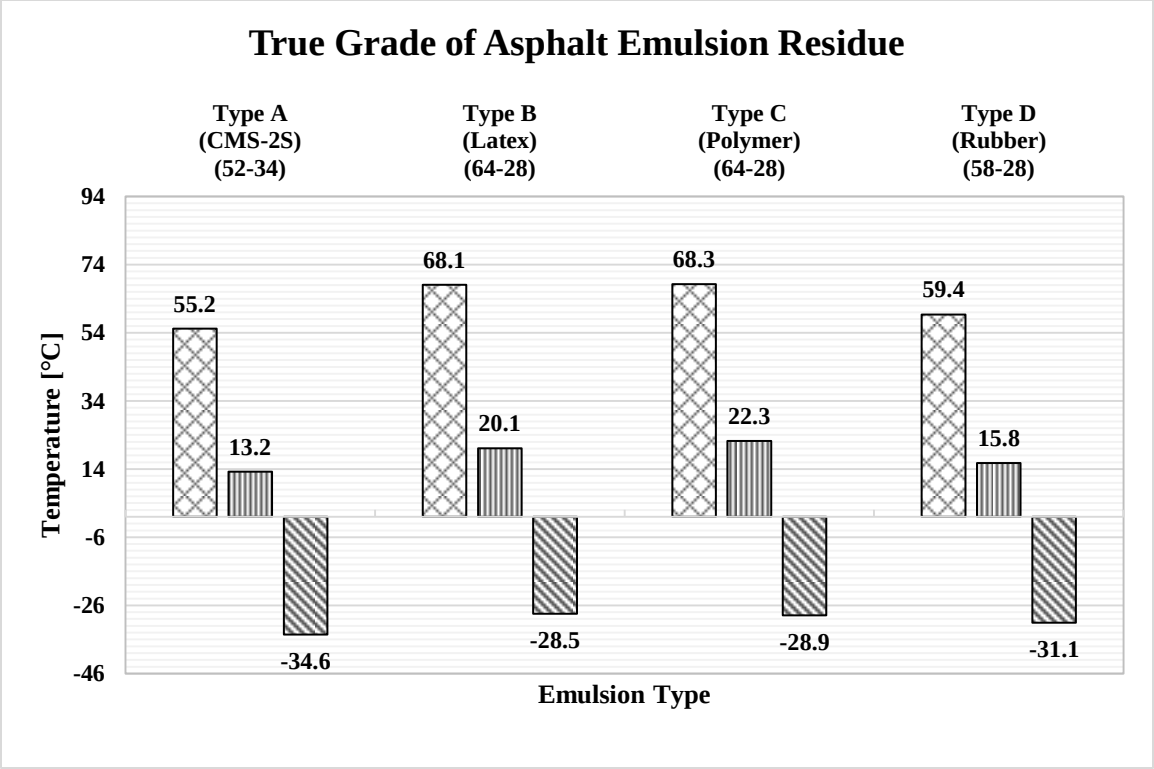

Figure 11. True grade of asphalt emulsion residue.

The physical properties of the original (unaged) asphalt binder residue (i.e., Complex modulus $G^*$and δ) are presented in Figure 7. The ratio $G^*/sin\delta$ is used to control rutting resistance of the asphalt binder at high temperatures. This parameter is inversely proportional to the work dissipated per loading cycle as can be seen in Equation(1:

$$\boldsymbol{W_c = \pi * \sigma_0^2 * \left(\frac{1}{G^*/sin\delta}\right)} \quad \textbf{(1)}$$

Where:

W_c : Work dissipated per loading cycle
σ_0 : Stress applied during loading cycle
G^* : Complex modulus
δ : Phase angle

The work dissipated per loading cycle can be decreased by increasing the complex modulus (G^*) and/or decreasing the phase angle (δ). This makes sense since a higher value of G^*means a stiffer and more resistant to rutting asphalt binder. Likewise, a low phase angle (δ) represents a more elastic and again more resistant to rutting asphalt binder. Based on the results shown in Figure 7, it can be concluded that emulsions Type B and C can resist rutting in environments where the pavement temperature goes up to 64°C, while emulsions A and D will be adequate for 52 and 58°C environments, respectively.

In spite of the Rolling Thin Film Oven (RTFO) test is recommended in AASHTO M320 for grading of asphalt binders, this test was not conducted in this research since the idea of this process is to simulate the asphalt binder aging during manufacture and construction process of HMA; and CIR will not be exposed to these levels of oxidation. The manufacturing and construction process of CIR does not require heat. Likewise, the expected flash point is not required since this rehabilitation technique will not require high temperatures.

The Rotational viscometer has been adopted in Superpave for determining the viscosity of asphalt binder at high construction temperatures (above 100°C) to ensure that the binder is sufficiently fluid for pumping and mixing [24]. Following the same logic mentioned in the paragraph above, this test was not conducted for the asphalt binder residue.

The long-term aging of the asphalt binder residue was conducted through the Pressure Aging Vessel (PAV) to simulate the aging that occurs during the in-service life of the

CIR pavement. However, the procedure established in AASHTO R28 [25] may simulate longer in-service life for the CIR layer since the layer is typically embedded under an AC overlay and may not age as much as a surface layer.

Because fatigue cracking generally occurs at intermediate pavement temperatures after the pavement has been in service for some time, the specification addresses the complex modulus (G^*) and phase angle (δ) measured with the DSR on the PAV residue to determine the critical temperature for fatigue cracking. Excessive stiffness at intermediate temperatures could be a contributing factor to fatigue cracking. [26]. The factor $G^*sin\delta$ was adopted to assess fatigue cracking susceptibility. The work dissipated per loading cycle at a constant strain can be expressed as:

$$\boldsymbol{W_c = \pi * \varepsilon_0^2 * (G^* sin\delta)} \quad (2)$$

Where:

W_c : Work dissipated per loading cycle
ε_0 : Strain applied during loading cycle

From Equation(2), it can be inferred that as $G^*$and/or δ increases, the work dissipated per a traffic loading cycle increases as well. On the other hand, as G^* decreases, the asphalt binder becomes less stiff and able to deform without building up large stresses. Likewise, asphalt binders with lower phase angle (δ) values present a more elastic behavior being able to regain their initial condition without dissipating too much work. Based on this analysis, the Superpave system recommends a maximum threshold of 5000kPa for the parameter $G^*sin\delta$ that is accepted in AASHTO M320 [23].

The critical fatigue temperatures for each emulsion are presented in Figure 11.

The Bending Beam Rheometer (BBR) was used to test the asphalt binder residues at low temperatures. Figure 9 presents the results of Creep Stiffness (S) at the testing temperatures. These values are a measure of the thermal stresses developed in the CIR as a result of thermal contraction. Superpave specifies a maximum threshold because as S increases, the thermal stresses developed in the pavement due to thermal shrinking also increase, and the thermal cracking becomes more likely.

A general rule of thumbs indicates that the Creep Stiffness (S) almost doubles for every 6 degrees decrease in temperature. This behavior was observed for emulsions type A, C, and D. The increase in Creep Stiffness for emulsion type B was only 1.4 times showing a flatter slope when compared with the other the emulsions. Considering that the flatter the curve of temperature vs S(t), the less thermal stresses are developed with decrease in temperature, it can be concluded that emulsion B may experience better resistance to thermal cracking.

The slopes of the stiffness vs temperature curve or "m-values" are presented in Figure 10. Superpave specifies a minimum threshold for m-value because as the slope of the asphalt binder stiffness curve flattens, the ability of the asphalt pavement to relieve thermal stresses by flow decreases.

Anderson et al. [27] suggested the ΔTc parameter to assess the susceptibility of the binder to aging at low temperatures. ΔTc is defined as the difference in continuous grade temperatures where binders reach their respective limits for S(60) of 300 MPa and m-value of 0.30. A negative value of ΔTc (Ts-Tm) indicates the controlling role of the relaxation properties of binder at low temperatures. A positive value of ΔTc represents

that the binder stiffening is a more influential factor for tested binder compared to ductility in low temperatures. Anderson et al. [27] verified the satisfactory correlation of ΔTc with ductility tests in several laboratory and field investigations. As a result, proposed the ΔTc thresholds of -2.5°C and -5°C as the correlation of ΔTc for the onset and significant cracking respectively.

The obtained values of ΔTc for all four asphalt residues indicate that none of the emulsions presents high susceptibility to low-temperature cracking. Type A and B emulsions are m-controlled (positive ΔTc) while Type C and D emulsions are S-controlled (negative ΔTc).

3.3. Additives (Hydrated Lime)

The benefits of hydrated lime in asphalt mixtures have been highlighted in several studies ([28]; [29]; [30]). The main benefit of the use of hydrated lime is its ability to control water susceptibility and its well-accepted capacity to act as an antistrip agent to inhibit moisture damage. Lime treatment of the CIR mixtures increases their initial stability, which allows early opening of the facility to traffic and improves its resistance to moisture damage, representing a significant extension of the useful life of the pavement [28]. Other benefits of hydrated lime in asphalt mixtures include:

- Acts as mineral filler, stiffening the asphalt binder and asphalt mixture in general.
- Improves the resistance to fracture growth at low temperatures.
- Favorably alters oxidation kinetics and interacts with products of oxidation to reduce their deleterious effects.

- Alters the plastic properties of clay fines to improve moisture stability and durability.

Cross [31] evaluated the impact of hydrated lime slurry on the moisture sensitivity of CIR mixtures in Kansas by means of the tensile strength and resilient modulus ratios. Figure 12 shows the retained tensile strength and resilient modulus ratios (i.e. ratio of conditioned over unconditioned property) of various CIR mixtures. It can be appreciated that the addition of hydrated lime represent a noteworthy impact on the retained tensile strength ratio (TSR), but not as significant on the retained resilient modulus ratio (except for the HFE emulsion where the hydrated lime slurry showed a significant impact on both ratios).

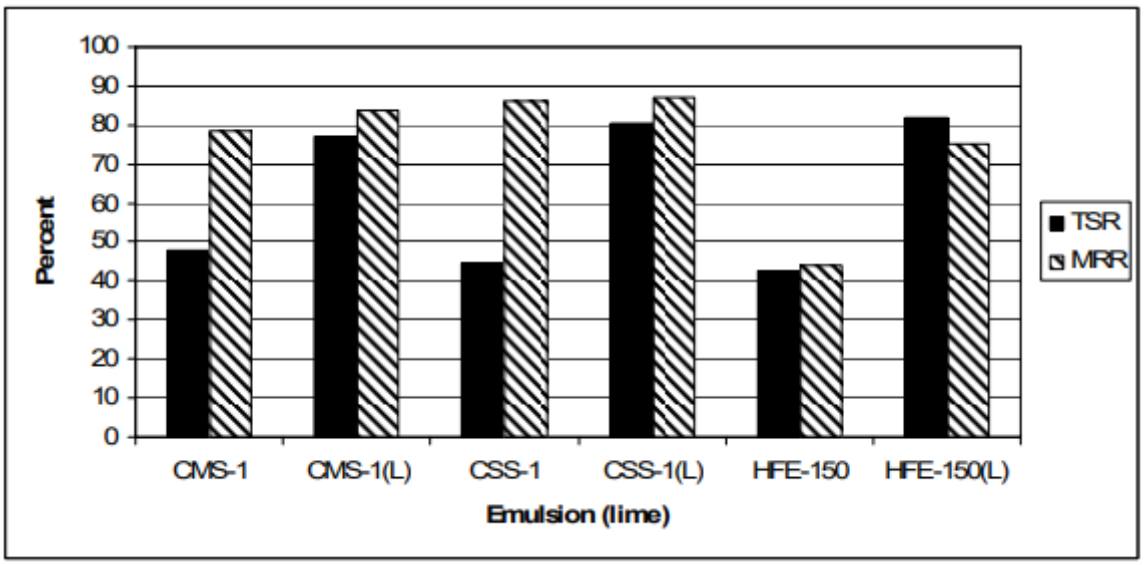

Figure 12. Tensile Strength Ratio (TSR) and Resilient Modulus Ratio (RMR) of Kansas CIR mixtures [31].

A similar finding was noted by Piratheepan in 2011 [32], when comparing the TSR of CIR mixtures with and without lime. The results are shown in Figure 13.

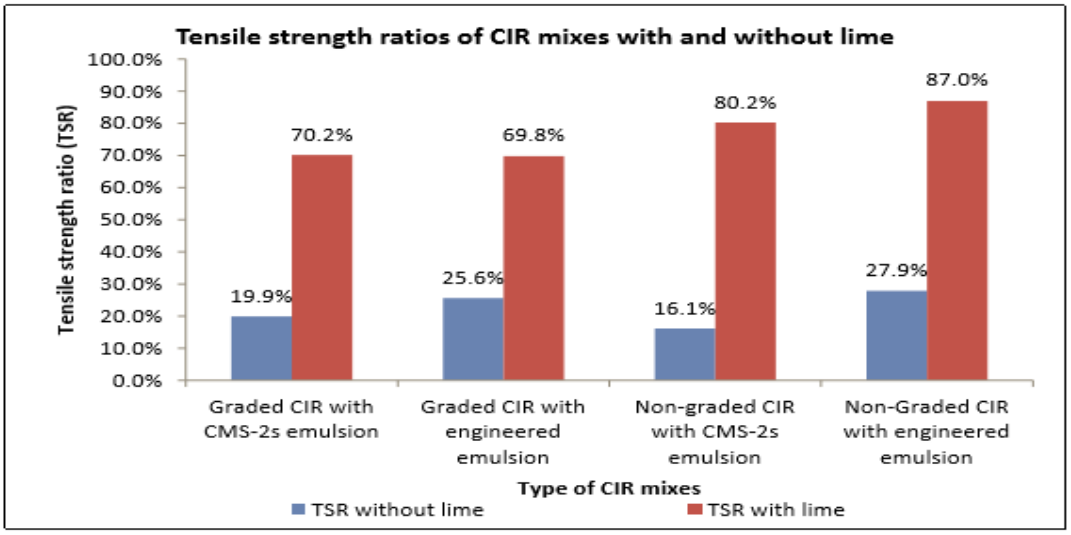

Figure 13. Tensile Strength Ratio (TSR) of CIR mixtures with and without lime [32].

The study conducted by Cross in the late 90's also assessed the impact of hydrated lime slurry on the rut resistance of CIR mixtures by means of the asphalt pavement analyzer (APA) after dry and submerged conditions.

Figure 14 presents the increase in rut depth when comparing the dry with the submerged conditions. A substantial influence of the hydrated lime slurry in reducing the percent change in the rut depth of the CIR mixtures can be observed, except for the HFE-150 mixture.

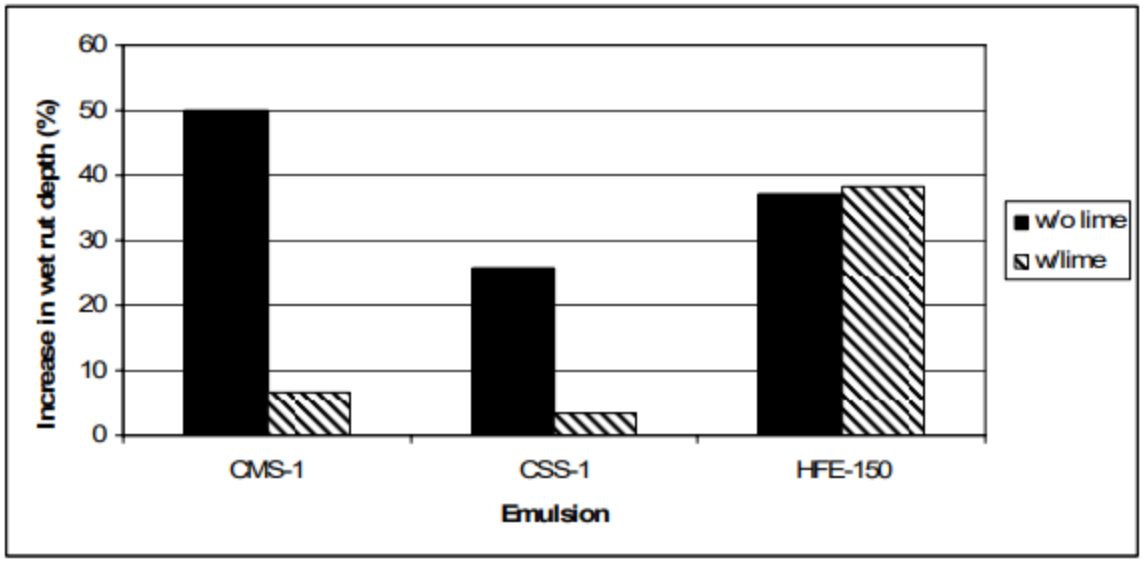

Figure 14. Percent increase in rut depth of Kansas CIR mixtures in the APA tester after 8000 cycles [31].

Another study conducted by the Kansas DOT in the late 90's constructed field test sections to evaluate the long-term performance of CIR mixtures treated with lime slurry and fly ash. This research showed that the fly ash section cracked soon after construction and had more cracking than the lime slurry section. In other words, the lime slurry section outperformed the fly ash test section [33].

In the early 2000's, Nevada DOT started looking into recycling most of the low-medium volume roads. A mix design procedure for CIR mixtures was developed to provide early stability (i.e, MR value above 150 ksi) and resistant to moisture damage (i.e. TSR $\geq$ 70%) [2]. This research concluded that in order to achieve early stability and improve resistance of the mixtures to moisture damage, the use of hydrated lime in CIR should be mandatory. After this study, NDOT mandates the use of lime in all CIR mixtures and excellent field performance has been observed.

Recent research conducted at the University of Nevada, Reno [11, 12] have validated the importance of hydrated lime in CIR mixtures when conducting mix design either by Superpave or Hveem methodologies.

In this research, two levels of lime slurry were considered: 6.0%, which is the actual level specified by NDOT and 4.5%, in order to study the impact of reducing the lime slurry on the cracking performance of CIR mixtures.

3.4. CIR Mix Design

Previous research conducted at UNR by Piratheepan, Castro, and Ayala [11, 12, 35] established the guidelines for the mix design of CIR. The main recommendations are summarized in this section:

3.4.1. Mixing Time

RAP is mixed with water (1-4%) for 1 minute, followed by 2 minutes mixing with lime slurry (6.0% or 4.5%) and 1 minute mixing with asphalt emulsion (1-4%). A visible satisfactory coating is required at the end of the complete mixing process. The percentage of water shall represent the actual combination of the water provided by the lime slurry and milling operation. The mixing time with emulsion shall be controlled in order to avoid break during the mixing process. Piratheepan [32] recommended maximum 1 minute mixing time with emulsion. A schematic overview of the mixing process is shown in Figure 15.

a) Dry RAP

b) RAP +1.5% Water

c) RAP +1.5% Water + Lime Slurry (LS)

d) RAP+1.5%Water + LS + Emulsion

Figure 15. Stages of CIR mixing process.

3.4.2. Determination of Theoretical Maximum Specific Gravity (G_{mm})

The measurement of the theoretical maximum specific gravity of the CIR mix was conducted as specified in AASHTO T209 [34].The test consists on calculating the maximum density the CIR mixture can achieve assuming zero air voids. For this purpose, the mass of dried loose mixture is divided by its volume. The volume of the sample is determined as the difference between the dry mass of the sample and the mass of the sample underwater at 77°F (25°C), as can be seen in Equation (**3**).

$$\boldsymbol{G_{mm} = \frac{A}{A - C}} \quad (3)$$

Where:
A: Mass of the oven dry sample in air (g)
C: Mass of the sample in water at 77°F (25°C)

3.4.3. Curing Time and Temperature for Compacted CIR Samples

The compacted CIR samples are cured for 48 hours at the temperature of 140°F (60°C) [11, 12].

3.4.4. Optimum Emulsion Content (OEC)

The optimum emulsion content percentages suggested by Ayala [9] obtained as a result of the Hveem mix design method using the California Kneading compactor were used in this research. The results are presented in Table 7 and Figure 16. It should clearly be noted that all percentages are expressed in terms of a percent of the dry weight of RAP. In addition, 6.0% lime slurry consists of 2.0% hydrated lime and 4.0% water and 4.5% lime slurry consists of 1.5% hydrated lime and 3.0% water

Table 7. Optimum Emulsion Content of CIR Mixtures for Hveem Mix Design [9].

Emulsion	Lime Slurry (%)	Aggregate	Hveem OEC (%)
Type A	4.5	Non-Graded	3.4
	6	Non-Graded	4
Type B	4.5	Non-Graded	3.8
	6	Non-Graded	3.5
Type C	4.5	Non-Graded	3.1
	6	Non-Graded	2.8
Type D	4.5	Non-Graded	3.6
	6	Non-Graded	4

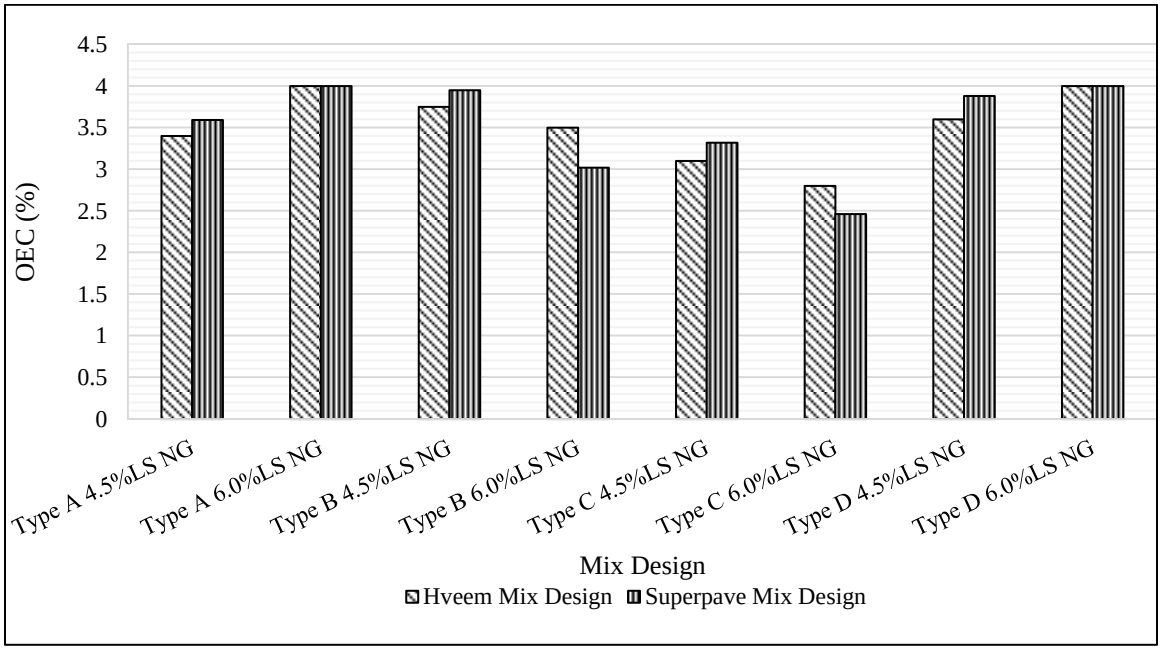

Figure 16. OEC according to Hveem & Superpave mix design [11, 12].

Chapter 4. Reflective Cracking behavior of Cold In-Place Recycling Mixtures

4.1. Introduction

Reflective cracking is a major challenge associated with pavement rehabilitation as it leads to premature failure of surface layer and allows water infiltration through the cracks, subsequently generating moisture damage and deterioration in all pavement layers.

Several methods have been investigated to determine effective alternatives to prevent or delay reflective cracking including metallic grids, different types of geosynthetics, asphalt-based interlayers, and fractured-slab approaches. Within those techniques, Cold-in Place recycling has been proven to be an effective mean of extending life of pavement rehabilitation projects and provide resistance against reflective cracking between two and three times that offered by conventional resurfaced control sections [18].

In this research, the reflective cracking resistance of the CIR mixtures was evaluated by means of the overlay tester device (OT). The OT measures the number of cycles to failure of specimens by simulating the opening and closing of cracks induced by temperature variations and tensile strains generated by traffic loads. Texas Department of Transportation (TxDOT) established a procedure to determine the susceptibility of bituminous mixtures to reflective cracking as per Tex-248-F standard [35].

Although the OT has been widely accepted to simulate effectively the cracking mechanism of AC mixes, the repeatability of the number of cycles to failure used as a performance index has been a major concern. A great effort developed by the University of Texas, El Paso and TxDOT was directed toward improving the characterization of the

cracking potential of mixes by evaluating the cracking properties in terms of crack initiation (Critical Fracture Energy) and crack propagation (Crack Progression Rate) [36]. These parameters were considered in this research and will be further explained in this chapter using examples of actual test results.

4.2. Experimental Plan

The Texas OT was performed on the eight mixtures presented in Table 7 in order to evaluate reflective cracking behavior and analyze the impact of lime content on the CIR mixtures. The process to perform the test is described in the following sections:

4.2.1. Sample Preparation

CIR samples were compacted in the Superpave Gyratory Compactor (SGC) in accordance with AASHTO R83. The dimensions of the samples were 6.0 inches (150 mm) diameter by 6.0 inches (150 mm) height, targeting 13±1% air voids. The compacted CIR samples were subjected to conditioning at 140^{o}F (60^{o}C) for 48 hours. Subsequently, SGC samples were cut to get the OT specimens consisting of a 6.0 inches (150mm) long by 3.0 inches (76 mm) wide and 1.5 inches (38mm) thick samples as shown in Figure 17 and Figure 18. A total of three samples were obtained from each SGC compacted sample. The bulk specific gravity (G_{mb}) of the cut samples were measured in accordance with ASTM D118 [37].

Figure 17. Laboratory molded specimen (left) and trimmed specimen (right).

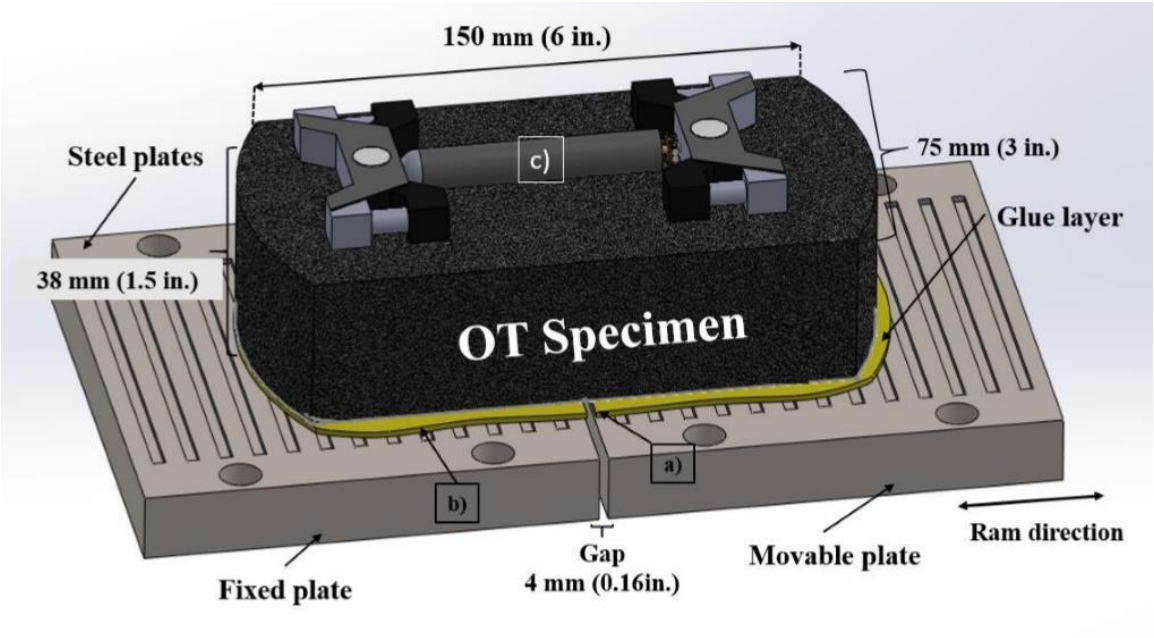

Figure 18. OT schematic layout and sample dimensions [36].

4.2.2. Sample Conditioning

As specified in Tex-248-F standard, the trimmed specimens were conditioned at 77 ± 1°F (25 ± 0.5°C) for at least 1hr before testing. [35]

4.2.3. Texas Overlay Test description

The OT measures the number of cycles to failure of specimens by simulating the opening and closing of joints and/or cracks induced by daily temperature variations and tensile strain generated by traffic loads. [36].The test is conducted in a controlled displacement mode until failure occurs at a loading rate of one cycle each 10 seconds. Each cycle consists of triangular load profile with 5 seconds of loading and 5 seconds of unloading. As the CIR mixture is subjected to the repeated openings and closings, its internal strength is reduced which is represented by a drop in the applied load needed to maintain the constant opening.

4.2.4. Opening Displacement

According to Tex-248-F [35], a maximum opening displacement of 0.025 in (0.635 mm) can be used to perform the Overlay Test. This value was derived by evaluating asphalt mixtures used in overlays on top of old concrete pavements in Texas and was calculated based on the thermal expansion of a 15-ft (4.5-m) long concrete slab under a 30 °F (17 °C) daily temperature variation [38]. In that study, two types of concrete slabs with gravel and limestone were considered. The average calculated thermal expansion of these two slabs was 0.025 in (0.635 mm), current value recommended as maximum in opening in the standard.

Equation (**4**) shows the expression used to calculate the maximum opening displacement (MOD) in the overly test recommended by Zhou and Scullion [38].

$$\Delta \boldsymbol{L} = \boldsymbol{\alpha} * \boldsymbol{L_{eff}} * \Delta \boldsymbol{T} * \boldsymbol{\beta} \quad (4)$$

Where:

ΔL : horizontal movement of the slab due to temperature change (m)
α : coefficient of linear thermal expansion ($10^{-6}/m/°C$)
L_{eff} : effective PCC joint spacing
ΔT : maximum 24-h temperature difference (°C)
β : PCC/Base friction factor

A second study conducted by Zhou et. Al [39] concluded that applying too large or too small opening displacement is not desirable for determining crack development. A large displacement causes the specimen to fail much more quickly. Small displacement lasts too long to perform the test. Zhou and Scullion [40] provided a recommended range of the MOD based on past studies. For 77 °F (25 °C) testing temperature, the MOD should be smaller than 0.08 inch (2.0 mm). For 32 °F (0 °C) testing temperature, the MOD should not exceed 0.005 inch (about 0.125 mm).

A study conducted by Ma [41] concluded that the maximum opening displacement of 0.025 inch (0.635 mm) is deemed too large for testing stiff asphalt mixtures with higher contents of RAP/RAS and the mixtures of asphalt overlay placed in different climate conditions.

Taking into account that the vast majority of CIR projects mill the top 2 to 3 inches of old AC and an AC overlay of 2 to 3 inches as a wearing course, a maximum opening displacement (MOD) of 0.01 inches (0.25 mm) was assumed to simulate field conditions.

4.2.5. Test Results

The analysis of the OT data was conducted in accordance with the latest procedures established in TxDOT test standard Tex-248-F [35], where the resistance of the mixture to reflective cracking is evaluated by means of three parameters: number of cycles to failure, crack initiation, and crack propagation.

The number of cycles to failure is defined by a drop of 93% of the maximum load measured on the first cycle. If the critical drop in the applied load is not reached, the test runs to 3,277 cycles (Maximum number of cycles that the machine can run).

The resistance of the mixture to crack initiation is defined as the dissipated energy required to initiate a crack. The area under the hysteresis loop of the first cycle obtained from the OT test is used to determine the critical fracture energy given by Equation 5:

$$\boldsymbol{G = W/A} \quad (5)$$

Where;

G : Energy (lbs.-in./in2)
W : Facture area (portion of the hysteresis loop)
A : Area of the cracked section (thickness multiplied by the width of the specimen: 1.5 in. x 3.0. in.)

Figure 19 shows an example of the hysteresis loop of one CIR specimen, mixed and compacted with asphalt emulsion type A, non-graded RAP, and 6.0% lime slurry. Calculations of the fracture energy are conducted as follows:

Maximum load: 398 lbs.

Displacement at maximum load: 0.0047 inches.

4th grade polynomial fitted to the hysteresis curve:

$$y = -8 * 10^{10}x^4 + 2 * 10^9x^3 - 3 * 10^7x^2 + 165575x + 75.961.$$

Fracture Area (W):

$$W = \int_0^{0.004748} -8 * 10^{10}x^4 + 2 * 10^9x^3 - 3 * 10^7x^2 + 165575x + 75.961\, dx$$

$$= 1.37\ lb \cdot in$$

Critical Fracture Energy:

$$G = \frac{W}{A} = \frac{1.37}{1.5 * 3.0} = 0.30\ lb \cdot in/in^2$$

The crack propagation rate provides an indication on the ability of the mix to attenuate the crack after it has been initiated. This property is quantified by fitting a power equation to the load reduction curve from the OT test. The crack propagation rate is defined as the coefficient in the power model; $y = x^{-b}$ (i.e., b-coefficient). Figure 20 shows the power model for the same CIR sample used to determine the critical fracture energy. In this case, the fitted power equation is; $y = x^{-0.439}$, and therefore the crack progression rate is defined as 0.44.

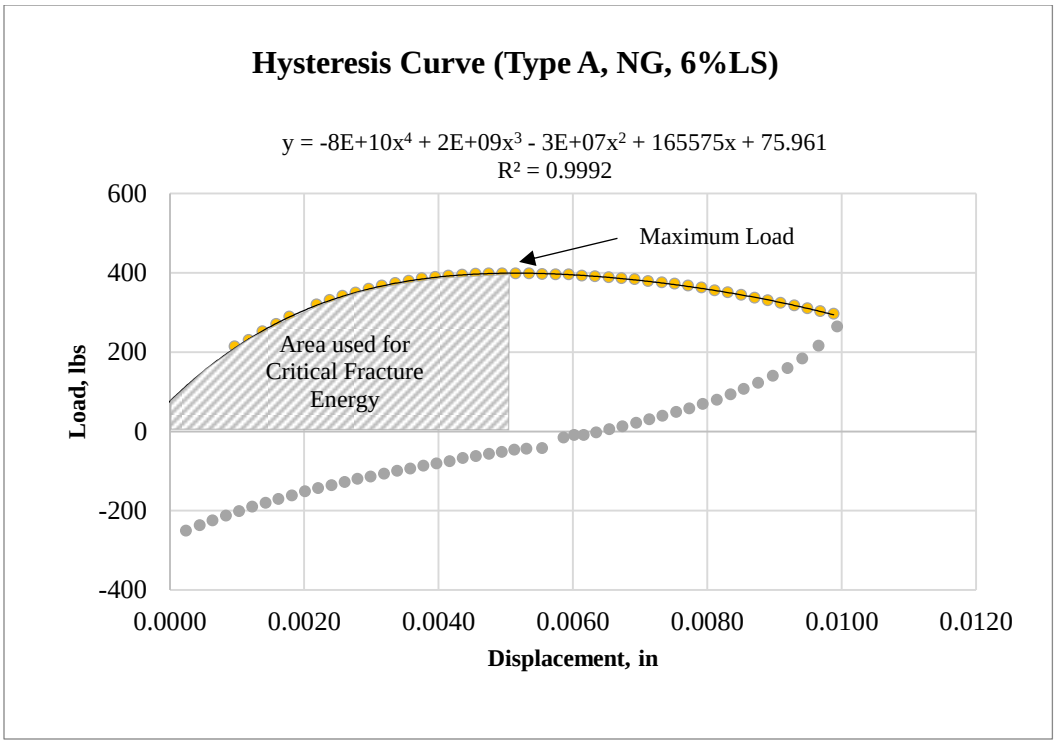

Figure 19. Hysteresis loop for CIR mixture under the first OT cycle.

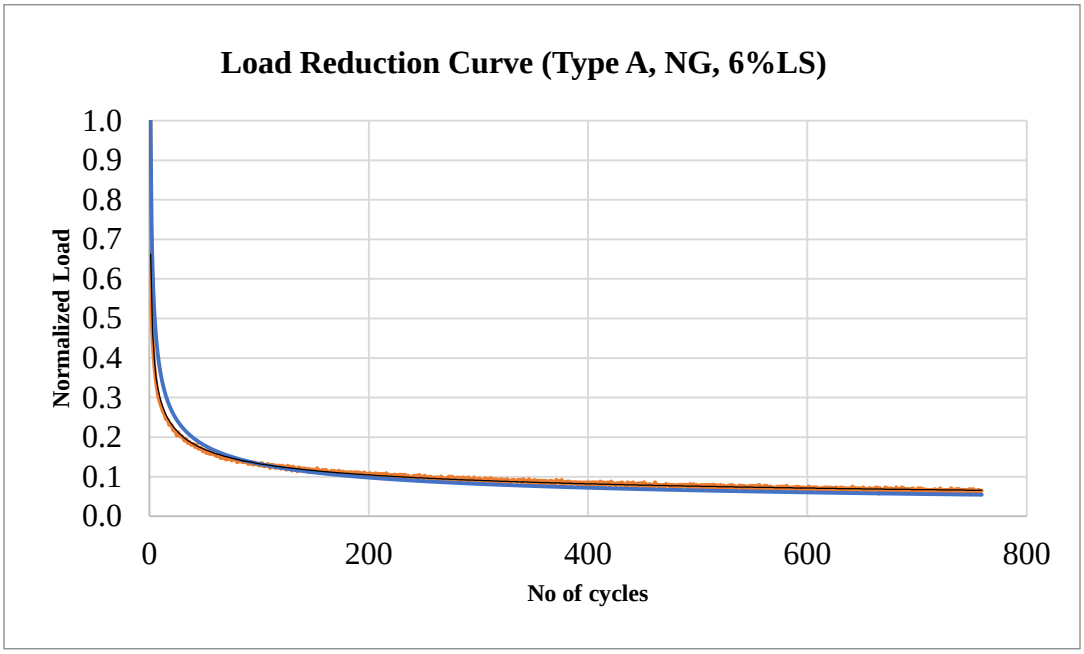

Figure 20. Power model fitting for CIR mixture in the OT.

A CIR mixture having high number of cycles to failure with high resistance to crack initiation and low rate of crack propagation is expected to exhibit excellent resistance to reflective cracking.

Table 8 summarizes the reflective cracking properties of the four CIR mixtures with non-graded RAP and 6.0% lime slurry designed with the Hveem method. The detailed dataset is presented in Appendix 9.2 .

Table 8. Summary of Reflective Cracking Characteristics of NG – 6.0% LS CIR Mixtures.

	No of Cycles to Failure			**Critical Fracture Energy**			**Crack Propagation Rate**		
Emulsion Type	Average	Std. Dev.	COV (%)	Average	Std. Dev.	COV (%)	Average	Std. Dev.	COV (%)
A	496	32	6%	0.33	0.0007	1%	0.44	0.0007	1%
B	132	26	20%	0.36	0.0163	4%	0.51	0.0198	4%
C	280	51	18%	0.20	0.0035	2%	0.41	0.0955	23%
D	1254	226	18%	0.24	0.0120	5%	0.35	0.0049	1%

Figure 21 to Figure 23 compare the reflective cracking properties of the 4 non-graded CIR mixtures with 6.0% LS. The whiskers over the bars represent the 95% confidence interval for each CIR mix. An overlap in the confidence intervals of any two CIR mixtures indicates that the represented properties are statistically similar.

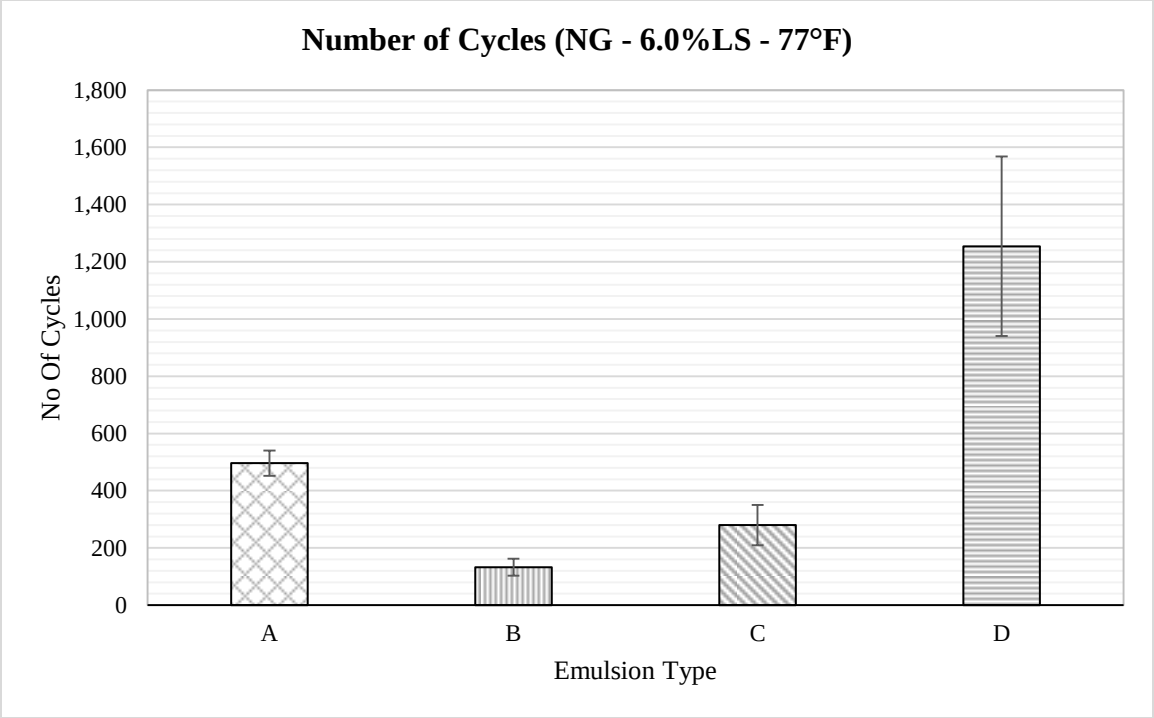

Figure 21. Cycles to failure of CIR mixtures; non-graded RAP and 6.0% lime slurry.

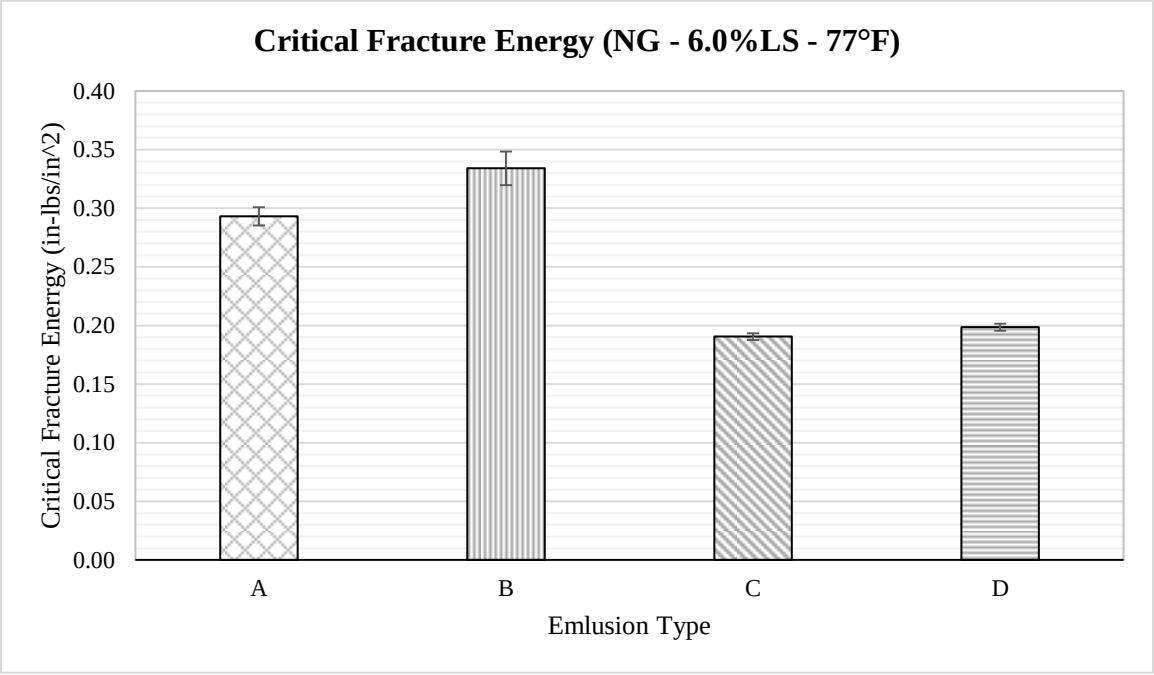

Figure 22. Critical fracture energy of CIR mixtures; non-graded RAP and 6.0% lime slurry.

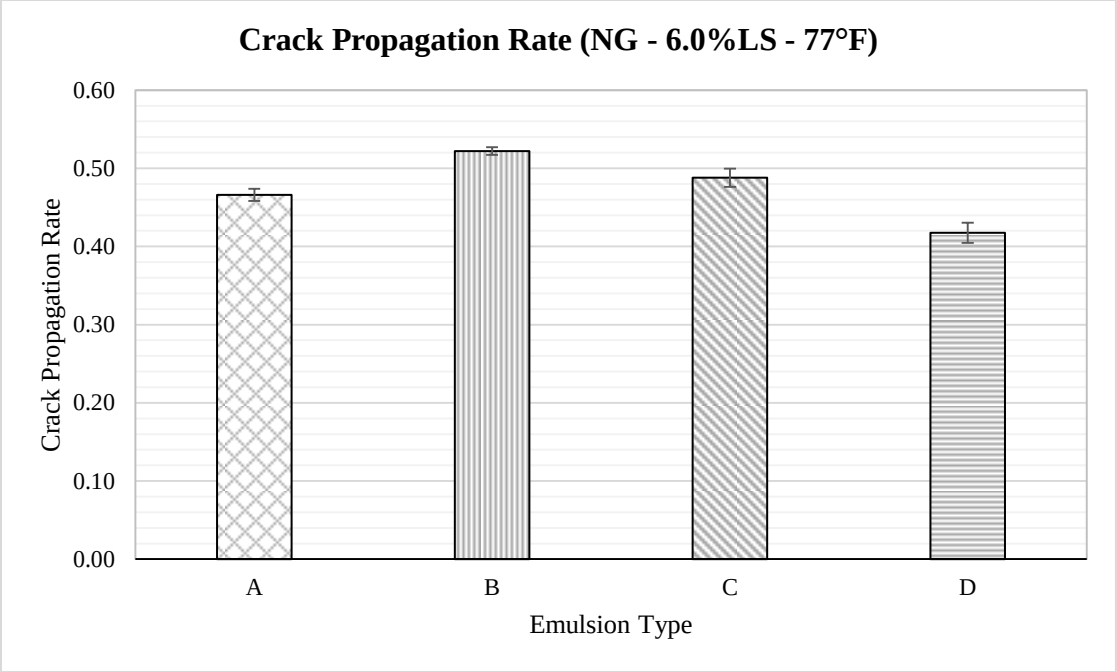

Figure 23. Crack propagation rate of CIR mixtures; non-graded RAP and 6.0% lime slurry.

Same evaluation was conducted for non-graded mixtures with 4.5% of Lime Slurry. The average, standard of deviation and coefficient of variation of the results from two replicates of each emulsion are presented in Table 9.

Table 9. Summary of Reflective Cracking Characteristics of NG – 4.5% LS CIR Mixtures.

	No of Cycles to Failure			**Critical Fracture Energy**			**Crack Propagation Rate**		
Emulsion Type	Average	Std. Dev.	COV (%)	Average	Std. Dev.	COV (%)	Average	Std. Dev.	COV (%)
A	282	56.57	20%	0.29	0.01	2%	0.47	0.0057	2%
B	76	19.09	25%	0.33	0.01	4%	0.52	0.0042	1%
C	155	23.33	15%	0.19	0.00	1%	0.49	0.0085	2%
D	391	58.69	15%	0.20	0.00	1%	0.42	0.0092	2%

Figure 24 to Figure 26 compare the reflective cracking properties of the 4 non-graded CIR mixtures with 4.5% of lime slurry. The whiskers over the bars represent the 95% confidence interval for each CIR mix.

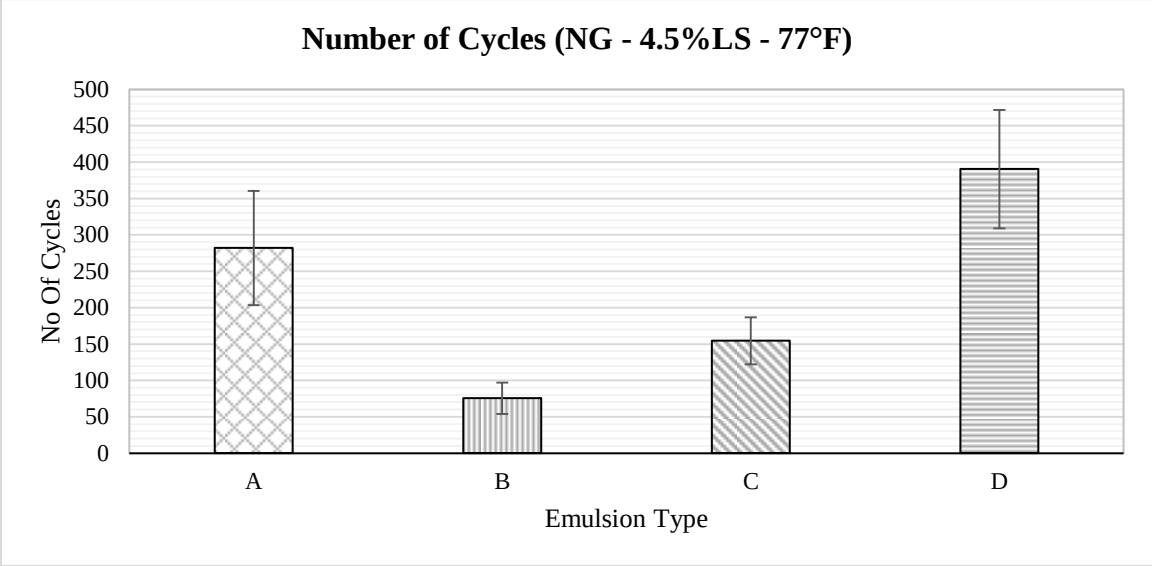

Figure 24. Cycles to failure of CIR mixtures, non-graded RAP and 4.5% lime slurry.

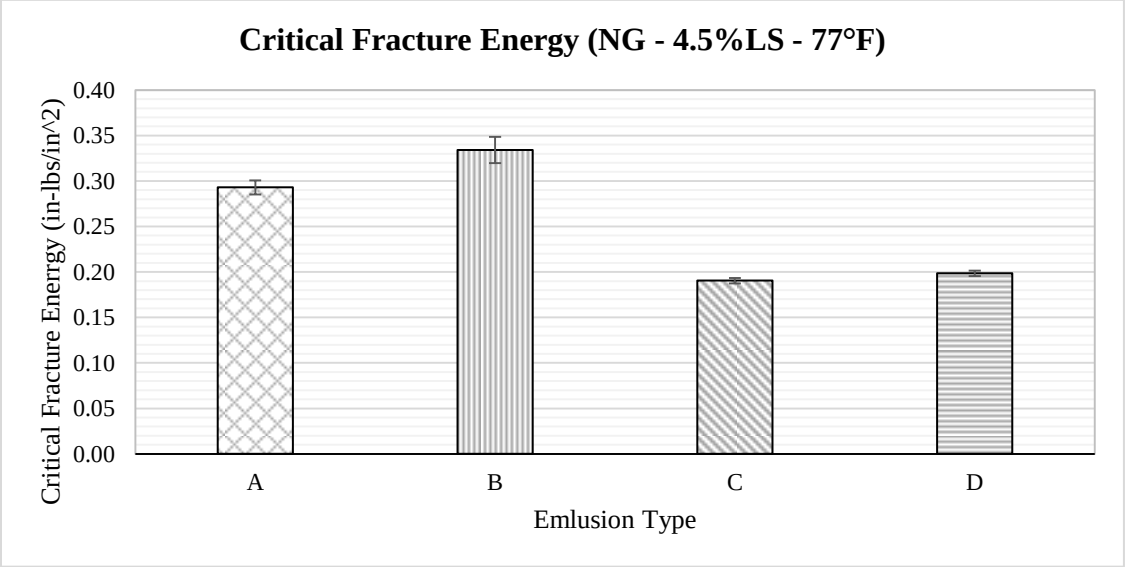

Figure 25. Critical Fracture Energy of CIR mixtures; non-graded RAP and 4.5% lime slurry.

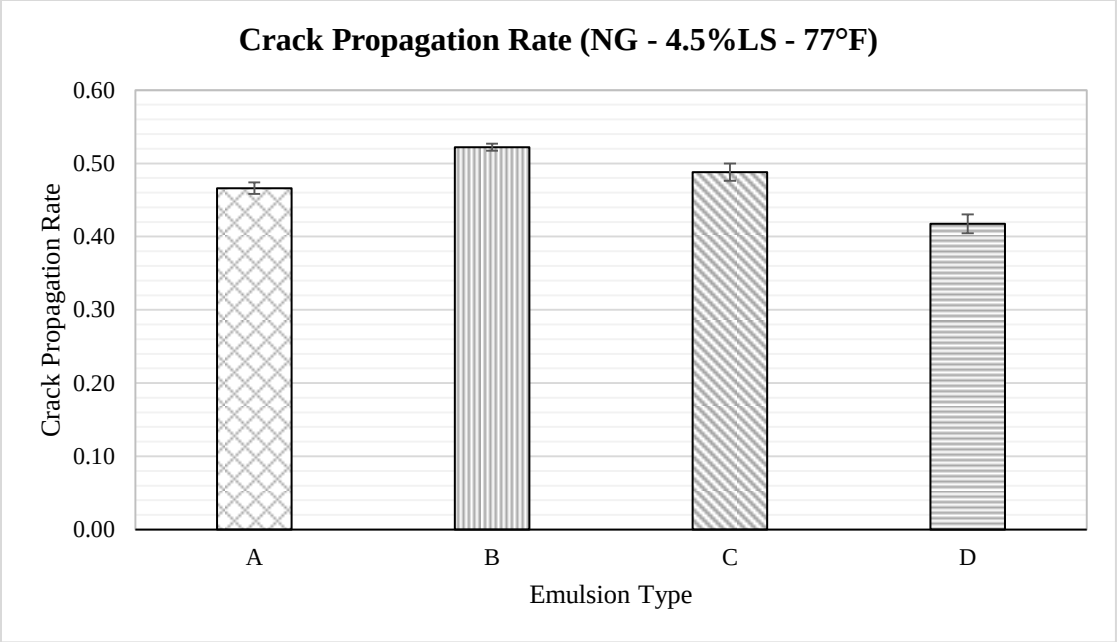

Figure 26. Crack propagation rate of CIR mixtures; non-graded RAP and 4.5% lime slurry.

4.2.6. Analysis of results

- **Number of Cycles**

The data show that the number of load cycles to failure has the highest variability (i.e., higher coefficients of variation) while the crack initiation and crack propagation rate have less variability.

Figure 27 presents a comparison between the number of cycles (NOC) to failure for the 6.0% and 4.5 % LS non-graded CIR mixtures.

The values in the boxes indicate the percentage of reduction in the number of cycles when decreasing the level of lime slurry from 6.0% to 4.5%.

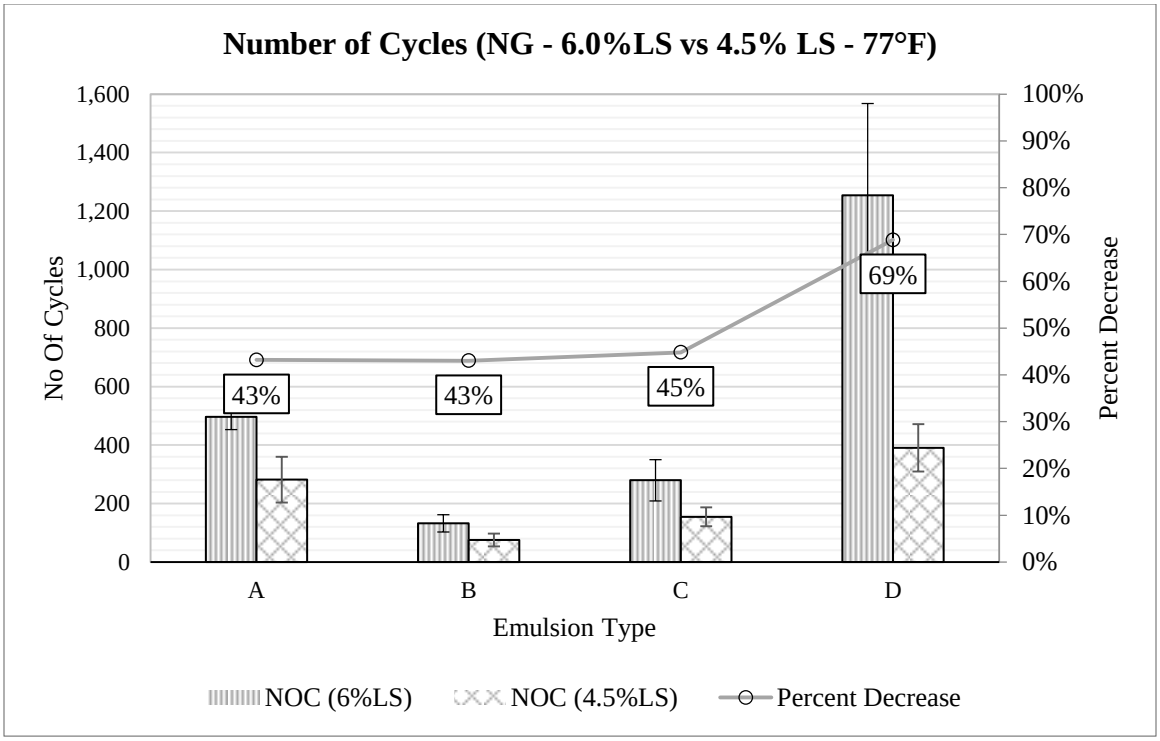

Figure 27. Number of cycles to failure comparison (6.0%LS vs 4.5% LS).

A consistent decreasing trend was observed when reducing the percentage of lime for the number of cycles (NOC) in all cases. Emulsions A, B and C exhibited similar percent reductions (≈ 45%) while emulsion D was the most affected with the decrease of lime slurry (69%). However, it should be mentioned that the high variability of the number of cycles to failure makes it an unreliable indicator of the resistance to reflective cracking.

- **Critical Fracture Energy (CFE)**

A comparison between the Critical Fracture Energies ($in - lbs/in^2$) of the non-graded emulsions with 6.0 and 4.5% of Lime Slurry is presented in Figure 28.

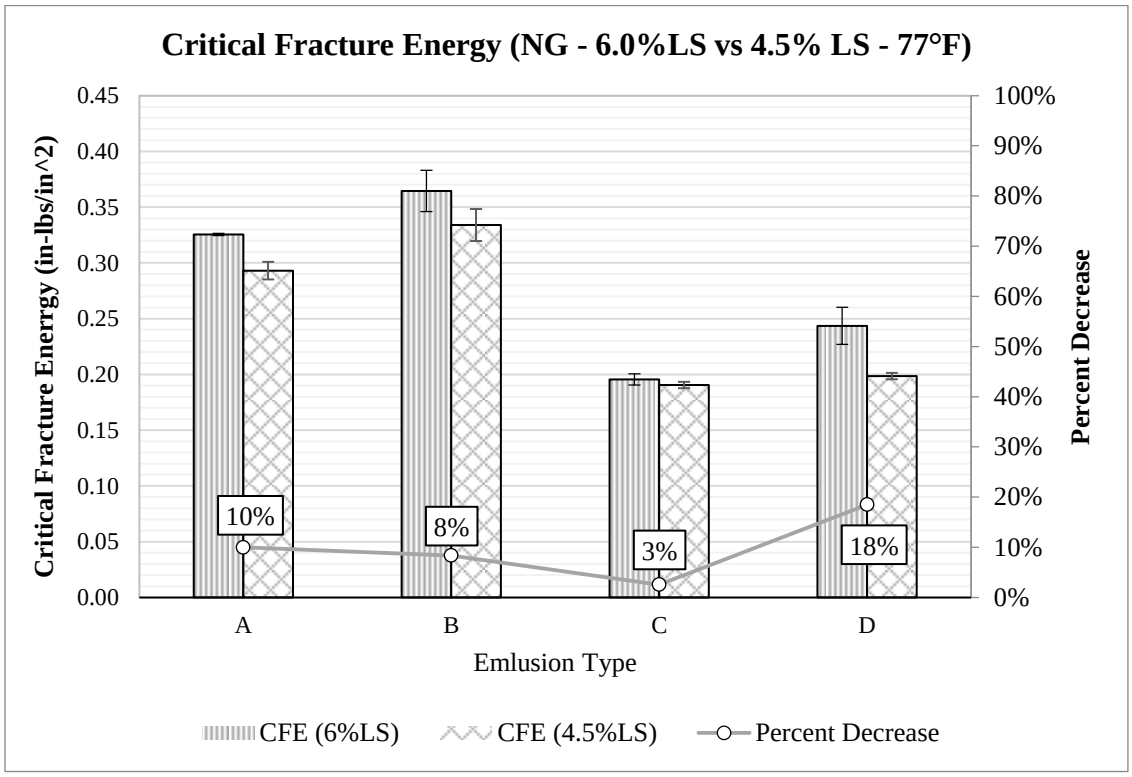

Figure 28. Critical Fracture Energy Comparison (6.0%LS vs 4.5% LS)

Similar to the number of cycles, a decrease in fracture energy is observed when reducing the percentage of lime slurry from 6.0 to 4.5%. However, the percent decrease in fracture energy (3-18%) is significantly lower than the percent decrease in the number of cycles to failure (43-69%). The variability among samples was lower as well, represented by a lower coefficients of variation.

The critical fracture energy can be described as the energy required to initiate a crack. Tough mixtures are desired to resist the propagation of a crack. Even though the CIR material exhibited higher levels of stiffness (i.e., high E*), the energy required to initiate a crack is low in comparison with the typical values presented by AC mixtures that are around 0.1 to 3 $in - lbs/in$^2 [36].

- **Crack Propagation Rate**

Figure 29 provides compares the crack propagation rates of the non-graded CIR mixtures with 6.0 and 4.5 % lime slurry.

The crack propagation rate reflects the ability of the CIR mix to retard the crack after it is initiated. A lower value of crack propagation rate is desired since it indicates that the material has good relaxation properties and the propagation of the crack to the overlay can be delayed.

In contrast with the number of cycles to failure and the critical fracture energy, the crack propagation rates increased with decreasing the percentage of lime slurry. This behavior is expected since hydrated lime has demonstrated a positive impact on the flexibility of the material [28]. In general, a decrease in flexibility and a decrease in the ability of the CIR mixture to retard crack propagation when decreasing the level of lime slurry was observed. The percent change in the crack propagation rate (6-18% increase) was lower than the percent change in the number of cycles to failure (43-69% decrease) as the slurry is reduced from 6.0 to 4.5%. It should be noted that the fracture energy and crack propagation rate exhibited similar changes with opposite trends as the slurry is reduced from 6.0 to 4.5%.

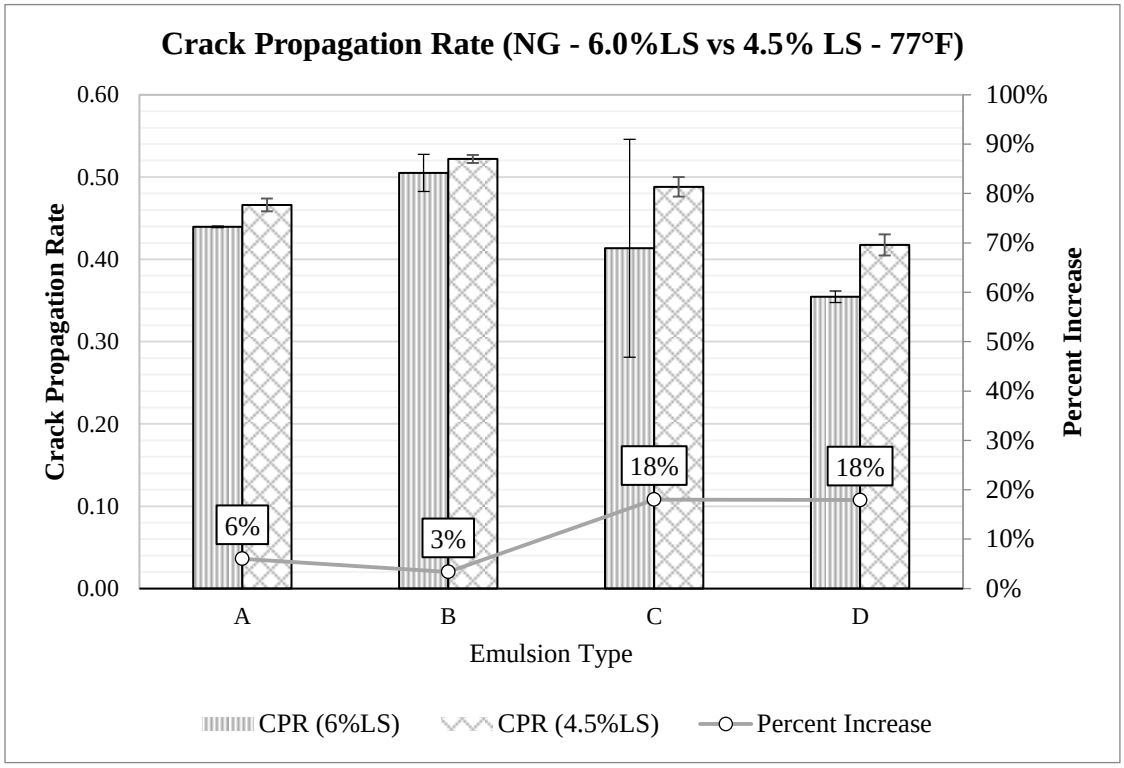

Figure 29. Crack Propagation Rate Comparison (6.0%LS vs 4.5% LS).

The OT data show some interesting trends where the standard CMS-2S and the latex-modified emulsions (A and B) seems to be able to resist the initiation of the reflective crack (i.e. higher fracture energy) but unable to slow down its propagation as good as the polymer and rubber modified emulsions (C and D).

Chapter 5. Fatigue Characteristics of Cold In-Place Recycling Mixtures

5.1. Introduction

It is well known that CIR offers an attractive alternative for rehabilitation of heavily damaged AC pavements. The most common use of this technique involves milling the top 2-3 inches of the old AC layer, laydown the CIR layer and overlay with 2-3 inches of AC, in such a way that the CIR and the new AC layer act as two asphalt bound layers.

On the other hand, one issue with CIR is that there is limited research information available regarding the fatigue cracking characteristics of this rehabilitation technique. Since fatigue cracking can start at the bottom face of any of the asphalt bound layers in a pavement system where the tensile stress exceeds the tensile strength, the fatigue behavior of each material needs to be properly evaluated.

This chapter presents the results of the evaluation of fatigue cracking characteristics of CIR mixtures by means of the flexural beam fatigue test, conducted at different temperatures and levels of microstrain.

5.2. Experimental Plan

5.2.1. Sample Preparation

Beam samples were mixed at the Hveem optimum emulsion content and compacted in the kneading compactor to air voids of 13±1%. The test beams of 2.5 x 2.0 x 15.0 inch were cut from the original compacted beams of 3.0 x 3.0 x 15.0 inch as shown in Figure 30.

Figure 30. Laboratory compacted specimens (left) and trimmed specimens (right).

5.2.2. Sample Conditioning

The flexural beam fatigue test was conducted at three different temperatures: 55°F (12.8°C), 70°F (21.1°C) and 85°F (29.4), a loading frequency of 10Hz, and various levels of microstrain. Samples were conditioned in the pneumatic beam fatigue machine chamber for at least two hours before testing. Unlike the HMA mixtures, CIR samples were not subjected to long term oven aging LTOA of 5 days at 185°F (85°C) as specified in AASHTO R30 [42]. The aforementioned aging protocol was not implemented since the CIR layer will be overlaid with a surface layer and will not experience the aging level that LTOA practices intend to simulate.

5.2.3. Flexural Beam Fatigue Test description

The resistance of the CIR mixtures to fatigue cracking was evaluated using the flexural beam fatigue test as per ASTM D7460: Standard Test Method for Determining Fatigue Failure of Compacted Asphalt Concrete Subjected to Repeated Flexural Bending [43] . In this test, the beam specimen is subjected to a 4-point bending with free rotation and horizontal translation at all load and reaction points. This produces a constant bending moment over the center portion of the specimen. In this research, constant strain tests were conducted at multiple strain levels between 250 and 800 microstrain using a repeated haversine load at a frequency of 10 Hz, and three test temperatures of 55, 70, and 85°F. All the flexural beam fatigue tests were conducted in the pneumatic testing system. **Figure 31** shows the testing set-up of the flexural beam fatigue test.

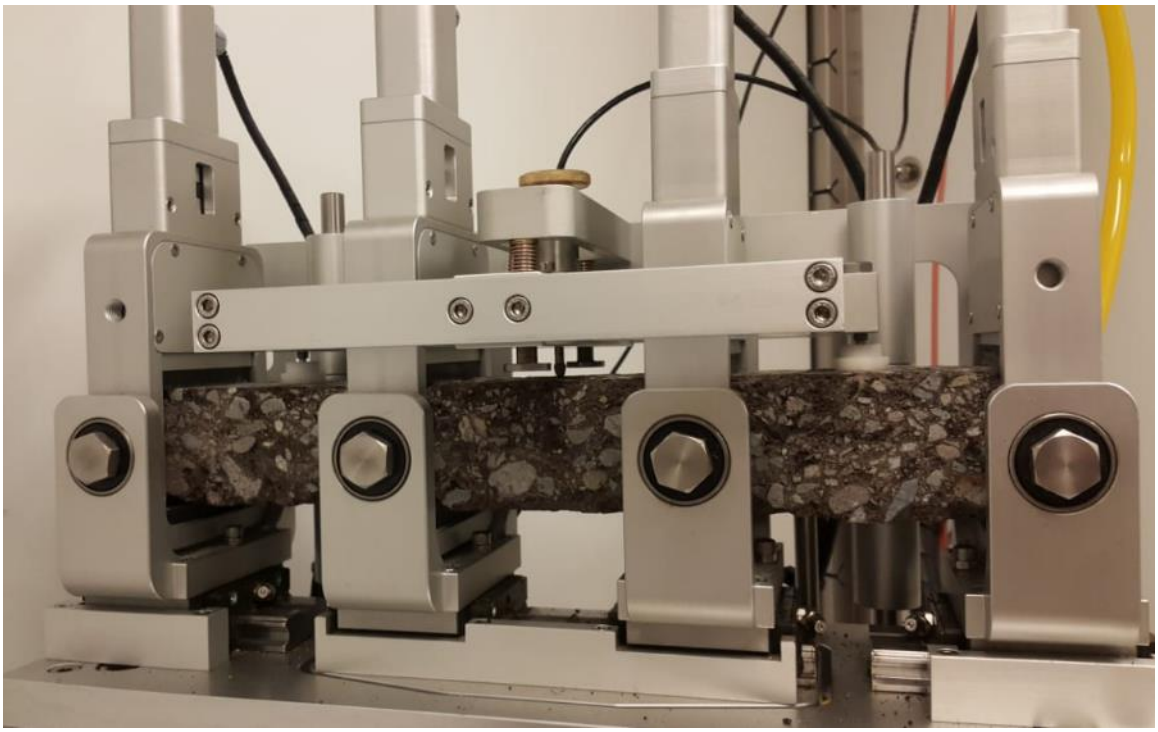

Figure 31. Flexural bending fatigue test on pneumatic machine

The flexural beam fatigue test can be conducted in controlled stress or controlled strain mode of loading. In the controlled stress mode, the haversine load of a constant amplitude is repeated until failure occurs. In this case, failure results when the sample actually breaks. In the controlled strain mode of loading, the deflection amplitude is maintained constant while the applied load is decreased appropiately with increasing cycles.

Experience has shown that thick asphalt pavements (more than 6 inches (150mm)) generally perform close to the controlled stress mode of loading, whereas thin asphalt pavements perform close to the controlled strain mode of loading [24] [44]. Considering that CIR layers are generally 2-3 inches thick and are usually overlaid with 2-3 inches of asphalt concrete, the strain mode of loading was considered appropriate.

Given that the controlled strain mode of loading was considered in this study, a verification of the tensile strain and the flexural beam stiffness was conducted for each tested specimen. The requirement was that the actual applied tensile strain had to reach the targeted tensile strain before the first 50 cycles. **Figure 32** (a) presents an acceptable test that reached the target strain before cycle 50 while (b) shows a discarded test since it took more than 200 cycles to reach the target strain. The amount of cycles required to reach the target strain was controlled by changing the Proportional-Integral-Derivative (PID) controllers of the machine. A PID controller continuously calculates an error value $e(t)$ as the difference between a desired setpoint (SP) and a measured process variable (PV) and applies a correction based on proportional, integral, and derivative terms (denoted P, I, and D respectively). In this case the SP was the desired level of microstrain.

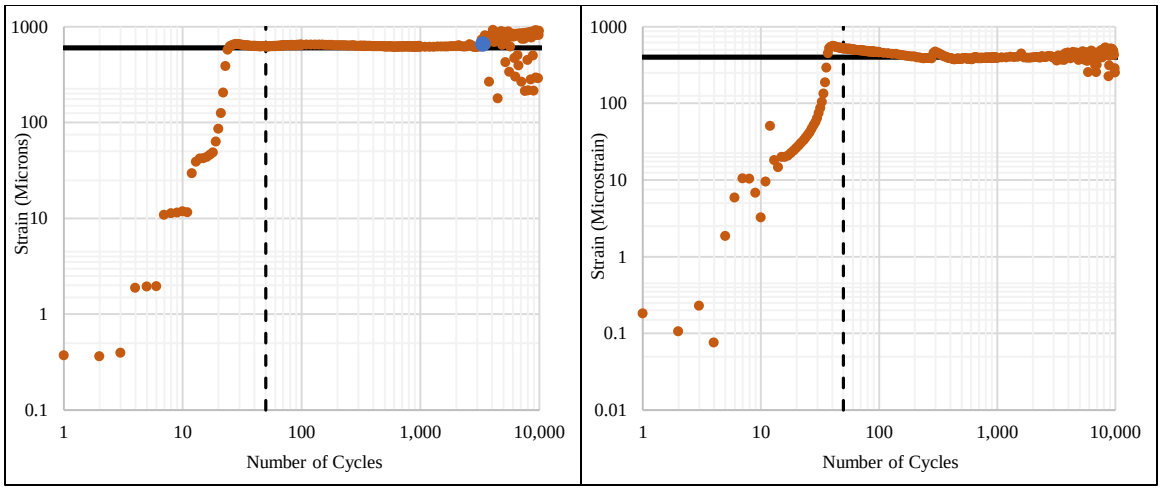

(a) **(b)**

Figure 32. Tensile strain vs number of cycles.

5.2.4. Testing Matrix

The general mathematical form of the fatigue cracking model commonly for asphalt bound materials is shown in Equation (**6** [47]. The form of the model is a function of the tensile strain at a given location and modulus of the asphalt bound layer.

$$N_f = K_1 * \left(\frac{1}{\varepsilon_t}\right)^{K_2} * \left(\frac{1}{E}\right)^{K_3} \quad (6)$$

Where:
N_f : Number of repetitions to failure by fatigue cracking
K_1, K_2, K_3 : Laboratory regression constants
ε_t : Tensile strain at the critical location
E : Stiffness of the material

In order to be able to implement this model for Cold in-Place Recycling mixtures, at least three temperatures and multiple levels of strains needed to be evaluated. Table 10 summarizes the testing conditions for the fatigue cracking experiment.

Table 10. Temperature and Microstrain Levels considered in the Experiment.

Temperature	Microstrain
55°F (12.8°C)	250
	400
	550
70°F (21.1°C)	250
	400
	550
85°F (21.1)	400
	550
	700

5.2.5. Test Results

The number of cycles to fatigue failure was determined in accordance to ASTM D7460 [43]. ASTM D7460 defines the failure point as the number of cycles at which the stiffness ratio (SR) is equal to 0.50. The stiffness ratio is defined as the ratio of the stiffness at any number of cycles over the initial stiffness measured at 50 cycles.

During the test, the maximum deflection (δ) in each cycle is used to calculate the resulting maximum tensile strain (ε_t) as shown in Equation (**7**). The maximum tensile stress (σ_t) is determined using Equation 8. Then, the flexural stiffness (S) is determined using Equation (**9**) [43].

$$\boldsymbol{\varepsilon_t = \frac{12\delta h}{(3L^2 - 4a^2)}} \quad (7)$$

Where:
ε_t : Maximum tensile strain (mm/mm)
δ : Maximum deflection at center of the beam (m)
a : Space between inside clamps (m)
L : Length of beam between outside clamps (m)

$$\boldsymbol{\sigma_t = \frac{3ap}{bh^2}} \quad (8)$$

Where:
σ_t : Maximum tensile stress (Pa)
a : Center to center spacing between clamps (Provided by Cox Equipment = 0.1190m)
P : Load applied by actuator (N)
b : Average specimen width (m)
h : Average specimen height (m)

$$\boldsymbol{S = \frac{\sigma_t}{\varepsilon_t}} \quad (9)$$

Finally, as mentioned before, the Stiffness ratio (SR) is calculated as:

$$\boldsymbol{SR = \frac{S_i}{S_{50}}} \quad (10)$$

Where:
SR : Beam Stiffness ratio (Pa/Pa)
S_i : Beam Stiffness at cycle i (Pa)
S_{50} : Initial beam stiffness at cycle 50 (Pa)

The failure point was determined at the SR of 50% as per ASTM D7460 [43] and initially recommended by Tsai, Harvey and Monismith [45]. The failure point in this criterion is estimated by solving Equation (11 for the value of N where the SR is equal to 0.5, i.e. 50% of reduction in initial beam stiffness.

$$\boldsymbol{Ln(-Ln(SR)) = \gamma * Ln(N) + Ln(\lambda)} \quad \textbf{(11)}$$

Where:
$Ln(-Ln(SR))$: The natural logarithm of the negative of the natural logarithm of SR
SR : Flexural beam stiffness ratio, beam stiffness at cycle i / initial beam stiffness
N : Number of cycles
γ : The slope of the linear regression of the $Ln(-Ln(SR))$ versus $Ln(N)$
$Ln(\lambda)$: The intercept of the linear regression of the $Ln(-Ln(SR))$ versus $Ln(N)$

Figure 33 shows an example of the Linear Regression of the natural logarithm of the negative of the natural logarithm of SR "$Ln(-Ln(SR))$" versus the natural logarithm of the number of cycles "$Ln(N)$" for a CIR non-graded sample mixed and compacted with emulsion type D and 6% of Lime Slurry, tested at 70°F and 400 με. In this case, the number of cycles where the SR is equal to 0.5, corresponds to 31,411. Detailed calculations are provided as follows:

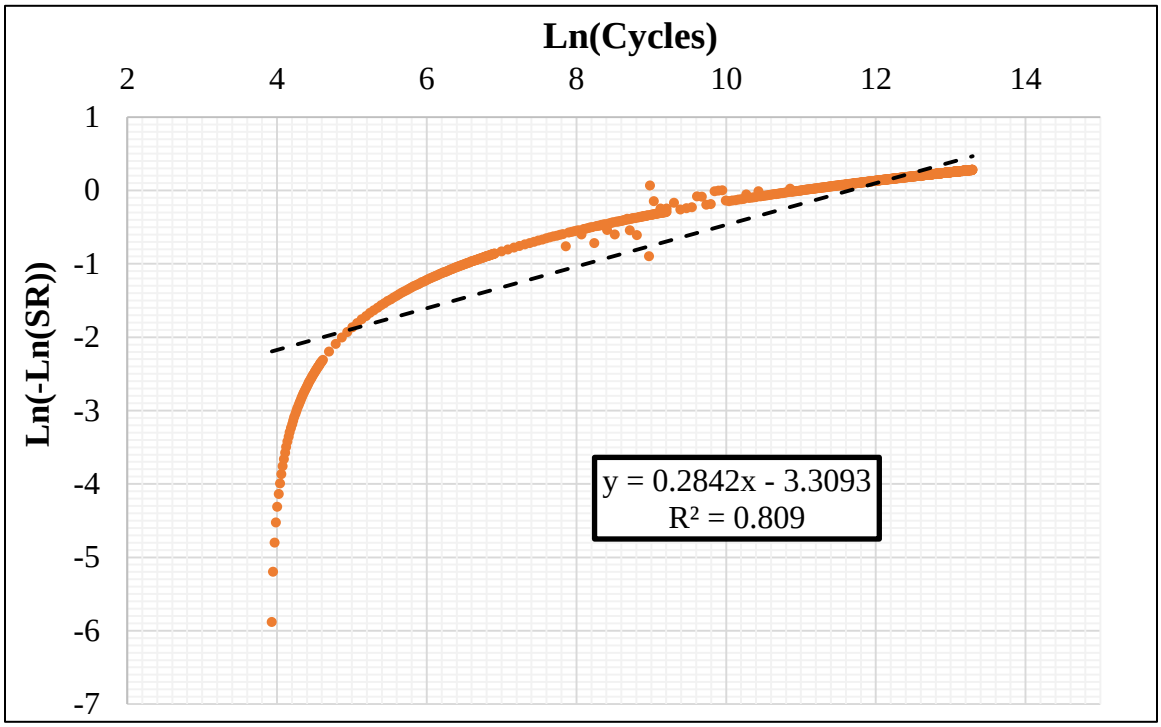

Figure 33. Example of linear regression.

$$Ln(-Ln(SR)) = \gamma * Ln(N) + Ln(\lambda)$$

$$Ln\big(-Ln(0.5)\big) = 0.2842 * Ln(N) - 3.3093$$

$$-0.367 = 0.2842 * Ln(N) - 3.3093$$

$$N = e^{\frac{-0.367+3.3093}{0.2842}}$$

$$N = 31{,}411\ cycles$$

Figure 34 to Figure 37 present the fatigue relationships for the CIR mixtures with non-graded RAP and 6.0% of lime slurry, designed with the Hveem method. Further details of test results can be found in Appendix 9.3.

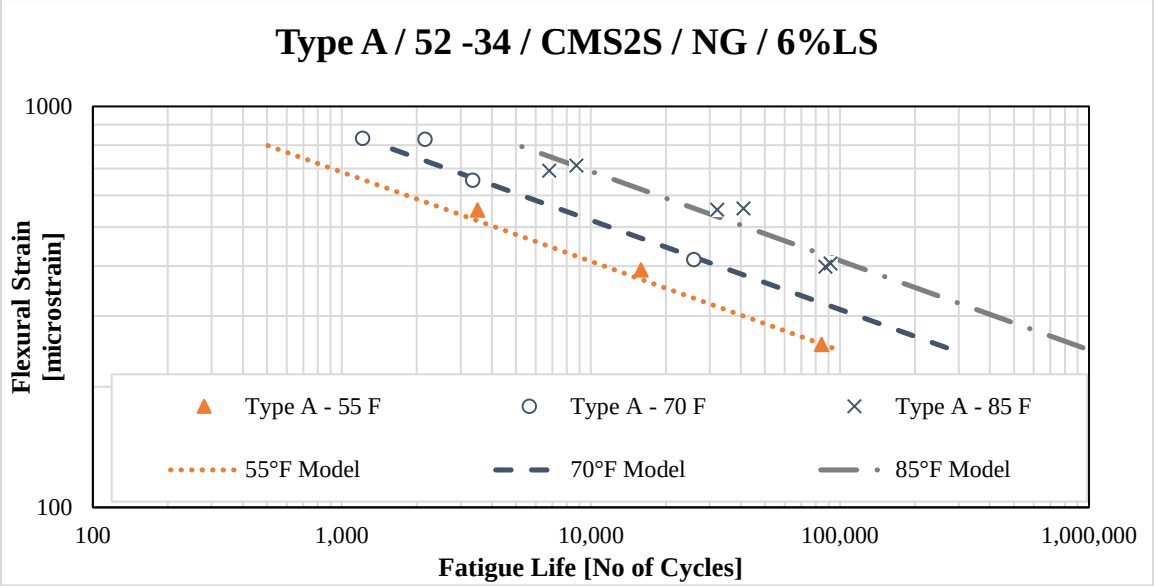

Figure 34. Fatigue relationships of CIR mixture type A.

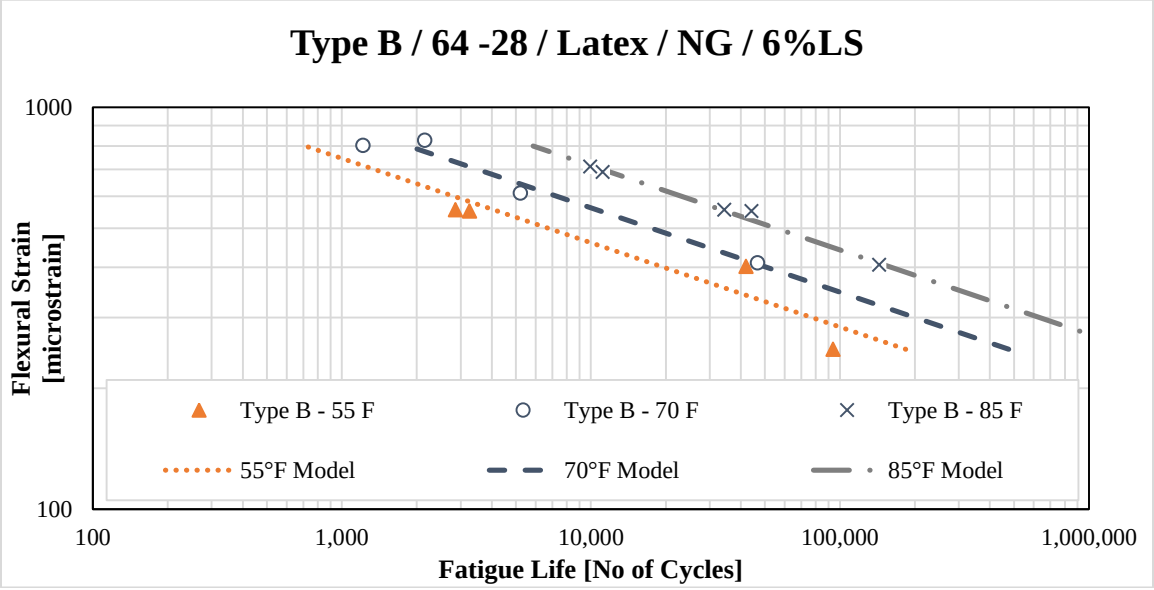

Figure 35. Fatigue relationships of CIR mixture type B.

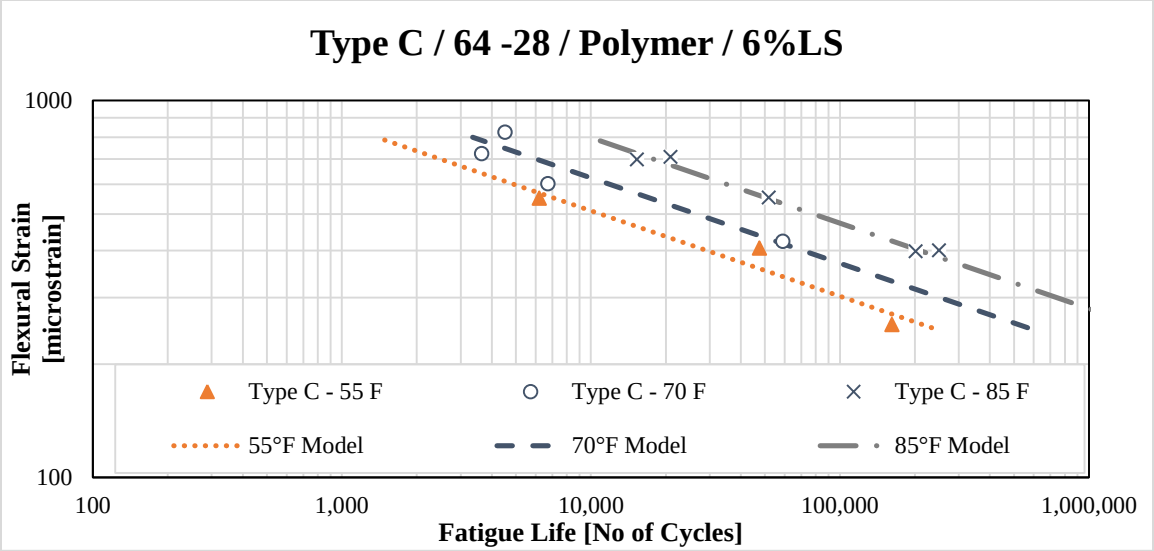

Figure 36. Fatigue relationships of CIR mixture type C.

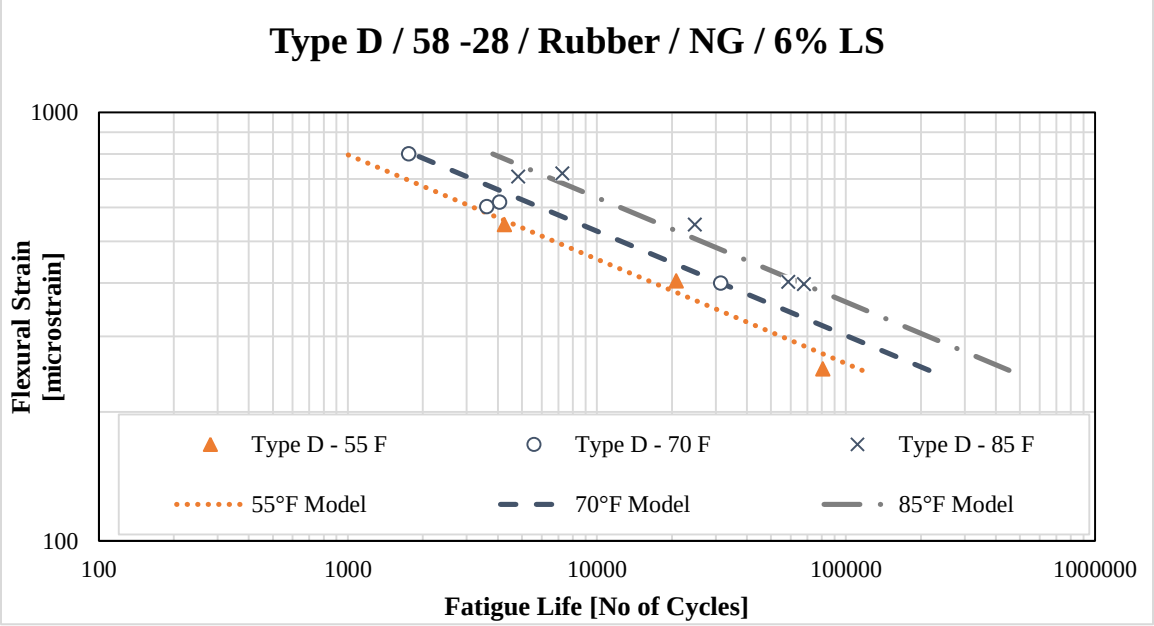

Figure 37. Fatigue relationships of CIR mixture type D.

Figure 38 to **Figure 41** present the fatigue relationships for the CIR mixtures with non-graded RAP and 4.5% of lime slurry, designed with the Hveem method. Details of the test results can be found in Appendix 9.3

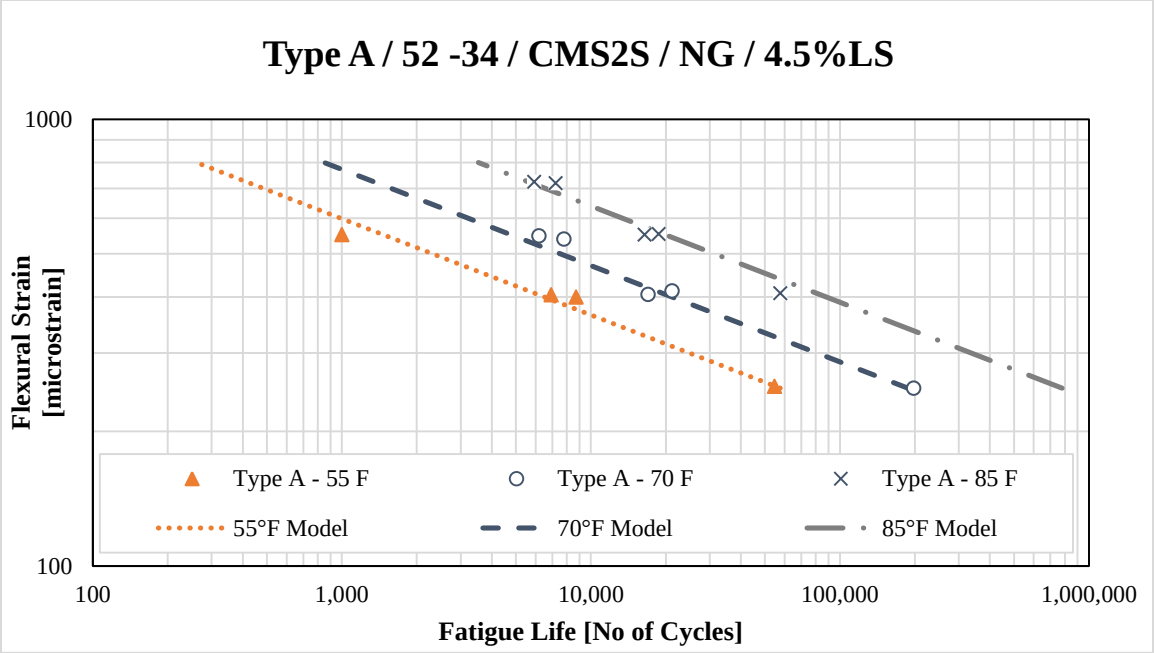

Figure 38. Fatigue relationships of CIR mixture type A.

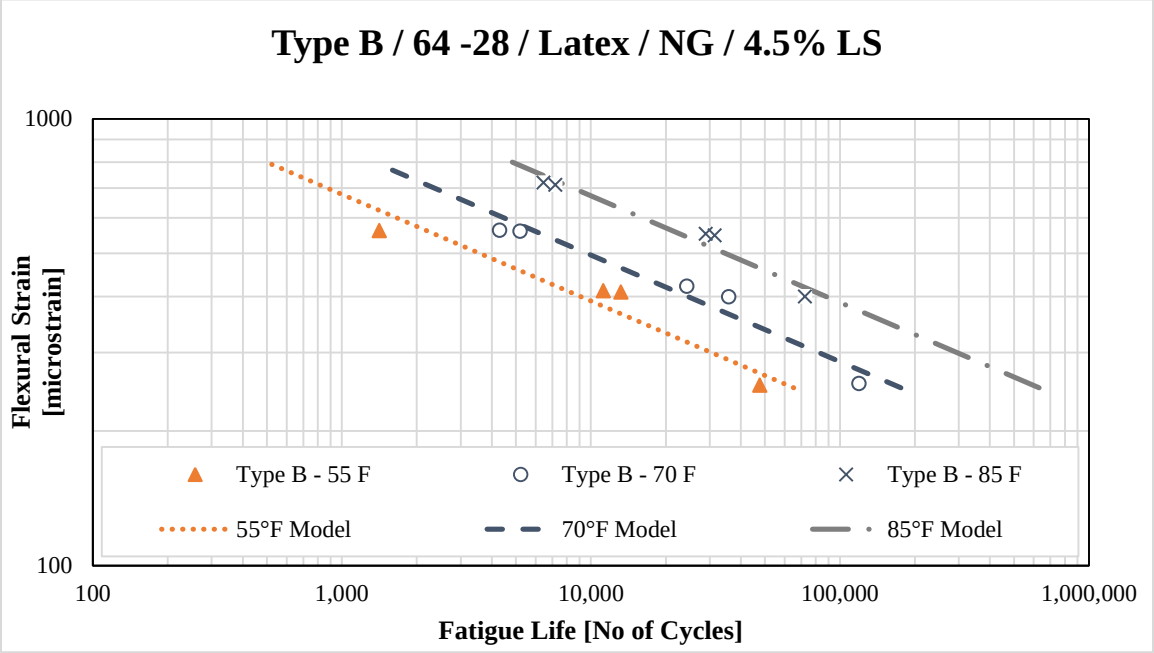

Figure 39. Fatigue relationships of CIR mixture type B.

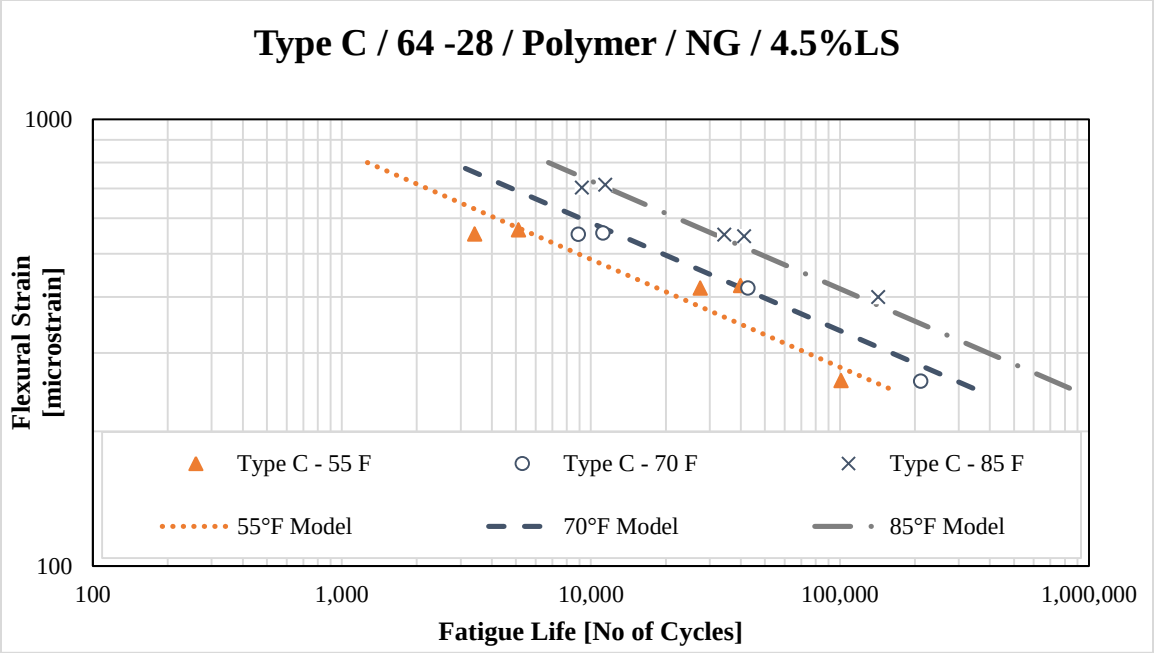

Figure 40. Fatigue relationships of CIR mixture type C.

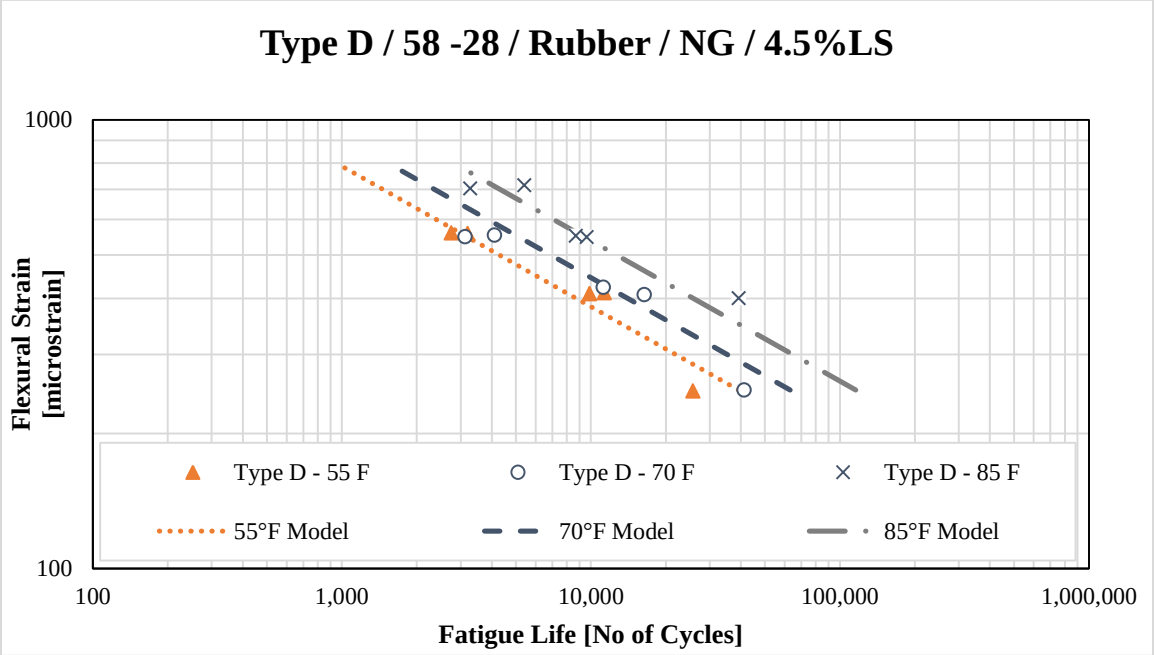

Figure 41. Fatigue relationships of CIR mixture type D.

5.2.6. Analysis of results

The number of cycles to failure at the different levels of microstrain and temperatures were used to develop the fatigue cracking models for the evaluated CIR mixture as presented in Equation (**6**.

$$\mathbf{N_f = k_1 \left(\frac{1}{\varepsilon_t}\right)^{k_2} \left(\frac{1}{E}\right)^{k_3}} \quad (6)$$

A multilinear regression analysis was conducted with Microsoft® Excel assuming $\log(N_f)$ as the dependent variable while $\log(1/\varepsilon_t)$ and $\log(1/E)$ were assumed as the independent variables.

Table 11 summarizes the fatigue models for the 4 CIR mixtures with non-graded RAP and 6.0%LS and Table 12 summarizes the fatigue models for the 4 CIR mixtures with non-graded RAP and 4.5% LS.

Table 11. Fatigue Performance Models for CIR mixtures with Non-Graded RAP and 6.0% Lime slurry.

Asphalt Emulsion	**Fatigue Model**
A: Standard CMS-2S	$\mathrm{N_f} = 4.40 * 10^{10} \left(\frac{1}{\varepsilon_t}\right)^{4.494} \left(\frac{1}{E}\right)^{3.749}$
B: Latex-Modified	$\mathrm{N_f} = 7.42 * 10^{10} \left(\frac{1}{\varepsilon_t}\right)^{4.771} \left(\frac{1}{E}\right)^{3.845}$
C: Polymer-Modified	$\mathrm{N_f} = 1.80 * 10^{13} \left(\frac{1}{\varepsilon_t}\right)^{4.409} \left(\frac{1}{E}\right)^{4.006}$
D: Rubber-Modified	$\mathrm{N_f} = 1.16 * 10^{5} \left(\frac{1}{\varepsilon_t}\right)^{4.104} \left(\frac{1}{E}\right)^{2.516}$

Table 12. Fatigue Performance Models for CIR mixtures with Non-Graded RAP and 4.5% Lime slurry.

Asphalt Emulsion	Fatigue Model
A: Standard CMS-2S	$N_f = 9.90 * 10^{13} \left(\frac{1}{\varepsilon_t}\right)^{4.639} \left(\frac{1}{E}\right)^{4.377}$
B: Latex-Modified	$N_f = 6.39 * 10^{16} \left(\frac{1}{\varepsilon_t}\right)^{4.188} \left(\frac{1}{E}\right)^{4.591}$
C: Polymer-Modified	$N_f = 1.19 * 10^{11} \left(\frac{1}{\varepsilon_t}\right)^{4.140} \left(\frac{1}{E}\right)^{3.483}$
D: Rubber-Modified	$N_f = 1.42 * 10^{5} \left(\frac{1}{\varepsilon_t}\right)^{3.198} \left(\frac{1}{E}\right)^{2.049}$

Figure 42 compares the fatigue models of the CIR mixtures with 6.0% LS at the fatigue critical temperature of 70°F. The following observations can be drawn from the data presented below:

- Considering that the higher and the flatter the fatigue curve, the better resistance to fatigue cracking, it can be concluded that the CIR mixture with asphalt emulsion Type C (64-28 Polymer modified) exhibits the best fatigue resistance followed by Type B (64-28 Latex modified). CIR mixtures with emulsions Type A (52-34) and D (58-28 Rubber modified) exhibit similar fatigue behavior. These findings are consistent with the observations based on the dynamic modulus properties [9].
- Several studies have demonstrated the positive influence of polymers in extending fatigue life of asphalt mixtures [46] [47] [48]. The obtained results confirm the benefit of modifiers represented by better fatigue behavior of the mixtures with polymer and latex-modified emulsions in comparison with the mixtures with unmodified asphalt emulsion.

- The percent of residue of the emulsified asphalt had a significant impact on the fatigue behavior of the evaluated CIR mixtures. The higher the percent residue, the better resistance to fatigue cracking.

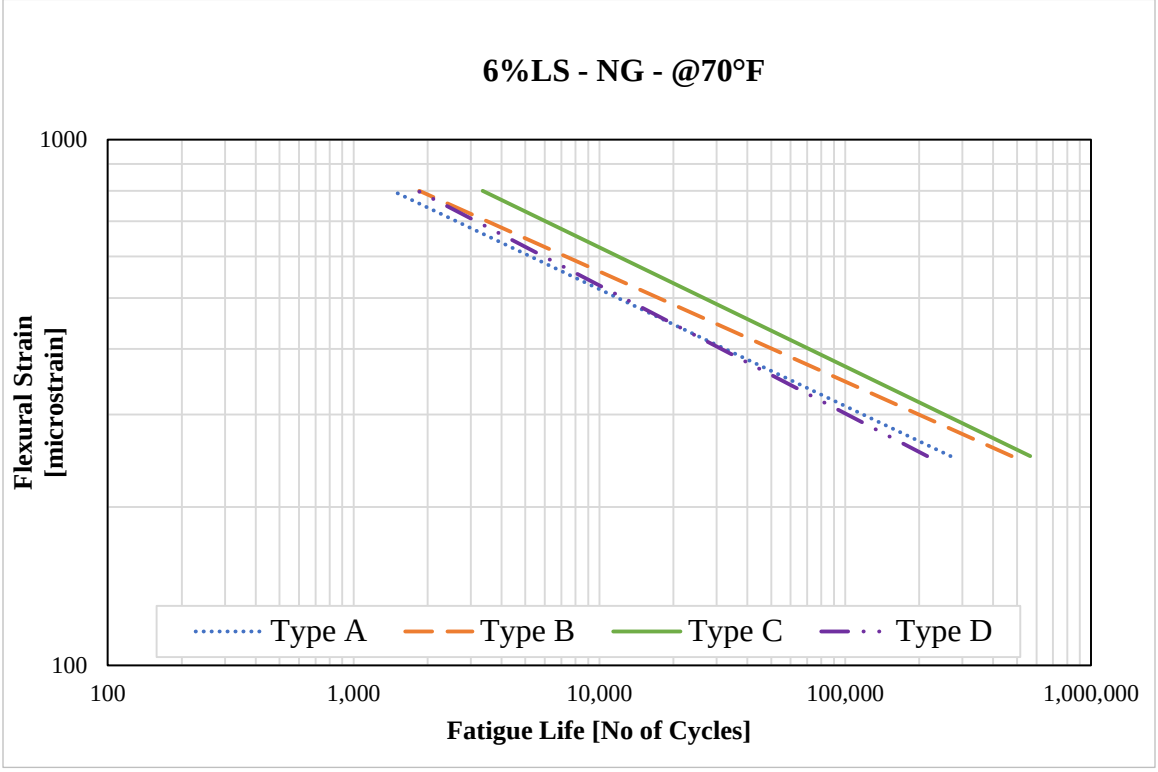

Figure 42. Fatigue relationships of CIR mixtures (6%LS / NG) at 70°F.

Likewise, a comparison of the fatigue models at 70°F for CIR mixtures with 4.5% of lime slurry is provided in Figure 43. As expected, and consistent with the results observed in the mixtures with 6% LS, mixtures with Emulsion Type B and C (64-28 Latex and 64-28 Polymer) exhibit longer fatigue life when compared to the Type A (52-34) and Type D (58-28) mixtures. A steeper slope was obtained by the mixture with emulsion type D, indicating more affectation when decreasing the level of lime slurry.

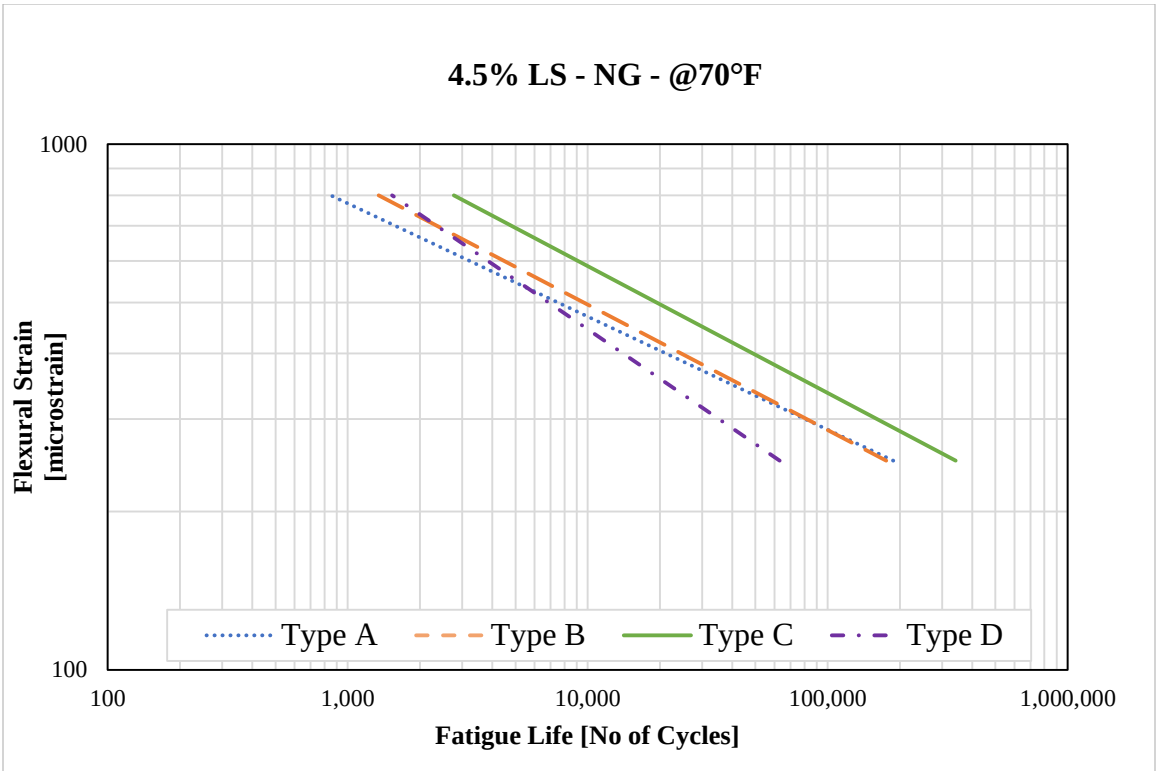

Figure 43. Fatigue relationships of CIR mixtures (4.5%LS / NG) at 70°F.

Given that the fatigue relationships presented similar trends for both 6.0 and 4.5 %LS, average models with 95% confidence intervals were proposed and are presented in Chapter 6.

It is noteworthy to mention that, a significant difference in the laboratory fatigue resistance does not necessarily mean that the same difference in the fatigue life will be observed in the field. Several factors affect the fatigue life of CIR pavements such as the age, stiffness, loading history, developed tensile strain under field loading and the interaction of these factors.

Fatigue Behavior of CIR Mixtures

Figure 44 presents the three different stages in a typical fatigue test of HMA mixture. The stiffness reduction process involves three phases. The first phase is called "internal heating" because dissipated energy is generated due to the materials viscous properties. According to Di Benedetto et al [49], this increase in temperature has a significant effect on the stiffness reduction and can be identified as the initial portion of the fatigue curve where the slope is very steep. As the cycling loading continues, two major stages can be identified. The second stage, or "formation of micro-cracks" where the stiffness is reduced by approximately 25-30% and the third stage or "crack formation" which reduces the stiffness by 35-40%. The failure of the specimen is expected once these two stages are realized.

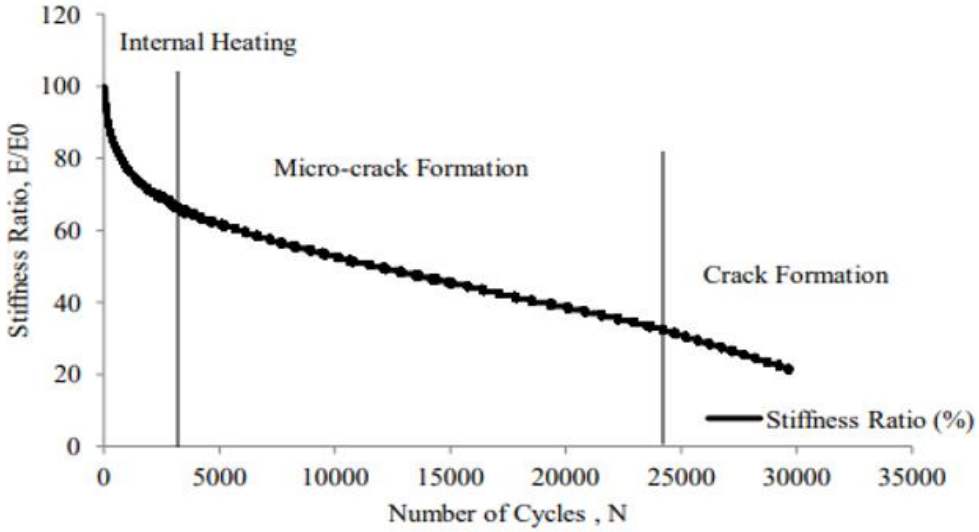

Figure 44. Three different stages in a typical fatigue test of HMA [50].

Figure 45 presents the typical flexural beam stiffness trend of CIR mixtures. In contrast with the HMA fatigue trends, the CIR mixtures exhibited greater reduction of stiffness ratio during the first stage “internal heating”. This is expected since CIR mixtures are very stiff due to the oxidation of the RAP material and the binder has lost most of its viscous properties. The elevated stiffness levels were positive when analyzing the rutting behavior of CIR mixtures [9], however, the fatigue evaluation identified the potential issue with brittleness of the CIR mixtures.

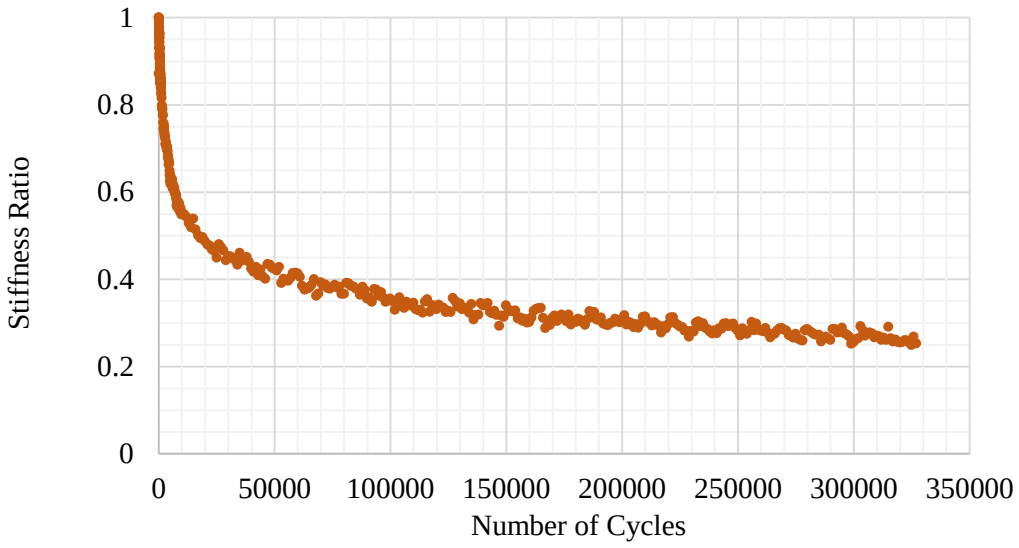

Figure 45. Typical flexural beam stiffness trend of CIR mixtures.

Chapter 6. Mechanistic Analysis of CIR Pavements

6.1. Introduction

The objective of this chapter is to incorporate the measured engineering properties fatigue and rutting characteristics of the evaluated CIR mixtures into mechanistic modelling of flexible pavement responses to traffic loading. A schematic overview of the general approach implemented in the mechanistic analysis is shown in Figure 46.

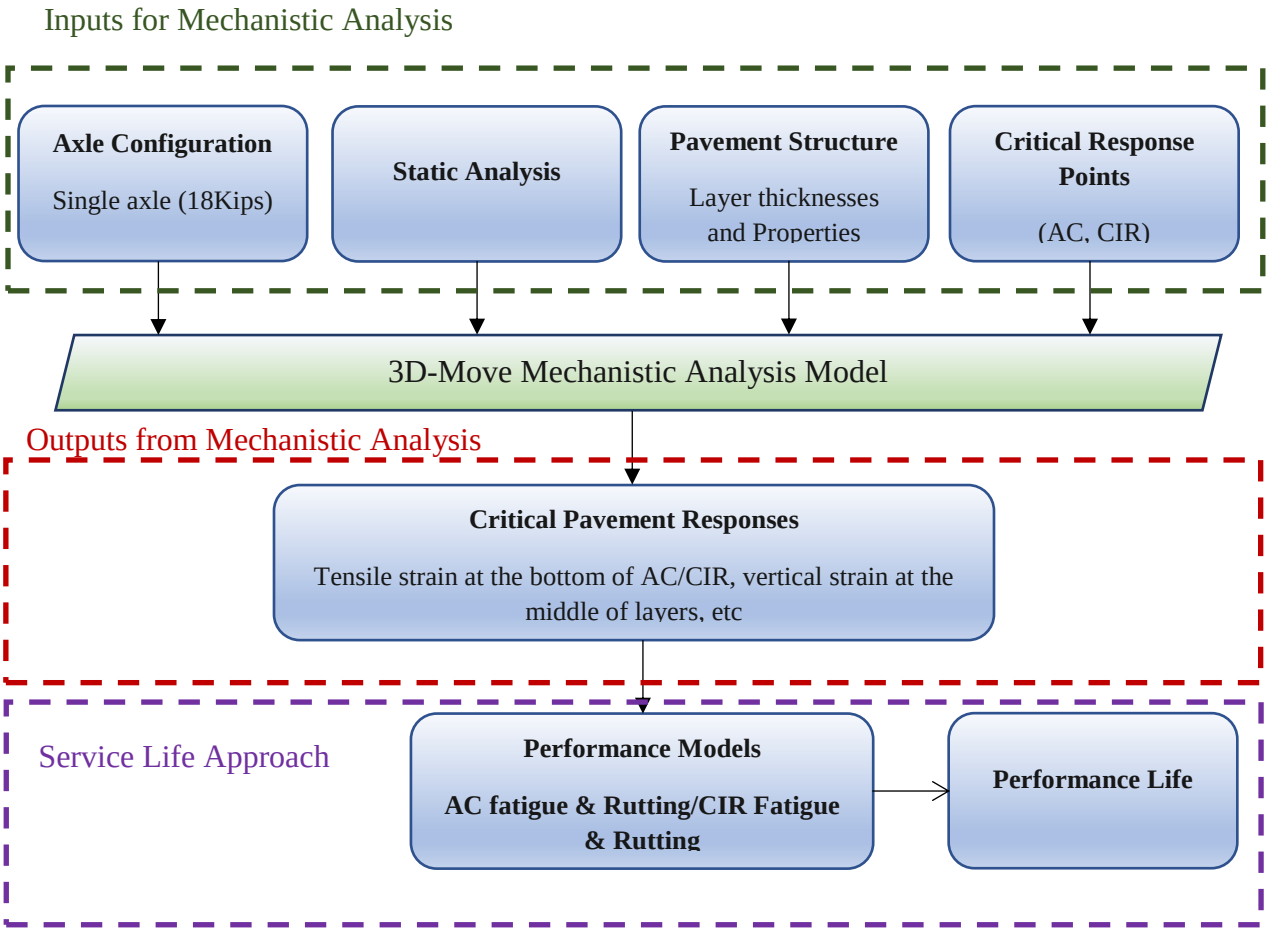

Figure 46. Flow chart of mechanistic analysis approach.

6.2. Experimental Plan

6.2.1. Pavement Structures

In order to conduct a mechanistic analysis based on fatigue and rutting characteristics of CIR mixtures, the following pavement structures were selected for the study:

- Old flexible pavement subjected to rehabilitation with CIR by milling the top 3.0 inches of the old AC layer followed by a 2.0 inches of new AC overlay (Figure 47).
- Old flexible pavement subjected to milling of the top 3.0 inches of the old AC layer followed by a new 2.0 inches AC overlay over a new AC layer at a thickness to be determined based on equal performance (Figure 48).

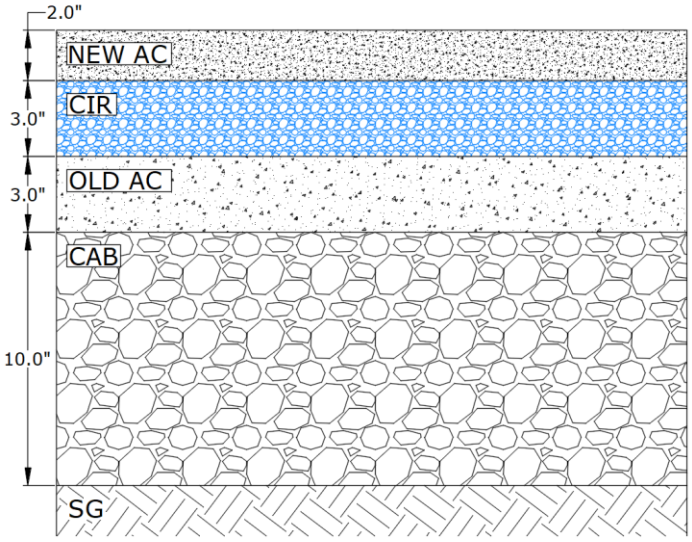

Figure 47. Flexible pavement rehabilitated using CIR [9].

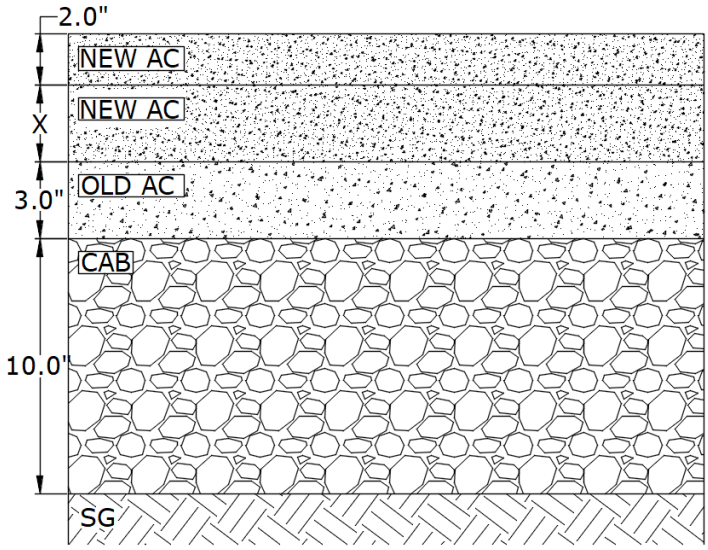

Figure 48. Flexible pavement rehabilitated using new AC overlay [9].

The control section was the flexible pavement with the CIR layer under the 2.0 inch AC overlay. The thickness of the new AC layer for the pavement structure without the CIR layer was determined based on achieving equal fatigue/rutting performance of the two pavements.

6.2.2. Selection of E* Average Model

As the AC and CIR materials are viscoelastic, the E* depends on the temperature and the loading frequency. The following sections describe the approach used to determine the representative E* for each layer.

a. Load Magnitude

A static single axle load of 18 kips on dual tires with inflation pressure of 120 psi was selected as the load for the analysis. For the purpose of identifying the appropriate loading frequency for E*, a speed of 1 mph was assumed.

b. Loading Frequency

The calculation of applicable load frequency was performed following the approach recommended in the MEPDG Section 3.3.3.4 [51] with additional assumptions. A stress distribution of 45° was assumed for the subgrade layer. the various AC and CIR layers were converted into equivalent thickness of the subgrade using the method of equivalent thickness (MET) in order to calculate the frequency at each effective depth using Equation (**12**) [52]. Figure 49 presents graphically how the MET will be applied

$$\mathbf{Z_{eff}} = \sum_{\mathbf{i=1}}^{\mathbf{n-1}} \left(\mathbf{h_i} \sqrt[3]{\frac{\mathbf{E_i}}{\mathbf{E_{SG}}}} \right) + \left(\mathbf{h_n} \sqrt[3]{\frac{\mathbf{E_n}}{\mathbf{E_{SG}}}} \right) \tag{12}$$

Where:

Z_{eff} : Effective depth
h_n : Thickness of the layer of interest
E_{SG} : Resilient modulus of subgrade layer
E_n : Modulus of elasticity of the layer of interest

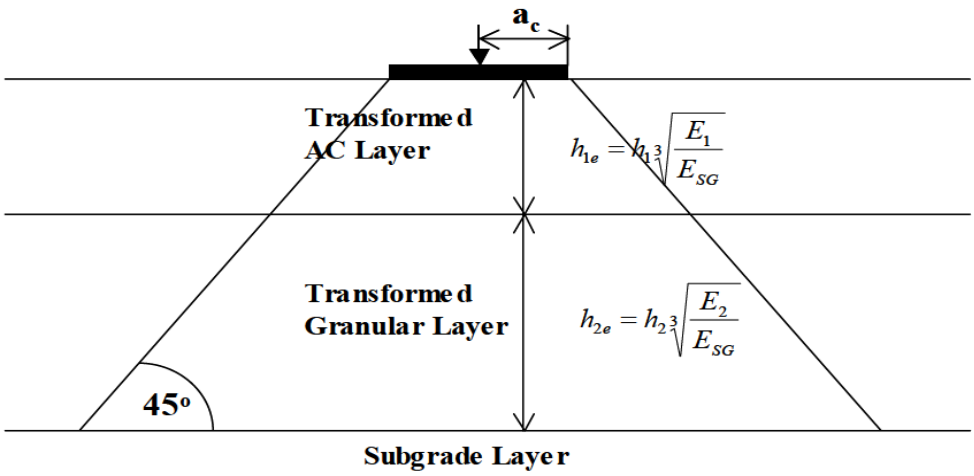

Figure 49. Method of equivalent thickness scheme. [52]

Once the effective depth is calculated, the effective length can be estimated using Equation (**13**. Using the effective length and the speed of the load, loading time can be calculated from kinematics using Equation (**14**. Finally, the frequency (in Hertz) is the inverse of the pulse time.

$$\boldsymbol{L_{eff} = 2 * a_c + 2 * Z_{eff}} \quad (13)$$

$$\boldsymbol{Pulse\ time = L_{eff}/v} \quad (14)$$

Figure 50 and Figure 51 present the structure used to calculate the loading frequency at the center of each sublayer. In the case of the pavement structure without CIR, the last sublayer (No. 6) of the AC layer will be the designed in order to achieve equal fatigue/rutting performance.

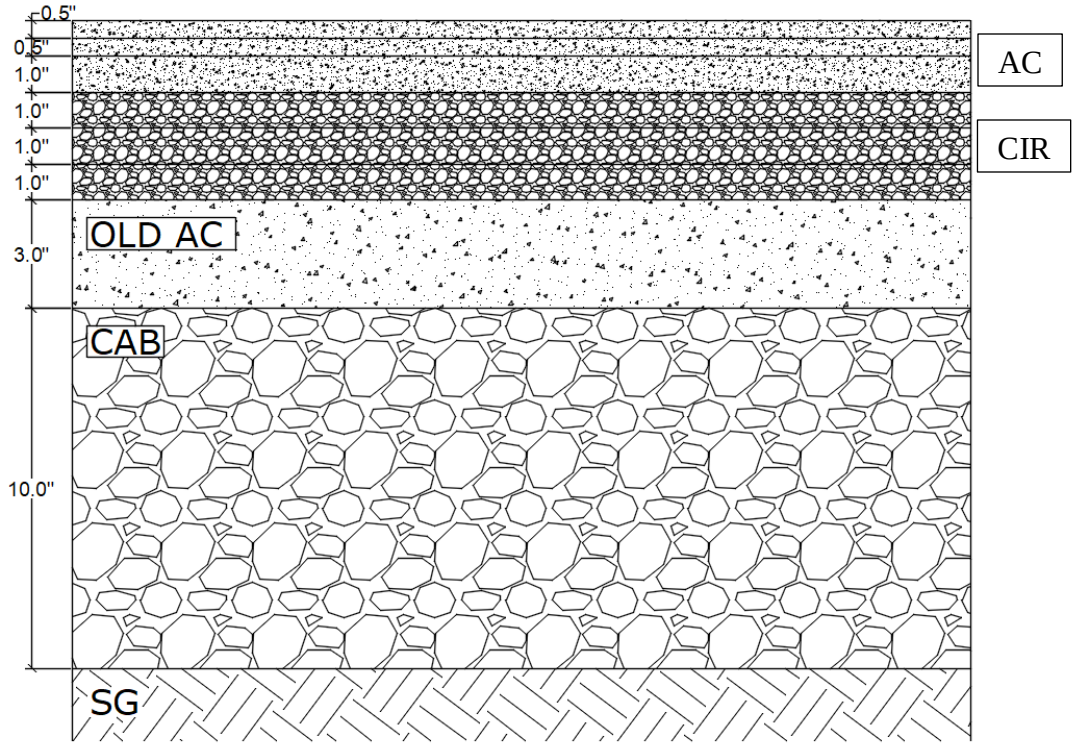

Figure 50. Sublayer distribution of the structure rehabilitated with CIR.

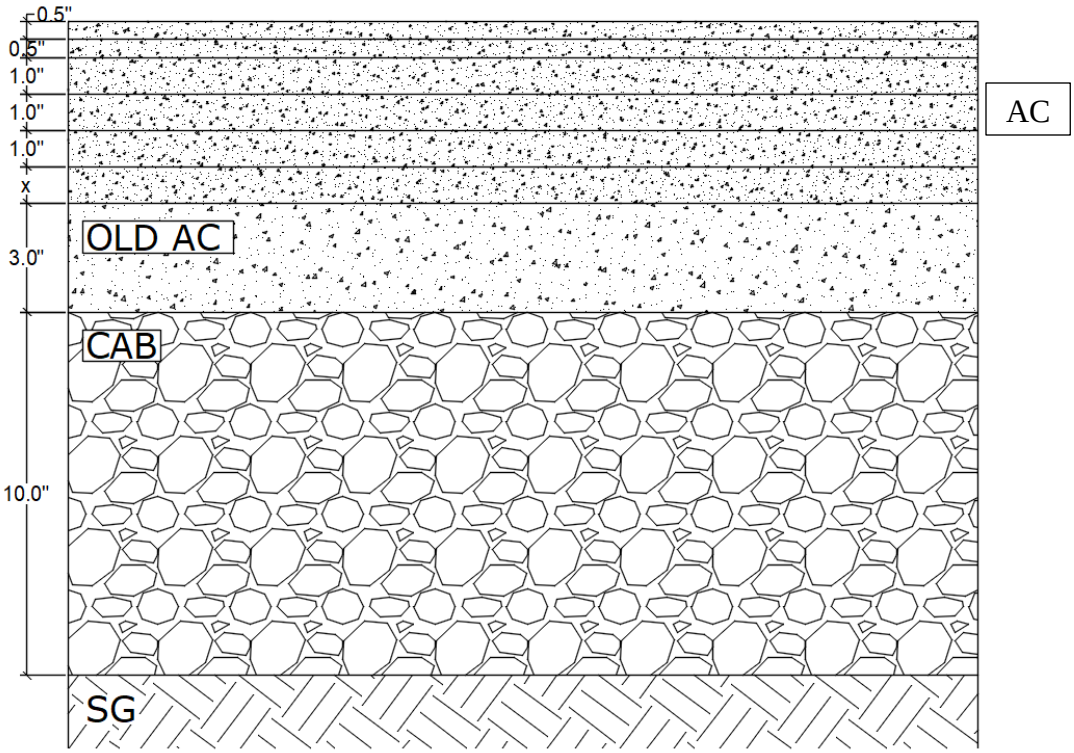

Figure 51. Sublayer distribution for structure rehabilitated with new AC.

c. Pavement Temperature

The temperature distribution throughout the AC and CIR layers must be determined in order to assign the appropriate E* property. Using the sublayers structures, the temperature at selected depth was calculated per Equation (**15** and (**16** obtained from El-Basyouny et al [56] approach for calculating the corresponding fatigue and rutting effective temperature. As this model was developed for the top two inches of the AC layer, the effective temperature was assumed constant for AC and CIR sublayers located deeper than 2.0 inch below the surface..

$$T_{eff} = -13.995 - 2.332(Freq)^{0.50} + 1.006(MAAT) + 0.876(\sigma_{MMAT}) - 1.186(Wind) + 0.549(Sunshine) + 0.071(Rain) \quad (15)$$

$$T_{eff} = 14.62 - 3.36\ln(Freq) - 10.940(z) + 1.121(MAAT) + 1.718(\sigma_{MMAT}) - 0.431(Wind) + 0.33(Sunshine) + 0.08(Rain) \quad (16)$$

Where:

$Freq$: Effective load frequency at interest point, Hz
z : Depth of interest point, in
$MAAT$: Mean annual air temperature, °F
σ_{MMAT} : Deviation of the mean monthly air temperature, °F
$Wind$: Mean annual wind speed, mph
$Sunshine$: Mean annual percentage sunshine, %
$Rain$: Annual cumulative rainfall depth, in

The following lists the references from where these data were obtained:

- MAAT obtained from MIRA climatic data. [53]
- Wind obtained from LTPP infoPave™ tool. [54]
- Sunshine obtained from LTPP infoPave™ tool. [54]
- Rain obtained from MIRA climatic data. [53]

Using the estimated temperature at various depths, the dynamic modulus of each sublayer was calculated using the master curve of the corresponding material. As the frequency calculation depends on the modulus of each sublayer and the temperature calculation depends on the loading frequency, an iterative process was performed until convergence.

The dynamic modulus of the old AC was calculated using similar procedure at corresponding frequency and temperature but including a reduction in the stiffness due to damage using Equation (**17**).

$$\boldsymbol{E^*_{dam} = 10^{\delta} + \frac{E^*_{Undam} - 10^{\delta}}{1 + e^{-0.3+5*logd_{AC}}}} \quad (17)$$

Where:
δ = minimum dynamic modulus obtained from fitting the master curve, psi
E^*_{Undam} = undamaged dynamic modulus, psi
d_{AC} = damage value

d. CIR Dynamic modulus (E*) Average Model

Figure 58 to Figure 61 present the dynamic modulus (E*) master curves for the CIR mixtures evaluated in this research. It can be seen that in both cases (6.0%LS and 4.5%LS) the master curves can be combined into a single average model where the 95% confidence interval will cover the full range of results. This indicates that, statistically, the E* master curves of the 4 CIR mixtures can be represented by the respective average model with 95% confidence.

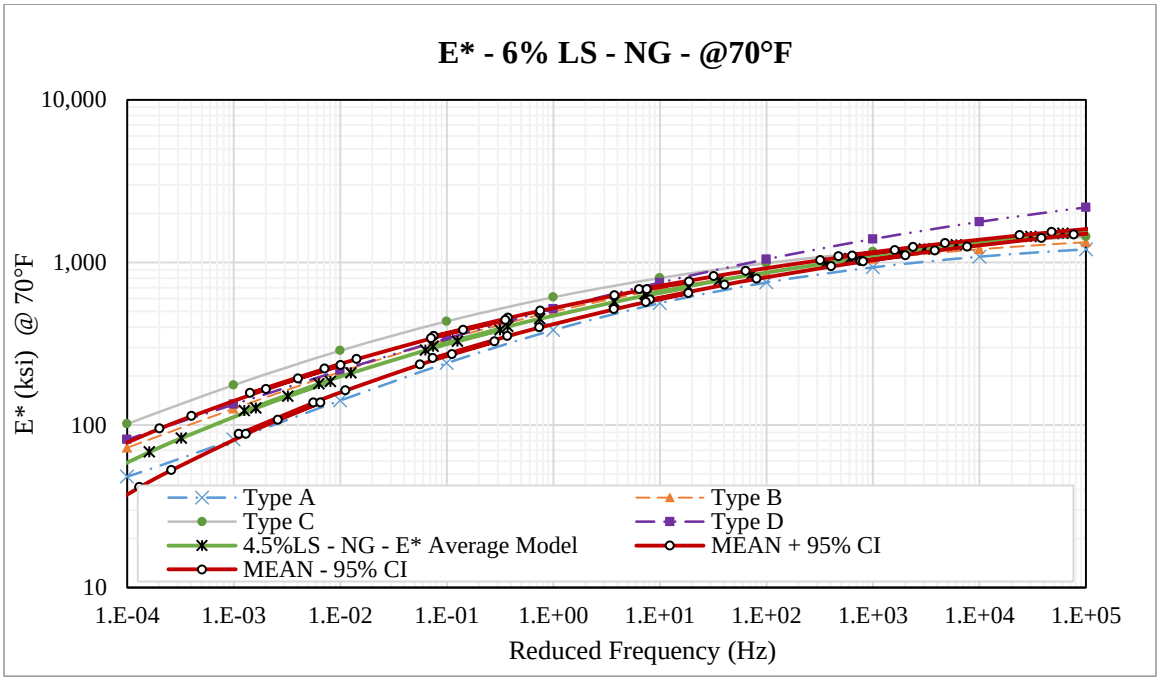

Figure 52. Dynamic modulus master curves for non-graded RAP and 6.0% LS.

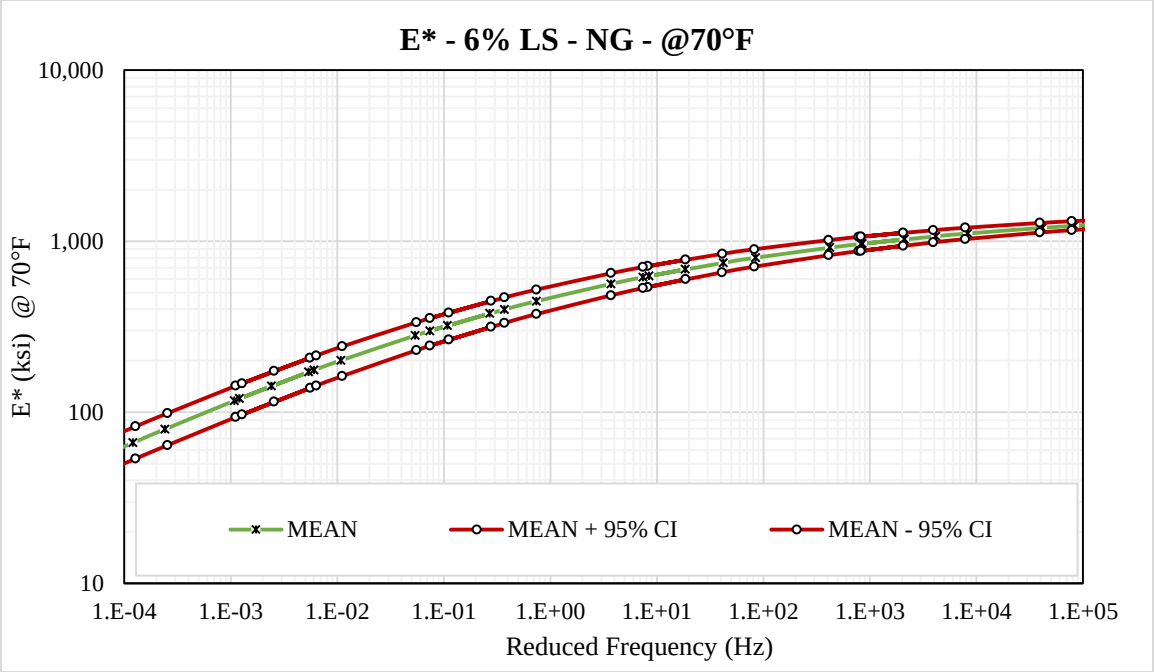

Figure 53. Average dynamic modulus master curves and 95% confidence intervals for non-graded RAP and 6.0% LS.

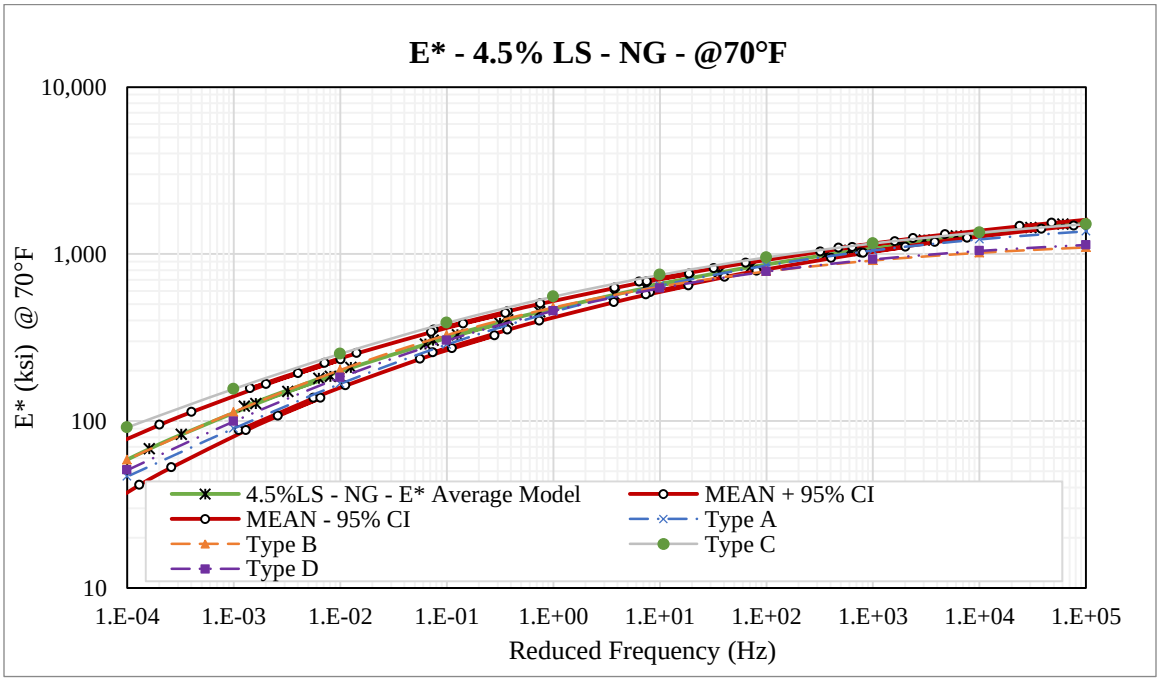

Figure 54. Dynamic modulus master curves for non-graded RAP and 4.5% LS.

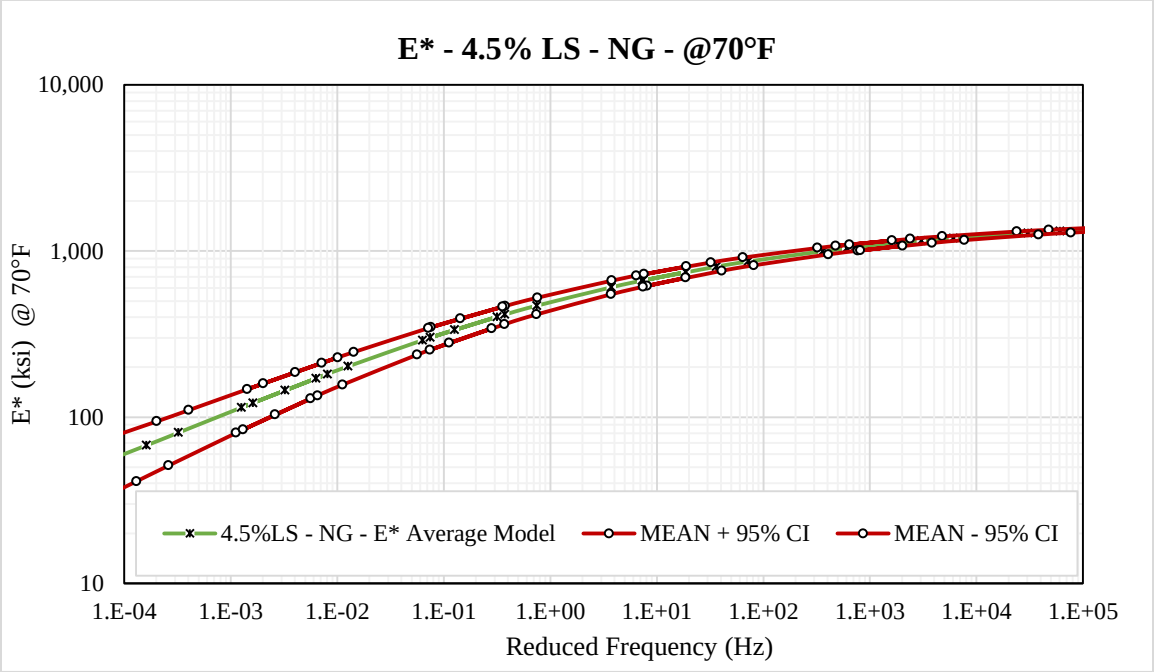

Figure 55. Average dynamic modulus master curves and 95% confidence intervals for non-graded RAP and 4.5% LS.

A comparison of the average E* master curves for non-graded RAP with 6.0% and 4.5% LS is provided in Figure 62. Likewise, these two master curves can be combined into a single average model with the 95% confidence intervals covering the full range of results.

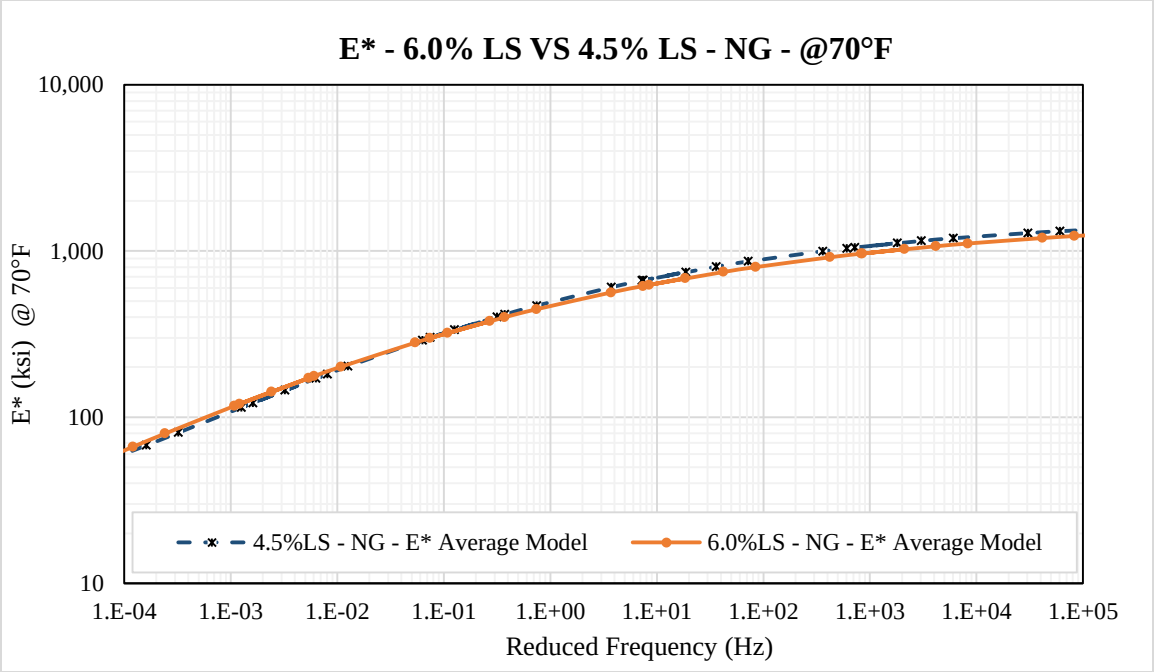

Figure 56. Comparison of average dynamic modulus master curves for non-graded RAP with 6.0%LS and 4.5% LS.

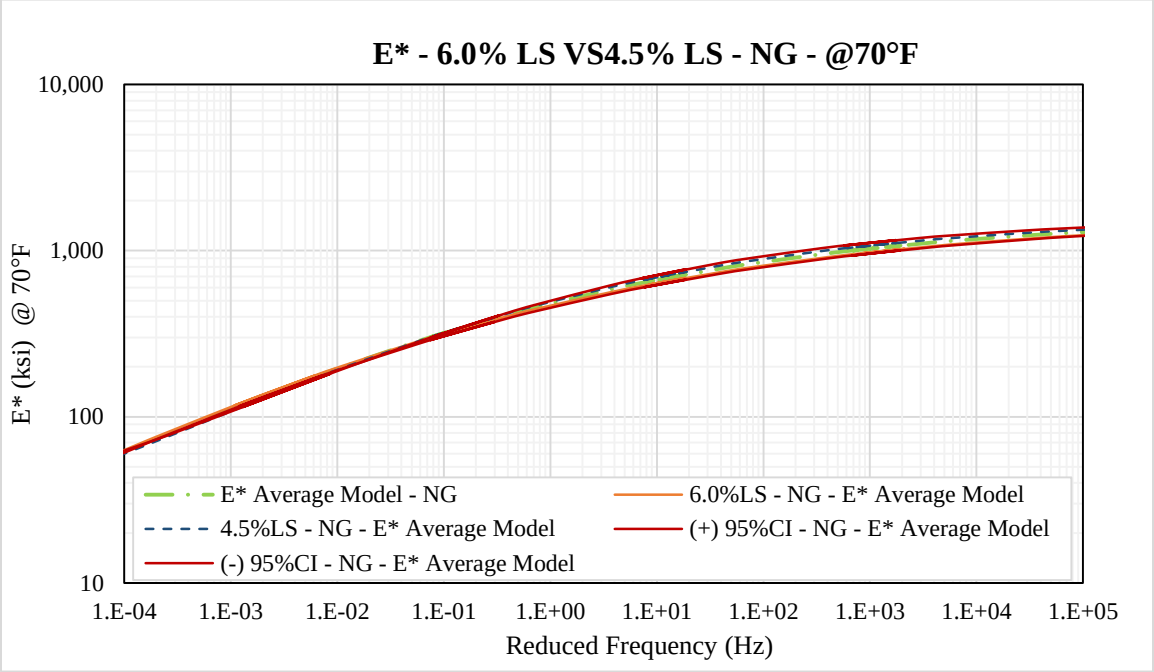

Figure 57. Average dynamic modulus master curves for non-graded RAP with 6.0%LS and 4.5% LS.

The general form of the dynamic modulus master curve equation is shown in a symmetrical sigmoidal model in Equation (**18**).

$$\boldsymbol{log(E^*) = \delta + \frac{Max - \delta}{1 + e^{\beta + \gamma \log f_r}}} \quad (18)$$

Where:
E* = dynamic modulus (psi)
Max = maximum modulus (psi)
f_r = reduced frequency (Hz)
β, δ, and γ = fitting parameters

The reduced frequency was calculated as using Equation$\boldsymbol{\log(f_r) = \log f + \log a_t}$ (**19**).

$$\boldsymbol{\log(f_r) = \log f + \log a_t} \quad (19)$$

Where:
f = actual frequency (Hz)
$\log a_t$ = (shift factor) can be calculated using Equation (**20**).

$$\boldsymbol{\log a_t = \frac{\Delta E_a}{19.14714}\left(\frac{1}{T} - \frac{1}{T_r}\right)} \quad (20)$$

Where, ΔE_a is a fitting parameter representing the activation energy, T is the test temperature in °K, and T_r is the reference temperature in °K.

Based on the findings presented in the previous section, the average dynamic modulus master curve will be defined by the parameters summarized in Table 13.

Table 13. Parameters of Average Dynamic Modulus Model for Non-Graded CIR Mixtures.

Parameter	Value
Delta (δ)	0.4532
Beta (β)	-1.446248
Gamma (γ)	-0.376021
ΔE_a	189185.02
T_r (°C)	20

6.2.3. Selection of Fatigue Average Model

Figure 58 to Figure 61 present the fatigue models for the CIR mixtures evaluated in this research. It can be seen that in both cases of 6.0%LS and 4.5%LS mixtures, the fatigue models can be combined into a single average model where the 95% confidence interval will cover the full range of results.

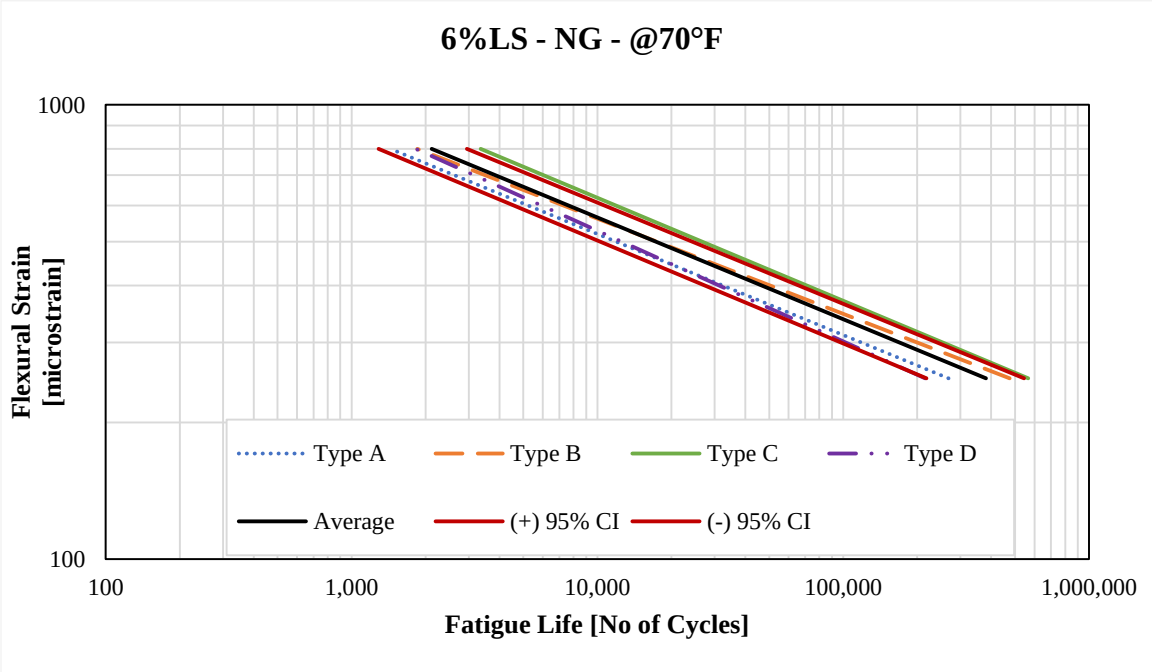

Figure 58. Average fatigue models for non-graded RAP and 6.0% LS.

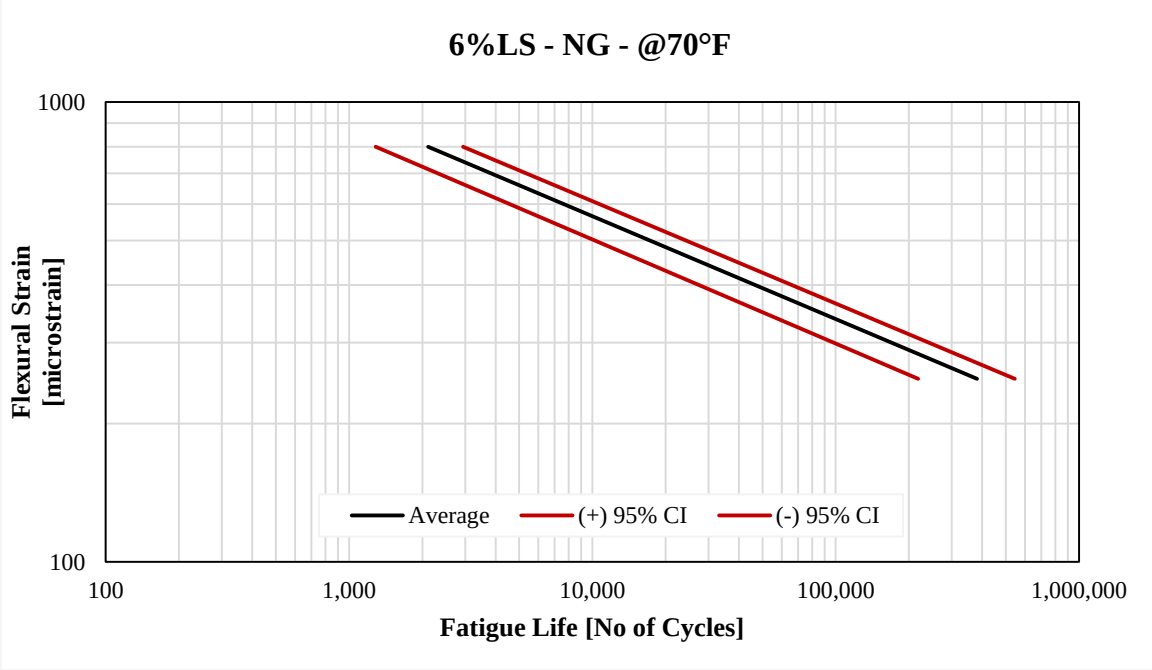

Figure 59. Average fatigue models and 95% confidence intervals for non-graded RAP and 6.0% LS.

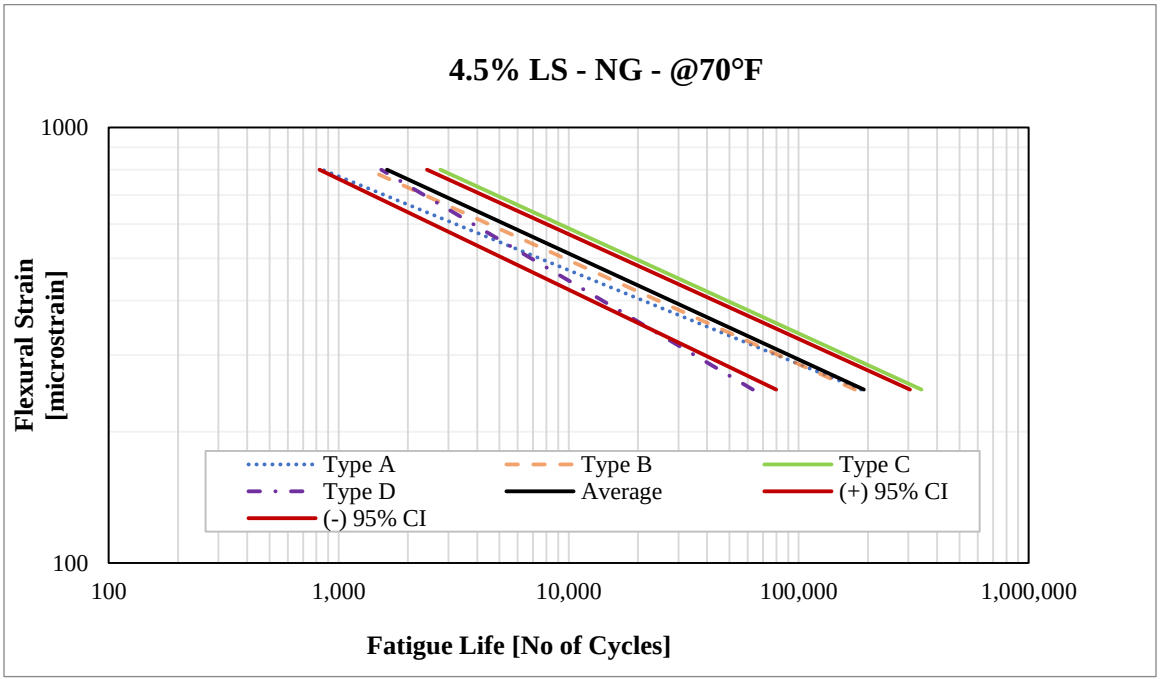

Figure 60. Average fatigue models for non-graded RAP and 4.5% LS.

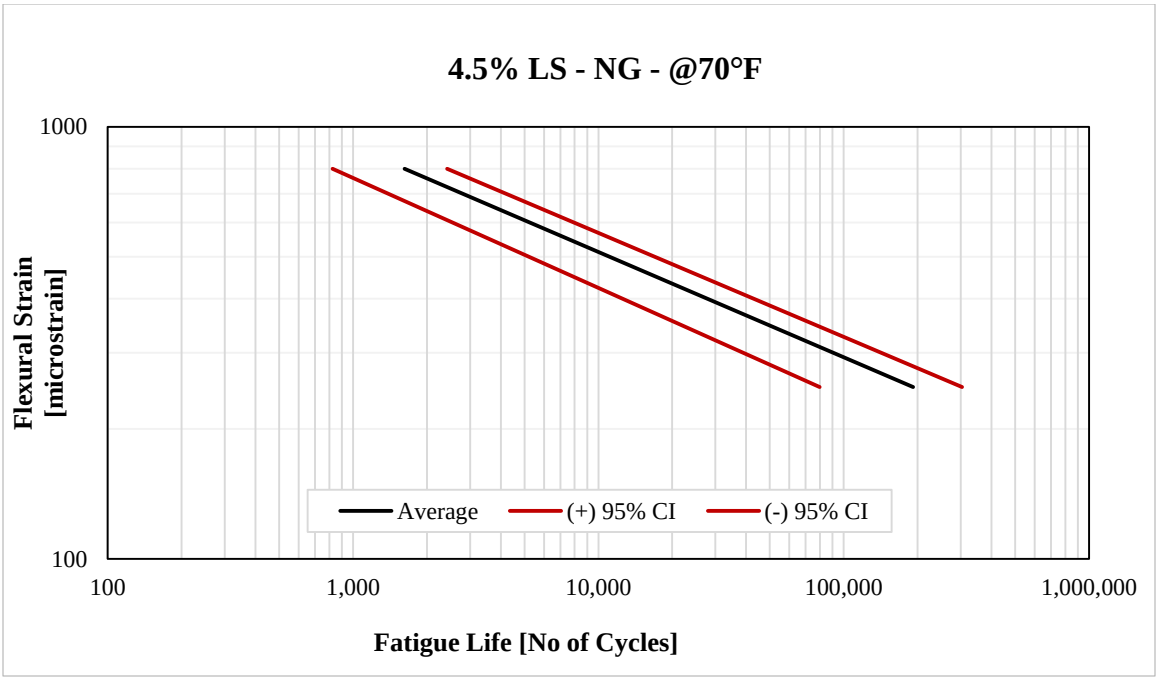

Figure 61. Average fatigue models and 95% confidence intervals for non-graded RAP and 4.5% LS.

A comparison of the average fatigue models for the CIR mixtures with non-graded RAP with 6.0% and 4.5%LS is provided in Figure 62. Likewise, these two fatigue models can be combined into one single average model with the 95% confidence intervals covering the full range of results. This indicates that, statistically, the fatigue models of the 8 non-graded CIR mixtures can be represented by a single average model with 95% confidence.

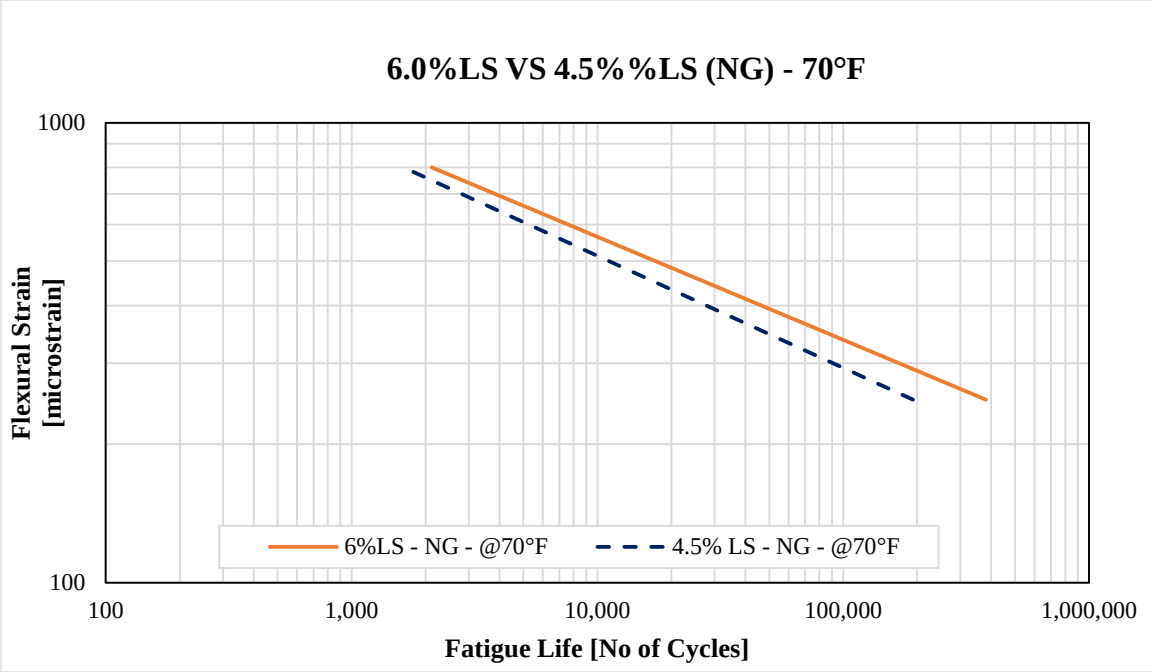

Figure 62. Comparison of average fatigue models for non-graded RAP with 6.0%LS and 4.5% LS.

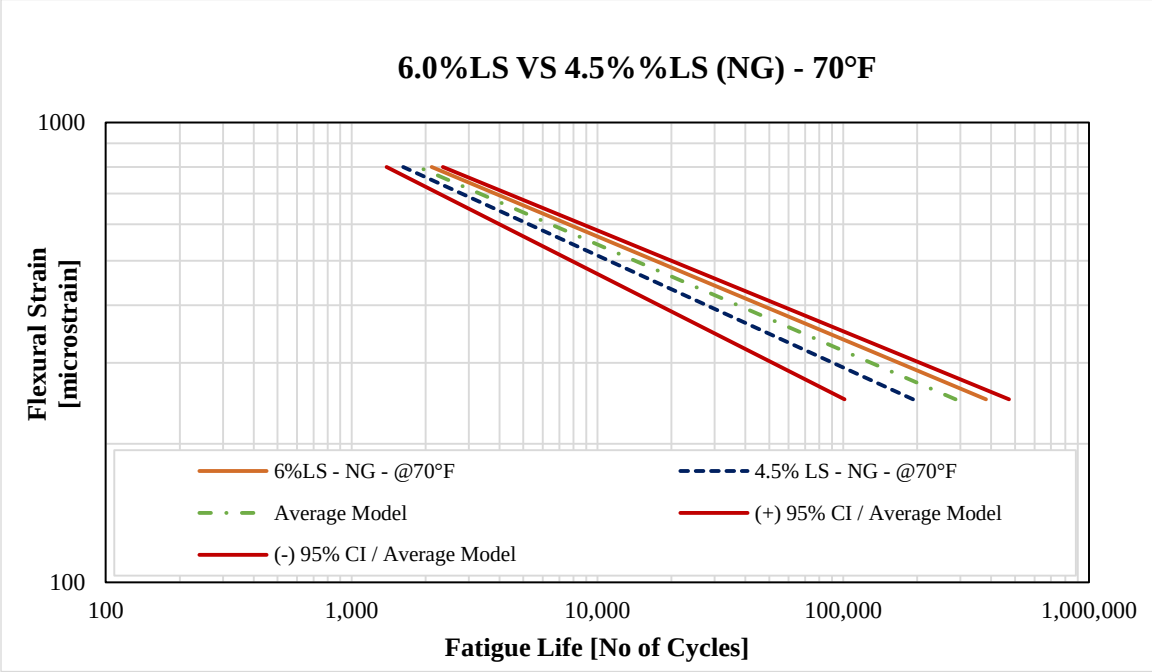

Figure 63. Average fatigue models for non-graded RAP with 6.0%LS and 4.5% LS.

Based on the findings presented in the previous section, the average fatigue model for the non-graded CIR mixtures evaluated in this research used for the mechanistical analysis is presented in Equation 21:

$$N_f = 1.19 * 10^9 * \left(\frac{1}{\varepsilon}\right)^{4.243} * \left(\frac{1}{E^*}\right)^{3.440} \quad (21)$$

6.2.4. Selection of Rutting Average Models

Ayala [11], conducted Repeated Load Triaxial test (RLT) to evaluate the rutting characteristics of CIR mixtures under repeated loading for the same CIR mixtures that were evaluated in this research. The permanent (ε_p) and resilient (ε_r) axial strains were measured during the RLT test as a function of the number of loading repetitions at three different temperatures 68°F (20°C), 97.7°F (36.5°C), and 127.4°F (53°C). It should be noted that common temperatures used for AC layers were not considered because CIR is not used as a surface course and will not be exposed to those levels of aging.

A similar analysis conducted for fatigue as presented in Section 6.2.3, was carried out for the rutting models suggested by Ayala [11]. Figure 64 to Figure 67 present the rutting models for the CIR mixtures evaluated by Ayala. It can be seen that in both cases of 6.0%LS and 4.5%LS CIR mixtures, the rutting models can be combined into a single average model where the 95% confidence interval will cover the full range of results.

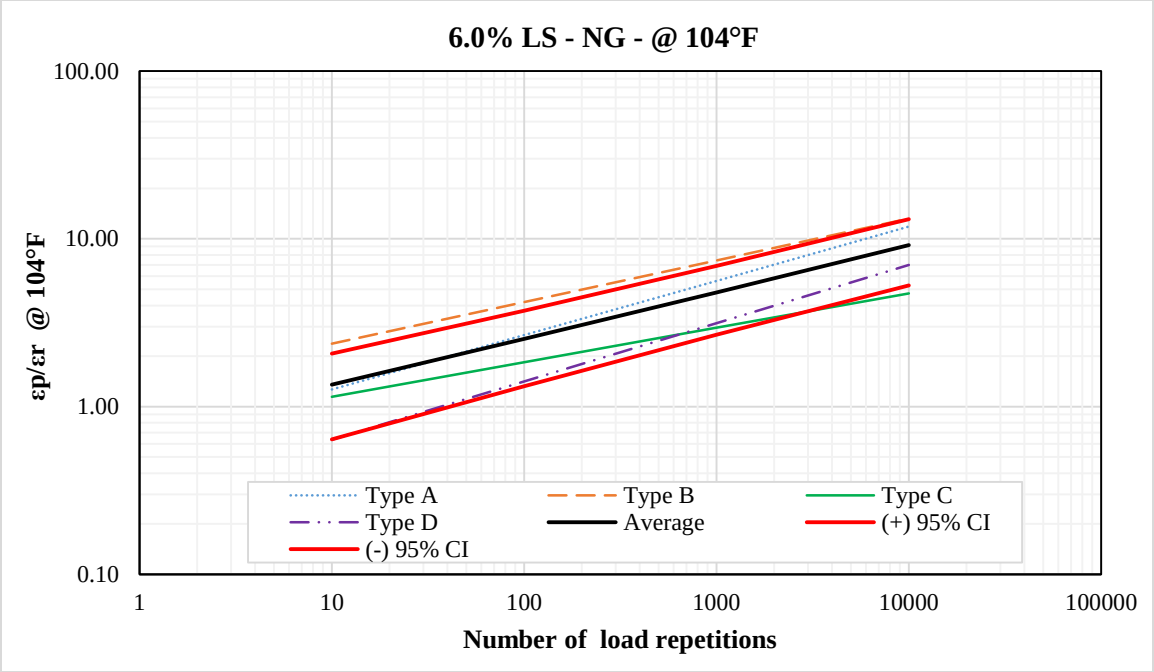

Figure 64. Average rutting models for non-graded RAP and 6.0% LS.

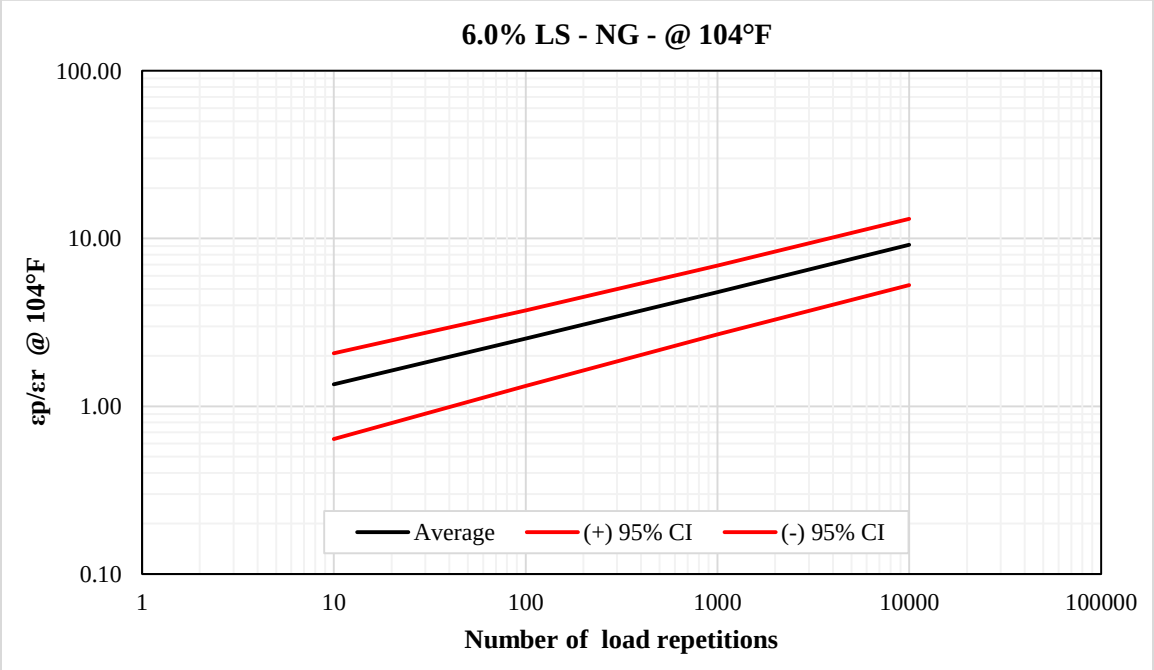

Figure 65. Average rutting models and 95% confidence intervals for non-graded RAP and 6.0% LS.

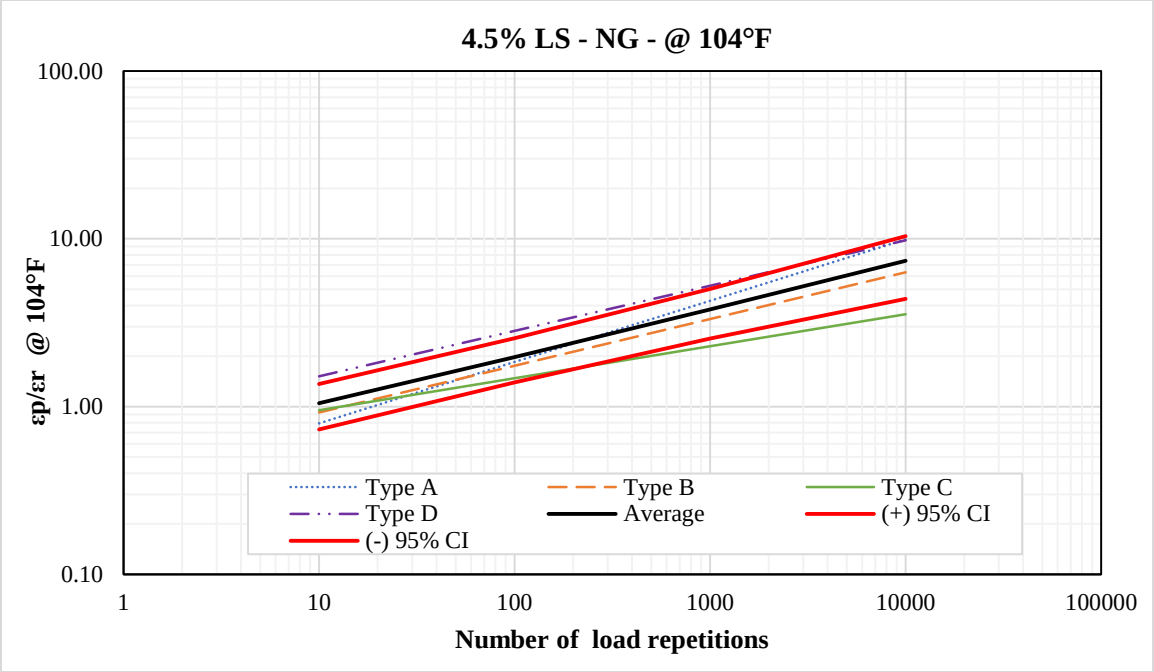

Figure 66. Average rutting models for non-graded RAP and 4.5% LS.

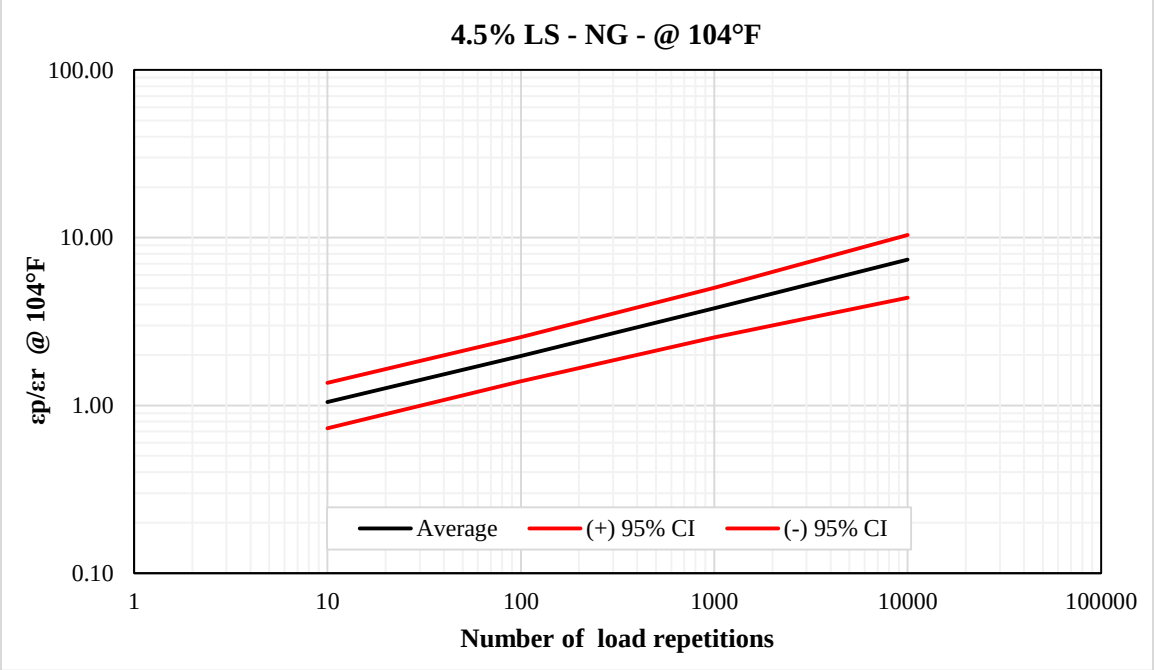

Figure 67. Average rutting models and 95% confidence intervals for non-graded RAP and 4.5% LS.

A comparison of the average rutting models for the CIR mixtures with non-graded RAP with 6.0%LS and 4.5% is provided in Figure 68. It is clear that the two rutting models can be combined into a single average model with the 95% confidence intervals covering the full range of results. This indicates that, statistically, the rutting models of the 8 non-graded CIR mixtures can be represented by a single average model with 95% confidence.

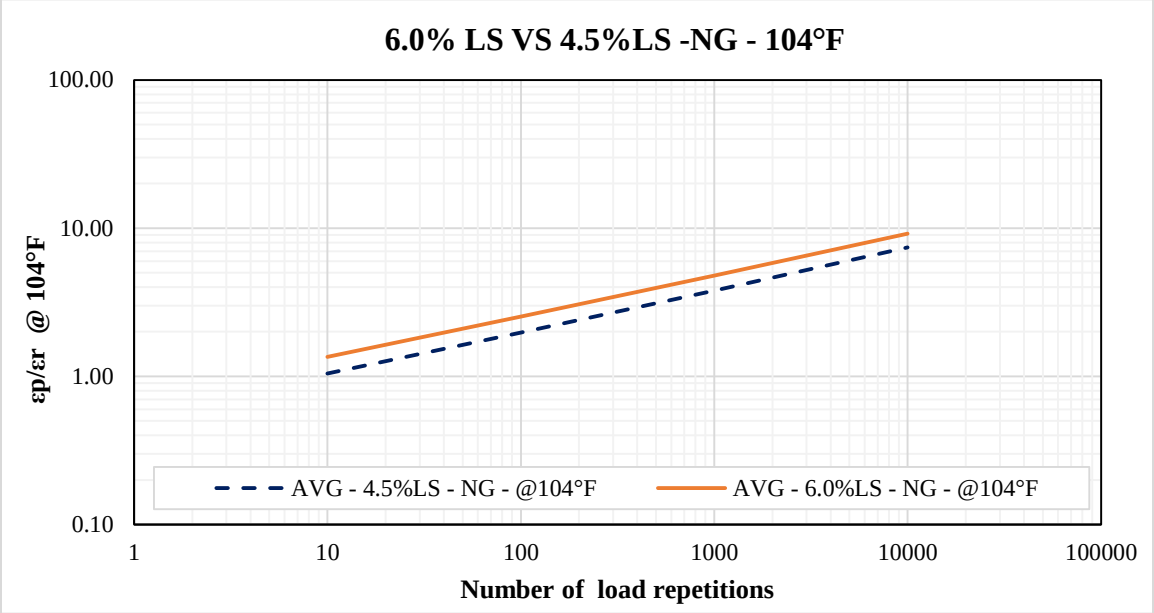

Figure 68. Comparison of average rutting models for non-graded RAP with 6.0%LS and 4.5% LS.

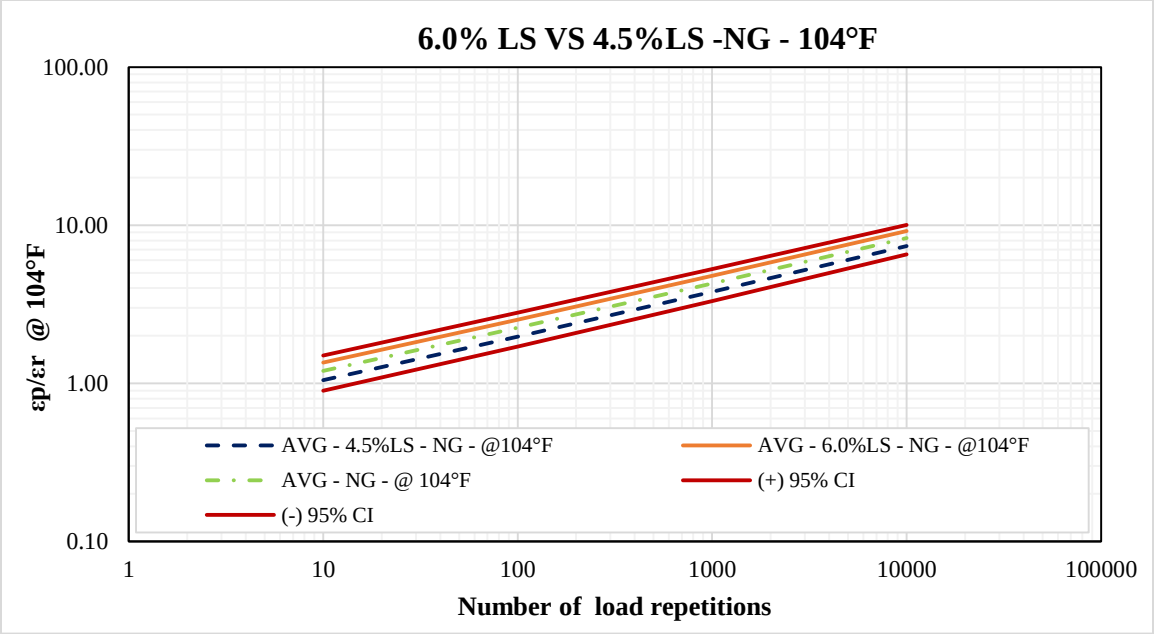

Figure 69. Average fatigue models for non-graded RAP with 6.0%LS and 4.5% LS.

Based on the findings presented in the previous section, the average rutting model for the non-graded CIR mixtures evaluated in this research , used for the mechanistical analysis is presented in Equation (**22**):

$$\frac{\boldsymbol{\varepsilon_p}}{\boldsymbol{\varepsilon_r}} = \mathbf{10}^{\mathbf{-6.4889}} * (\boldsymbol{N})^{\mathbf{0.2338}} * (\boldsymbol{T})^{\mathbf{1.8759}} \quad (22)$$

Where:

ε_P = Permanent strain, in/in
ε_r = Resilient strain, in/in
N = Number of load repetitions
T = Temperature, °F

6.2.5. Calculation of Pavement Responses

The 3D-Move pavement analysis software was used to determine the pavement responses due to applied load. [55]. The 3D-Move model is based on finite-layer approach and uses the Fourier transform technique to evaluate the responses of the layered medium subjected to a moving load traveling along the x axis at a constant speed. The properties for the AC layer can be either linear elastic (i.e., for static analyses such as the conducted in this study) or viscoelastic (i.e., for dynamic analyses). The properties of the unbound layers are linear elastic. Material properties are assumed to be uniform and constant within the layer.

The 3D-Move model can handle any number of layers with the complex loading at the surface and any number of response evaluation points.

For the purpose of this research, the pavement structure was subdivided in various layers with corresponding moduli and subjected to the load induced by a single axle with dual tires spaced 14 inches (axis to axis) and uniform circular load of 4500 lbs. each. The response points were selected under the center of the tire load, edge of the load, and center of the dual tires; at the middle (rutting) and at the bottom (fatigue) of each asphalt bound layer (i.e., CIR and AC).

6.2.6. Estimation of equivalent pavement structures

The approach used to calculate equivalent pavement structures for fatigue performance was based on using the fatigue performance models and the tensile strain at the critical locations (bottom of AC or CIR layer).

For rutting performance, the approach was based upon using the rutting performance models and a fixed number of cycles to reach an equivalent rut depth in both pavement structures. NDOT specifies 0.15 inches as the maximum allowed rut depth in the AC layers

In both cases, the following assumptions were made [9]:

- Temperature of CIR was assumed constant and equal to the AC layer temperature at 2 inches below the pavement surface.
- For the pavement structure rehabilitated with new AC layer and AC overlay, the temperature at 1 inch was selected for the top 2 inches of the AC layer, and the temperature at 2 inches was selected for the remaining depth of the AC layer.
- Loading frequencies were calculated for a speed of 1 mph.
- Performance models of AC layer were obtained from NDOT's M-E-Design database [56].
- Dynamic modulus of the existing AC layer was calculated using the same master curve assumed for the new AC overlay at corresponding frequency and temperature with a damage value of d_{ac}= 0.6 (Equation (**17**)).

With the properties of each sublayer, the tensile strains were calculated at the bottom of the CIR layer. The number of cycles to fatigue failure was calculated with the average performance model presented in section 6.2.3. The tensile strain required to reach that number of cycles was determined with the respective performance fatigue models for typical mixtures in northern and southern Nevada. The final step was determining the required thickness of the new AC layer to get the same or lower strain value.

In the case of the rutting analysis, the resilient strains at the middle of each sublayer were calculated. Using the resilient strain, maximum rut depth, thickness, analysis temperature, and the performance model of each sublayer; the numbers of cycles (N) to reach the selected rut depth of 0.15 inch were calculated for the CIR pavement. Finally, the required thickness of the new AC layer to achieve the same rut depth (i.e., 0.15 inch) under the same number of load cycles was determined.

6.2.7. Fatigue Endurance Limit

Monismith et al. suggested that the relationship between strain at the bottom of the AC layer and the number of cycles to fatigue seems to undergo a significant slope change at lower strain levels [57]. This level of stress or strain below which no fatigue damage originating from the bottom of the AC layer occurs is denominated as the: "endurance limit" [58]. Multiple approaches have been suggested to estimate a fatigue life endurance limit of an evaluated mixture at a given temperature and frequency. The Strategic Highway Research Program (SHRP) suggested that any strain value which results in a laboratory fatigue life of 50 million loading cycles can be considered as the fatigue endurance limit. Conducting a laboratory fatigue test for 50 million cycles would take an impractical amount of time and extrapolation techniques have been accepted to predict fatigue life under low strains. Using the average fatigue model developed for the CIR mixtures, the tensile strain to reach 50 cycles ($\varepsilon_{t-50\ million\ cycles}$) at a given temperature and loading frequency is estimated as:

$$\boldsymbol{\varepsilon_{t-50\ million\ cycles} = 10^{\left(-\frac{1}{k_2}\right)*\log\left[\left(\frac{50*10^6}{k_1}\right)*\left(\frac{1}{E_{CIR}}\right)^{k_3}\right]}} \quad (23)$$

A draft AASHTO standard of practice related with the prediction of endurance limit of AC mixtures specifies that the difference between the logs of the fatigue lives (i.e., $\log(sample\ 1) - \log(sample2)$) of two properly conducted test at a given temperature should not exceed 0.69 in the same laboratory . Consequently, the fatigue endurance limit can be calculated using Equation (**24**).

$$\log \varepsilon_{t-EL} = \log \varepsilon_{t-50\ million\ cycles} - \frac{\Delta \log \varepsilon_t}{2} = \log \varepsilon_{t-50\ million\ cycles} + \frac{0.69}{k2} \quad (24)$$

The endurance limit for the CIR pavement structures was calculated to be 194 microstrain. The endurance limit was compared with the obtained microstrain at bottom of the CIR layer determined from the 3D-Move analysis. If the mechanistic analysis determined a strain lower than ε_{t-EL}, it means that the pavement section will not experience fatigue failure under the evaluated loading magnitude and configuration. In this case, ε_{t-EL} is considered in the analysis to determine an AC section with similar fatigue performance life of the CIR pavement structure.

6.2.8. Calculation of CIR Structural layer coefficient based on fatigue performance

The final step of the process was to determine the structural layer coefficient for the CIR layer controlled by fatigue performance and verified by rutting performance. Based on the equivalent structure methodology described earlier, it was assumed that the pavement rehabilitated with CIR and the reconstructed pavement have the same structural number (SN). The coefficient of the CIR layer was calculated by equating the SN's of the two pavement structures along with the known coefficients of all other layers in the

pavement. Equation 25 can be used to determine the structural number of the entire pavement structure.

$$\boldsymbol{SN = \sum_{i}^{n-1} D_i * a_i} \quad (25)$$

Where:

D_i = thickness of interest layer, in
a_i = layer coefficient of interest layer
n = number of layers including the SG

6.3. Fatigue Mechanistic Analysis Results

The fatigue characteristics of the 8 different non-graded CIR mixtures were evaluated using the flexural beam fatigue test as per ASTM D7460 at three temperatures and multiple strain levels. A single average fatigue model was proposed by combining the fatigue models developed for each CIR mixture, presented in Table 11 and Table 12. The critical tensile strain (ε_t) at the bottom of the CIR layer was determined from the 3-D Move mechanistic analysis, and the number of cycles to fatigue failure was determined using the average fatigue model.

The dynamic modulus (E*) of the CIR layer, required for the fatigue model, was determined using the average dynamic modulus master curve presented in Figure 57. The frequency at which E* was computed was determined based on the MEPDG stress distribution concept using Odemark's equivalent thickness method, presented in section 6.2.2. Once the fatigue life of CIR was determined, the matching performance life approach was used to determine the equivalent AC layer thickness. The AC layer section was determined to achieve the same fatigue service life (i.e., number of cycles to fatigue failure) as the corresponding CIR control pavement sections.

6.3.1. Northern Nevada Pavement Structure

The mechanistical analysis indicated that the tensile strain at the bottom of the CIR layer structure with and a PG64-28 overlay (as shown in Figure 47) was 199 microstrain. This level of microstrain leads to 7,368,742 cycles cycles to failure when used in the CIR fatigue model. The tensile strain required to reach the same number of cycles to failure for a typical mixture in northern Nevada (PG64-28) was found to be 201 microstrain. Finally, the required thickness of the new AC layer to get the same or lower strain was found as shown in Figure 70.

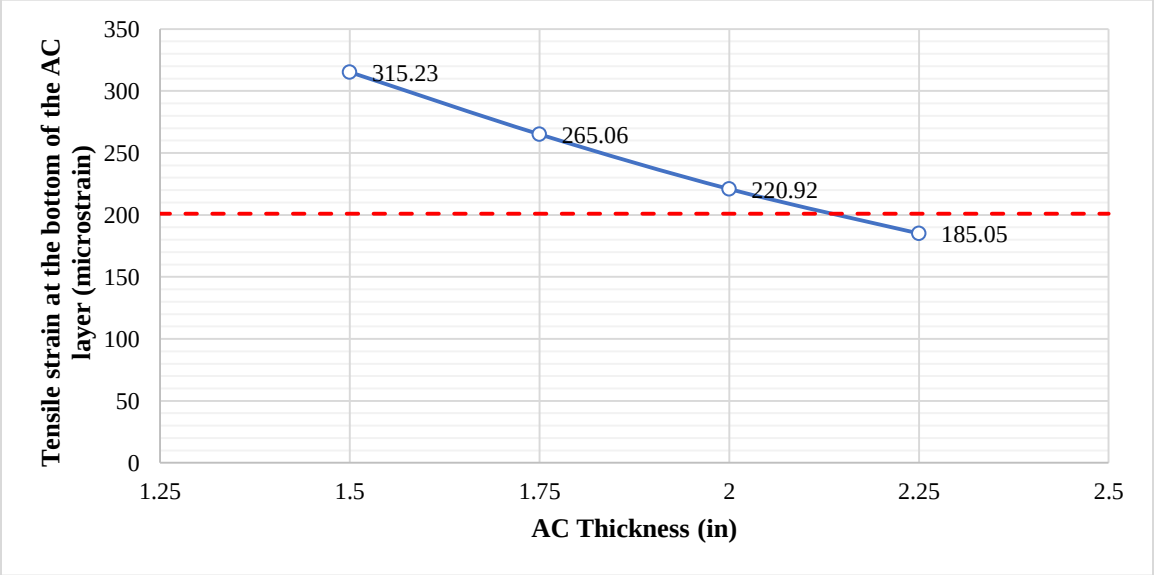

Figure 70. Tensile strain at the bottom of AC layer as a function of AC layer thickness.

The results indicated that 3.0 inches of CIR layer are equivalent to 2.25 inches of standard AC layer manufactured with a PG64-28NV asphalt binder. **Table 14** summarized the data used in the calculation of the CIR structural layer coefficient in northern Nevada. The analysis resulted in a fatigue-based coefficient of 0.26.

Table 14. Structural Layer Coefficients of Assumed Pavements Structures in Northern Nevada.

CIR structure			AC structure		
Type	**Thickness, in**	**a**	**Type**	**Thickness, in**	**a**
AC	2.0	0.35	AC	2.0	0.35
CIR	3.0	**0.26**	AC	2.25	0.35
OLD AC	3.0	0.29	OLD AC	3.0	0.29
CAB	10.0	0.1	CAB	10.0	0.1
SN	**3.358**		**SN**	**3.358**	

6.3.2. Southern Nevada Pavement Structure

The mechanistical analysis indicated that the tensile strain at the bottom of the CIR layer structure with and a PG76-22 layer (as shown in Figure 47) was 198 microstrain. This level of microstrain leads 22,043,998 cycles to failure when used in the CIR fatigue model. The tensile strain required to reach the same number of cycles to failure for a typical mixture in southern Nevada (PG76-22) was found to be 187 microstrain. Finally, the required thickness of the new AC layer to get the same or lower strain was found as shown in Figure 71.

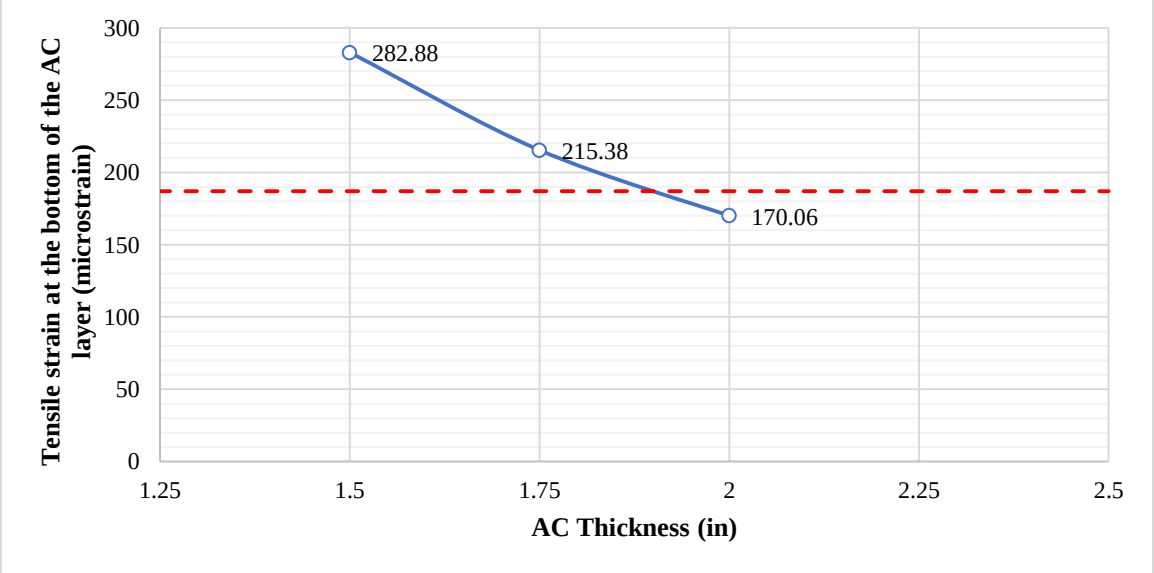

Figure 71. Tensile strain at the bottom of AC layer as a function of AC layer thickness.

The mechanistical analysis indicated that 3.0 inches of CIR layer are equivalent to 2.0 inches of standard AC overlay manufactured with a PG76-22NV asphalt binder. **Table 14** summarized the data used in the calculation of the CIR structural layer coefficient in southern Nevada. The analysis resulted in a fatigue-based coefficient of 0.23.

Table 15. Structural Layer Coefficients of Assumed Pavements Structures in Southern Nevada.

CIR structure			**AC structure**		
Type	**Thickness, in**	**a**	**Type**	**Thickness, in**	**A**
AC	2.0	0.35	AC	2.0	0.35
CIR	3.0	**0.23**	AC	2.0	0.35
OLD AC	3.0	0.29	OLD AC	3.0	0.29
CAB	10.0	0.1	CAB	10.0	0.1
SN	**3.270**		**SN**	**3.270**	

6.4. Verification for Rutting Performance

Based on the RLT test results and the average rutting model presented in section 6.2.4, a full mechanistic analysis was conducted for the non-graded CIR mixtures. The procedure and assumptions used to study the rutting performance were quite similar to those used in the approach to evaluate the fatigue performance. The main difference was that the approach used to determine equivalent pavement structures for rutting performance is based upon using the rutting performance models and a fixed number of cycles to reach an equivalent rut depth in both pavement structures. In this case, NDOT specifies 0.15 inches as the maximum allowed rut depth in the AC layers.

For the purpose of this study, the resilient strains at the middle of each sublayer were calculated. Using the resilient strain, maximum rut depth, thickness, analysis temperature, and the performance model of each sublayer; the number of cycles (N) to reach the

selected rut depth of 0.15 inch were calculated for the CIR pavement. The final step was determining the required thickness of the new AC layer to achieve the same rut depth (i.e., 0.15 inch) under the same number of load cycles. This analysis used the properties of typical mixtures from northern (64-28NV) and southern (76-22NV) Nevada.

6.4.1. Northern Nevada Pavement Structure

Table 16 and Table 17 summarize the rutting results of each pavement sublayer for the structure rehabilitated with CIR and the structure rehabilitated with new AC layer and overlay, respectively.

Table 16. Rut Depth of Each Sublayer in the CIR Structure in Northern Nevada.

Type	ID sublayer	Thickness, in	Temperature, °F	Z rutting, in	Rutting, in
AC	h sublayer 1	0.5	101.5	0.25	0.00894
AC	h sublayer 2	0.5	101.5	0.75	0.03396
AC	h sublayer 3	1.0	101.5	1.50	0.10688
CIR	h sublayer 4	1.0	91.8	2.50	0.00012
CIR	h sublayer 5	1.0	91.8	3.50	0.00007
CIR	h sublayer 6	1.0	91.8	4.50	0.00004
Number of Cycles for a rut depth of 0.15 in				**80,969,942**	**0.15**

Table 17. Rut Depth of Each Sublayer in the AC Structure in Northern Nevada.

Type	ID sublayer	Thickness, in	Temperature, °F	Z rutting, in	Rutting, in
AC	h sublayer 1	0.5	101.5	0.25	0.00057
AC	h sublayer 2	0.5	101.5	0.75	0.02798
AC	h sublayer 3	1.0	101.5	1.50	0.07852
AC	h sublayer 4	1.0	91.8	2.50	0.03006
AC	h sublayer 5	1.0	91.8	3.50	0.01376
AC	h sublayer 6	**6.5**	91.8	10.50	0.00163
Number of Cycles for a rut depth of 0.15 in				**80,969,942**	**0.15**

The M-E analysis indicated that the 3.0 inches CIR layer is equivalent to 8.5 inches of the standard AC layer with a PG64-28NV asphalt binder. Table 18 summarizes the data used in the calculation of the coefficient for the CIR layer in northern Nevada. The analysis resulted in a rutting-based layer coefficient of 0.99 for a CIR mixture used in northern Nevada.

Table 18. Layer Coefficients of Assumed Pavements Structures in Northern Nevada.

CIR structure [RD=0.15"]			**AC structure [RD=0.15"]**		
Type	**Thickness, in**	**a**	**Type**	**Thickness, in**	**A**
AC	2.0	0.35	AC	2.0	0.35
CIR	3.0	**0.99**	AC	8.5	0.35
OLD AC	3.0	0.29	OLD AC	3.0	0.29
CAB	10.0	0.1	CAB	10.0	0.1
SN	**5.545**		**SN**	**5.545**	

6.4.1. Southern Nevada Pavement Structure

Table 19 and Table 20 summarize the rut depth of each sublayer for the structure rehabilitated with CIR and the structure rehabilitated with new AC layer and overlay, respectively.

Table 19. Rut Depth of Each Sublayer in the CIR Structure in Southern Nevada.

Type	**ID sublayer**	**Thickness, in**	**Temperature, °F**	**Z rutting, in**	**Rutting, in**
AC	h sublayer 1	0.5	126.0	0.25	0.00913
AC	h sublayer 2	0.5	126.0	0.75	0.03398
AC	h sublayer 3	1.0	126.0	1.50	0.10392
CIR	h sublayer 4	1.0	116.1	2.50	0.00170
CIR	h sublayer 5	1.0	116.1	3.50	0.00088
CIR	h sublayer 6	1.0	116.1	4.50	0.00039
Number of Cycles for a rut depth of 0.15in				**38,090**	**0.15**

Table 20. Rut Depth of Each Sublayer in the AC Structure in Southern Nevada.

Type	ID sublayer	Thickness, in	Temperature, °F	Z , in	Z rutting, in	Rutting, in
AC	h sublayer 1	0.5	126.0	0.50	0.25	0.00061
AC	h sublayer 2	0.5	126.0	1.00	0.75	0.02826
AC	h sublayer 3	1.0	126.0	2.00	1.50	0.07573
AC	h sublayer 4	1.0	116.1	3.00	2.50	0.03118
AC	h sublayer 5	1.0	116.1	4.00	3.50	0.01381
AC	h sublayer 6	6.5	116.1	10.50	7.25	0.00155
Number of Cycles for a rut depth of 0.15in					**38,090**	**0.15114**

The M-E analysis indicated that the 3.0 inches CIR layer is equivalent to 8.5 inches of the standard AC layer with a PG76-22NV asphalt binder. Table 21 summarizes the data used in the calculation of the coefficient for the CIR layer in southern Nevada. The analysis resulted in a rutting-based layer coefficient of 0.99 for a CIR mixture used in southern Nevada.

Table 21. Layer Coefficients of Assumed Pavements Structures in Southern Nevada.

CIR structure [RD=0.15"]			**AC structure [RD=0.15"]**		
Type	**Thickness, in**	**a**	**Type**	**Thickness, in**	**a**
AC	2.0	0.35	AC	2.0	0.35
CIR	3.0	**0.99**	AC	6.5	0.35
OLD AC	3.0	0.29	OLD AC	3.0	0.29
CAB	10.0	0.10	CAB	10.0	0.10
SN	**5.545**		**SN**	**5.545**	

Chapter 7. Findings, Conclusions and Recommendations

7.1. Findings and Conclusions

The overall objective of this research effort was to evaluate the cracking behavior of Cold In-Place Recycling mixtures. For this purpose, eight different combinations of CIR mixtures were assessed, including four types of emulsions and two levels of lime slurry. Full Performance Grading (PG) of the asphalt emulsions was also conducted. The number of cycles to failure based on the 50% reduction in flexural stiffness was used to assess the fatigue behavior of CIR mixtures, while the number of cycles, crack initiation and crack propagation parameters were analyzed to address the reflective cracking performance. Based on the analysis of the data generated from this extensive evaluation, the following findings and recommendations can be made:

- The data generated from the fatigue evaluation indicate that the fatigue behavior at 70°F of the CIR mixture with the polymer-modified emulsion (C) presents the best resistance to fatigue cracking followed by the CIR mixture made with the latex-modified emulsion (B). CIR mixtures with Rubber-modified (D) and Standard CMS-2S (A) emulsions showed similar fatigue behavior. In general, all evaluated mixtures presented similar fatigue performance and an average fatigue model can be recommended with 95% confidence to estimate the fatigue performance of CIR mixtures manufactured with different asphalt emulsions and percentages of lime slurry.

- The data generated from the overlay tester showed that the resistance of the CIR mixtures to reflective cracking is sensitive to the type of asphalt emulsion. As previous studies in Nevada showed, CIR mixtures offer good resistance to reflective cracking, this study employed a new approach to assess resistance to reflective cracking in terms of crack initiation and propagation. The analysis of the reflective cracking data indicated that some CIR mixtures are less resistant to crack initiation but more resistant to crack propagation than others.
- Even though, the energy required to initiate a fracture was observed to be mixture-dependent, the crack propagation rates were closer for the whole range of mixtures. This indicates that the material will resist the initiation of the crack depending on the emulsion type but all mixture will offer similar propagation rates regardless of the emulsion type or lime content.
- Based on the fatigue-based mechanistic analysis conducted, a range of structural layer coefficient of CIR from 0.23 to 0.26 is recommended. These values are similar to the values recommended in the current literature for NDOT CIR mixtures.
- The fatigue-based structural layer coefficient for CIR mixtures was verified for rutting performance. The rutting-based analysis provided a structural layer coefficient of 0.99. This verification process concluded that the controlling distress of CIR mixtures is fatigue and not rutting. This makes sense since CIR is done with 100% recycled materials that are not as flexible as new pavements, but at the same time, its high stiffness levels provide elevated rutting resistance.

- The percentage of emulsion residue plays an important role in the fatigue behavior of CIR mixtures. The mixtures with higher percentage residue exhibited better fatigue behavior regardless of the level of lime slurry.
- In contrast with the results obtained in the fatigue analysis, the percentage of emulsion residue was not a critical factor in the reflective cracking behavior of the CIR mixtures. Conversely, the emulsion with the lower percentage residue presented the higher number of cycles to failure. This may be attributed to the effect of additives, in this case, tire rubber.
- Based on the conclusions of this study, and the conclusions presented in previous studies conducted at UNR, it can be concluded that decreasing the percentage of lime slurry by 1.5 percent will not compromise the structural performance of the CIR mixtures.
- The mechanistic analysis conducted to verify rutting performance of CIR layers indicated that this rehabilitation technique may represent a significant improvement on the overall rutting performance of the pavement structure. Knowing that the CIR mixture is manufactured with 100% RAP material, it is expected to observe its superior rutting performance as compared to the AC mixtures with 100% virgin materials.
- The level of lime slurry does not have a significant impact on the E* master curve of the CIR mixtures manufactured with non-graded RAP. An average model was suggested and can be used with 95% of statistical confidence.

- Likewise, the level of lime slurry does not have a significant impact on the rutting performance of the CIR mixtures manufactured with non-graded RAP. An average model was suggested and can be used with 95% of statistical confidence.

7.2. Recommendations

- This study evaluated the cracking behavior of CIR mixtures. Some CIR techniques include the addition of Portland cement during the construction process. A recommendation for further studies would be to assess the cracking behavior of CIR mixtures including cement.
- The models proposed in this study are laboratory calibrated. In order to be used in the AASHTO Ware Pavement ME software, a calibration of the laboratory-to-field coefficients (betas) is required
- The cracking behavior of CIR mixtures can be further evaluated with other devices such as Semi Circular Bend (SCB) test, Ideal Cracking Test (Ideal CT) among others.
- The low-temperature cracking behavior of the CIR mixtures can be evaluated with the Uniaxial Thermal Stress and Strain Test (UTSST)
- The field density (air voids) and emulsion content play an important role in the cracking behavior of the CIR mixture, therefore, monitoring density and emulsion content during construction process is highly recommendable.

Chapter 8. References

[1] Williams, B. A., Copeland, A., & Ross, T. C., " Asphalt Pavement Industry Survey on Recycled Materials and Warm-Mix Asphalt Usage," *National Asphalt Pavement Association,* 2017.

[2] Sebaaly, P. E.; Bazi, G.: Hitti, E.; Weitzel, D.; Bemanian, S., "Performance of Cold In-Place Recycling in Nevada," *Transportation Research Record: Journal of the Transportation Research Board, No. 1896,* pp. 162-169, 2004.

[3] Kazmierowski, T. J., Bradbury, A., Cheng, S., & Raymond, C. , "Performance of cold in-place recycling in Ontario.," *Transportation Research Record, (1337).,* 1992.

[4] Charmot, S., & Romero, P., " Assessment of Fracture Parameters to Predict Field Cracking Performance of Cold In-Place Recycling Mixtures," *ransportation Research Record: Journal of the Transportation Research Board, (2155),,* pp. 34-42..

[5] Epps, J. A., "Cold-recycled bituminous concrete using bituminous materials," *Transportation Research Board.,* 1990.

[6] Kearney, E., & Huffman, J., "Full-depth reclamation process.," *ransportation Research Record: Journal of the Transportation Research Board, (1684),* pp. 203-209, 1999.

[7] Forsberg, A., Lukanen, E., & Thomas, T., "Engineered cold in-place recycling project: blue Earth county state aid highway 20, Minnesota.," *Transportation Research Record: Journal of the Transportation Research Board, (1813),,* pp. 111-123, 2002.

[8] Mallick, R., Bonner, D., Bradbury, R., Andrews, J., Kandhal, P., & Kearney, E. , "Evaluation of performance of full-depth reclamation mixes.," *Transportation Research Record: Journal of the Transportation Research Board, ,* pp. 199-208, 2002.

[9] Ayala, F., "Hveem Mix Design and Engineering Properties of Cold In-Place Recycling Mixtures," *Master Thesis, University of Nevada, Reno,* 2018.

[10] Castro-Ortiz, J., "Cold In-Place Recycling Mix Design, In-Place Density, and Long-Term Performance in Nevada," University of Nevada Reno, Reno, NV, 2017.

[11] Niazi, Y., & Jalili, M., "Effect of Portland cement and lime additives on properties of cold in-place recycled mixtures with asphalt emulsion.," *Construction and Building Materials, 23(3),* pp. 1338-1343., 2009.

[12] Milton, L. J., & Earland, M. G., "Design guide and specification for structural maintenance of highway pavements by cold in-situ recycling. Wokingham," *Transport Research Laboratory.*, 1999.

[13] Lin, J., Hong, J., & Xiao, Y., "Dynamic characteristics of 100% cold recycled asphalt mixture using asphalt emulsion and cement.," *Journal of Cleaner Production,* pp. 337-344., 2017.

[14] Gao, L., Ni, F., Ling, C., & Yan, J., "Evaluation of fatigue behavior in cold recycled mixture using digital image correlation method," *Construction and Building Materials,* pp. 393-402, 2016.

[15] Yan, J., Ni, F., Yang, M., & Li, J., "An experimental study on fatigue properties of emulsion and foam cold recycled mixes.," *Construction and Building Materials, 24(11),* pp. 2151-

2156., 2010.

[16] Kavussi, A., & Modarres, A., "Laboratory fatigue models for recycled mixes with bitumen emulsion and cement.," *Construction and Building Materials*, pp. 1920-1927., 2010.

[17] Ruenkrairergsa, T., Phromsorn, C., Silarom, P., & Ketnoot, W., "Engineering Properties of Foam Bitumen Mixtures in Thailand," *8th Conference on Asphalt Pavements for Southern Africa*, p. 16, 2004.

[18] Morian, D., Oswalt, J., & Deodhar, A., "Experience with cold in-place recycling as a reflective crack control technique: Twenty years later.," Transportation Research Record: Journal of the Transportation Research Board, 2004.

[19] AASHTO , "T -27 Standard Method of Test for Sieve Analysis of Fine and Coarse Aggregates," 2014.

[20] Asphalt Institute, "MS-19 Basic Asphalt Emulsion Manual," 2008.

[21] ASTM D7497, "Standard Practice for Recovering Residue from Emulsified Asphalt Using Low Temperature Evaporative Technique," 2009.

[22] Kim, Y. R., Adams, J., Castorena, C., Ilias, M., Im, J. H., Bahia, H., & Johannes, P. T., "Performance-Related Specifications for Emulsified Asphaltic Binders Used in Preservation Surface Treatments (No. Project 09-50).," *NCHRP 9-50,* 2017.

[23] AASHTO M320, "Standard Specification for Performance-Graded Asphalt Binder," 2017 .

[24] Brown, E. R.; Khandhal, P. S.; Roberts, F.; Kim, Y. R.; Lee, D. Y.; Kennedy, T., "Hot Mix Asphalt Materials, Mixture Design and Construction," *National Center for Technology*

NCAT, pp. 365-367, 2009.

[25] AASHTO R28, "Standard Practice for Accelerated Aging of Asphalt Binder Using a Pressurized Aging Vessel (PAV)," 2012.

[26] Asphalt Institute, "MS-26 Asphalt Binder Handbook," 2011.

[27] Anderson, R.M., King, G.N., Hanson, D.I., Blankenship, P.B.,, "Evaluation of the Relationship between Asphalt Binder Properties and Non-Load Related Cracking," *Journal of the Association of Asphalt Paving Technologists,* pp. 615-664, 2011.

[28] Little, D. N., Epps, J. A., & Sebaaly, P. E., "Hydrated lime in hot mix asphalt.," *National Lime Association,* no. Arlington, VA., 2006.

[29] Lesueur, D., Petit, J., & Ritter, H. J., "The mechanisms of hydrated lime modification of asphalt mixtures: a state-of-the-art review.," *Road Materials and Pavement Design, 14(1),* pp. 1-16, 2013.

[30] Niazi, Y., and M. Jalili., " "Effect of Portland cement and lime additives on properties of cold in-place recycled mixtures with asphalt emulsion."," *Construction and Building Materials 23.3* , pp. 1338-1343, 2009.

[31] Cross, S. A., ""“Experimental Cold In-Place Recycling with Hydrated Lime"," *Transportation Research Record,* pp. 186-193, 1999.

[32] Piratheepan, M., "Designing Cold Mix Asphalt (CMA) and Cold In-place Recycling (CIR) Using SUPERPAVE Gyratory Compactor," MSc Thesis, University of Nevada, Reno, 2011.

[33] Fager, G.A.,, ""“Lime Slurry in Cold In Place Recycle”," *Final Report to Kansas DOT,* 2004.

[34] AASHTO, "Standard Method of Test for Theoretical Maximum Specific Gravity (Gmm) and Density of Hot Mix Asphalt (HMA)," AASHTO, 2015.

[35] Texas Departrment of Transportation, "TxDOT Designation: TEX-248-F. Overlay test," 2009.

[36] Garcia, V., Miramontes, A., Garibay, J., Abdallah, I., & Nazarian, S, "Improved overlay tester for fatigue cracking resistance of asphalt mixtures," TxDOT, Texas, 2017.

[37] ASTM, "Standard Test Method for Bulk Specific Gravity and Density of Compacted Bituminous Mixtures Using Coated Samples," ASTM Int'l, 2015.

[38] Zhou, F., & Scullion, T, "Upgraded overlay tester and its application to characterize reflection cracking resistance of asphalt mixtures (FHWA/TX-04/0-4467-1).," Transportation Institute, Texas A&M University System., 2003.

[39] Zhou, F., Hu, S., & Scullion, T., "Development and verification of the overlay tester based fatigue cracking prediction approach (FHWA/TX-07/9-1502-01-8).," Texas Transportation Institute, Texas A&M University System., 2007.

[40] Zhou, F., & Scullion, T., "Overlay tester: a rapid performance related crack resistance test (FHWA/TX-05/0-4467-2)," Overlay tester: a rapid performance related crack resistance test (FHWA/TX-05/0-4467-2), 2005.

[41] W. Ma, "Proposed Improvements to Overlay Test for Determining Cracking Resistance of Asphalt Mixtures," 2014.

[42] AASHTO, "R-30 Standard Practice for Mixture Conditioning of Hot Mix Asphalt (HMA),"

2002.

[43] ASTM, "D7460 - Standard Test Method for Determining Fatigue Failure of Compacted Asphalt Concrete Subjected to Repeated Flexural Bending," 2010.

[44] ARA, Inc., ERES Consultants Division, "Guide for Mechanistic–Empirical Design of New and Rehabilitated Pavement Structures. Final Rep.," *NCHRP Project 1-37A.*, 2004.

[45] Tsai, B. W., Harvey, J. T., and Monismith, C. L.,, "High Temperature Fatigue and Fatigue Damage Process of Aggregate-Asphalt Mixes," *Journal of the Association of Asphalt Paving Technologists*, p. 345–385, 2002.

[46] Habbouche, J., Hajj, E. Y., Sebaaly, P. E., & Piratheepan, M. , " A critical review of high polymer-modified asphalt binders and mixtures," International Journal of Pavement Engineering, 2018.

[47] Goodrich, J. L., "Asphalt and polymer modified Asphalt properties related to the performance of Asphalt concrete mixes (with discussion)," In Association of Asphalt Paving Technologists Proc (Vol. 57), 1988.

[48] Khattak, M., & Baladi, G, "Fatigue and permanent deformation models for polymer-modified asphalt mixtures.," Journal of the Transportation Research Board, Transportation Research Record (1767), 2001.

[49] Di Benedetto, H., Ashayer S., and Chaverot, P., "Fatigue Damage for Bituminous Mixtures.," *Proceedings of the 5th Int. RILEM Symposium MTBM*, pp. 263-270, 1997.

[50] D. Bateman, "Laboratory investigation of fatigue endurance limits in asphalt concrete,"

Master Thesis, 2012.

[51] National Cooperative Highway Research Program, "Guide for Mechanistic-Empirical Design," NCHRP, Champaign, Illinois, 2004.

[52] Al-Qadi, I., Elseifi, M., Yoo, P., Dessouky, S., Gibson, N., Harman, T., D'Angelo, J. and Petros, K., , "Accuracy of Current Complex Modulus Selection Procedure from Vehicular Load Pulse," Transportation research board, Washington, D.C, 2008.

[53] Climte-data, "Climate Data," 2018. [Online]. Available: https://en.climate-data.org/location/1457/. [Accessed 19 April 2018].

[54] "LTPP InfoPAve," Federal Highway Administration Long-Term Pavement Performance, 2018. [Online]. Available: https://infopave.fhwa.dot.gov/Data/ClimateTool. [Accessed 19 April 2018].

[55] Siddharthan R.V., Hajj E.Y., Sebaaly P.E., and Nitharsan R, "Formulation and Application of 3D-Move: A dynamic Pavement Analysis Program, Report FHWA-RD-WRSC-UNR-201506," Western Regional Superpave Center (WRSC), University of Nevada, Reno, 2015.

[56] Hajj, Elie Y.; Sebaaly, Peter E.; Nabhan, P., "Manual for Designing Flexible Pavements in Nevada Using AASHTOWare Pavement-ME Design," University of Nevada, Reno, Reno, NV, 2017.

[57] Monismith, C. L., J. A. Epps, D. A. Kasianchuk, and D. B. McLean., "Asphalt Mixture Behavior in Repeated Flexure. Report TE 70-5.," *Institute of Transportation and Traffic Engineering, University of California*, 1970.

[58] Prowell B.D., Brown E. R., Aderson R. M., Daniel J.S., Quintus H. V, Shen S., Carpenter S.H., Bhattacharjee S., and Maghsoodloo S., , "Validating the Fatigue Endurance Limit for Hot Mix Asphalt," *National Cooperative Highway research Program,* 2010.

[59] National Cooperative Highway Research Program, "Recycling and Reclamation of Asphalt Pavements Using In-Place Methods," National Academy of Sciences, Washington, D.C., 2011.

[60] Nevada Department of Transportation, "Standard specification of road and bridge construction," Nevada Department of Transportation, Carson City, 2014.

[61] Y. Kim, H. Lee and M. Heitzman, "Dynamic Modulus and Repeated Load Tests of Cold In-Place Recycling Mixtures Using Foamed Asphalt," ASCE, 2009.

[62] K. Yongjoo, I. Soohyok and L. Hosin, "Impacts of Curing Time and Moisture Content on Engineering Properties of Cold In-Place Recycling Mixtures Using Foamed or Emulsified Asphalt," ASCE, 2011.

[63] AASHTO, "Standard Method of Test for Resistance of Compacted Asphalt Mixtures to Moisture-Induced," AASHTO, 2015.

[64] AASHTO, "Standard Method of Test for Preparation of Test Specimens of Hot Mix Asphalt (HMA) by Means of California Kneading Compactor," AASHTO, 2015.

[65] AASHTO, "Standard Method of Test for Determining the Dynamic Modulus and Flow Number for Asphalt Mixtures Using the Asphalt MixturePerformance Tester (AMPT)," AASHTO, 2015.

[66] AASHTO, "Standard Practice for Developing Dynamic Modulus Master Curves for Asphalt Mixtures Using the Asphalt Mixture Performance Tester (AMPT)," AASHTO, 2017.

[67] National Cooperative Highway Research Program, "Calibration of Rutting Models for Structural and Mix Design," Transportation Research Board, Washington, 2012.

[68] AASHTO, "Standard Method of Test for Determining Dynamic Modulus of Hot Mix Asphalt (HMA)," AASHTO, 2015.

[69] AASHTO, "Standard Practice for Developing Dynamic Modulus Master Curves for Asphalt Mixtures," AASHTO, 2015.

[70] Lewis, A. J. N. and Collings, D. C., "Cold in Place Recycling: A Relevant process for Road Rehabilitation and Upgrading," *7th Conference on Asphalt Pavement Process for Southern Africa*, 1999.

[71] Jitareekul, P, "An Investigation into Cold In-Place Recycling of Asphalt Pavements," *Doctoral dissertation, PhD Thesis, University of Nottingham,* 2009.

[72] Glover, C. J., Davison, R. R., Domke, C. H., Ruan, Y., Juristyarini, P., Knorr, D. B., & Jung, S. H. , "Development of a new method for assessing asphalt binder durability with field validation.," *Texas Dept Transport*, 2005.

[73] P. E. Sebaaly, G. Bazi, E. Hitti, D. Weitzel and S. Bemanian, "Performance of Cold In-Place Recycling in Nevada," *Transportation Research Record: Journal of the Transportation Research Board, No. 1896,* pp. 162-169, 2004.

[74] Piratheepan, M.; Sebaaly, P.; Hajj, E.; Selvaratnam, S., "Evaluation of Long-term Performance of Cold In-Place Recycling Pavements in Nevada," University of Nevada,

Reno, 2014.

[75] Huang, Y. H., "Pavement Analysis and Design," Prentice Hall, 1993.

[76] Lee, K. Wayne; Brayton, Todd E.; Veyera, George; Huffman, John; Harrington, Jason, "MODIFIED SUPERPAVE MIX-DESIGN FOR COLD IN-PLACE RECYCLING ASPHALT MIXTURES," 2nd International Symposium on Maintenance and Rehabilitation of Pavements and Technological Control, Auburn, Alabama, 2001.

[77] Thapa, S., "Design of Cold-In-Place Recycling (CIR) Using Superpave Gyratory Compactor," University of Nevada Reno, Reno, NV, 2015.

[78] Thomas, T.; Kadrmas, A., "Performance-Related Tests and Specifications for Cold In-Place Recycling: Lab and Field Experience," Transportation Research Board 2003 Annual Meeting, 2003.

[79] El-Basyouny, M.; Jeong, M., "Effective Temperature for Analysis of Permanent Deformation and Fatigue Distress on Asphalt Mixtures," Transportation Research Board, Washingotn, D.C, 2009.

Chapter 9. Appendices

9.1. Performance Grading (PG) test results

9.1.1. Emulsion Type A

Table 22. Emulsion Type A: Dynamic Shear Rheometer Original.

Test	Temperature, °C	S1	S2	Average	CV (1s%)	Spec	d2s (%)	Spec
|G*|/sin(delta) Original, Kpa	**46**	3.401	3.383	3.392	0.3	2.3	0.5	6.4
	52	1.59	1.511	1.551	2.5	2.3	5.1	6.4
	58	0.732	0.729	0.731	0.2	2.3	0.4	6.4

Table 23. Emulsion Type A: Dynamic Shear Rheometer (PAV Residue).

Test	Temperature, °C	S1	S2	Average	CV (1s%)	Spec	d2s (%)	Spec
G*sinδ PAV, Kpa	**13**	5224	5148	5186	0.7	4.9	1.5	13.8
	16	3165	3115	3140	0.8	4.9	1.6	13.8
	19	1998	1822	1910	4.6	4.9	9.2	13.8

Table 24. Emulsion Type A: Bending Beam Rheometer (BBR).

Test	Temperature, °C	S1	S2	Average	CV (1s%)	Spec	d2s (%)	Spec
Stiffness BBR, MPa	**-18**	104	113	108.5	4.1	2.5	8.3	7.2
	-24	269	270	269.5	0.2	2.5	0.4	7.2
Test	**Temperature, °C**	**S1**	**S2**	**Average**	**CV (1s%)**	**Spec**	**d2s (%)**	**Spec**
m-value BBR	**-18**	0.404	0.398	0.401	0.7	1.0	1.5	2.9
	-24	0.324	0.325	0.325	0.2	1.0	0.3	2.9

9.1.2. Emulsion Type B

Table 25. Emulsion Type B: Dynamic Shear Rheometer Original.

Test	Temperature, °C	S1	S2	Average	CV (1s%)	Spec	d2s (%)	Spec
|G*|/sin(delta) Original, Kpa	**58**	3.799	3.825	3.812	0.3	2.3	0.7	6.4
	64	1.812	1.728	1.770	2.4	2.3	4.7	6.4
	70	0.865	0.859	0.862	0.3	2.3	0.7	6.4

Table 26. Emulsion Type B: Dynamic Shear Rheometer (PAV Residue).

Test	Temperature, °C	S1	S2	Average	CV (1s%)	Spec	d2s (%)	Spec
G*sinδ PAV, Kpa	**19**	5696	5924	5810	2.0	4.9	3.9	13.8
	22	3800	3980	3890	2.3	4.9	4.6	13.8
	25	2685	2666	2676	0.4	4.9	0.7	13.8

Table 27. Emulsion Type B: Bending Beam Rheometer (BBR).

Test	Temperature, °C	S1	S2	Average	CV (1s%)	Spec	d2s (%)	Spec
Stiffness BBR, MPa	**-18**	291	293	292.0	0.3	2.5	0.7	7.2
	-24	410	415	412.5	0.6	2.5	1.2	7.2
Test	**Temperature, °C**	**S1**	**S2**	**Average**	**CV (1s%)**	**Spec**	**d2s (%)**	**Spec**
m-value BBR	**-18**	0.305	0.308	0.307	0.5	1.0	1.0	2.9
	-24	0.250	0.247	0.249	0.6	1.0	1.2	2.9

9.1.3. Emulsion Type C

Table 28. Emulsion Type C: Dynamic Shear Rheometer Original.

Test	Temperature, °C	S1	S2	Average	CV (1s%)	Spec	d2s (%)	Spec
|G*|/sin(delta) Original, Kpa	**58**	3.554	3.456	3.505	1.4	2.3	2.8	6.4
	64	1.609	1.674	1.642	2.0	2.3	4.0	6.4
	70	0.763	0.794	0.779	2.0	2.3	4.0	6.4

Table 29. Emulsion Type C: Dynamic Shear Rheometer (PAV Residue).

Test	Temperature, °C	S1	S2	Average	CV (1s%)	Spec	d2s (%)	Spec
G*sinδ PAV, Kpa	**19**	---	---	---	---	---	----	---
	22	5250	5203	5227	0.4	4.9	0.9	13.8
	25	3211	3181	3196	0.5	4.9	0.9	13.8

Table 30. Emulsion Type C: Bending Beam Rheometer (BBR).

Test	Temperature, °C	S1	S2	Average	CV (1s%)	Spec	d2s (%)	Spec
Stiffness BBR, MPa	**-18**	229	231	230	0.4	2.5	0.9	7.2
	-24	487	467	477	2.1	2.5	4.2	7.2
Test	**Temperature, °C**	**S1**	**S2**	**Average**	**CV (1s%)**	**Spec**	**d2s (%)**	**Spec**
m-value BBR	**-18**	0.310	0.308	0.309	0.3	1.0	0.6	2.9
	-24	0.249	0.253	0.351	0.8	1.0	1.6	2.9

9.1.4. Emulsion Type D

Table 31. Emulsion Type D: Dynamic Shear Rheometer Original.

Test	Temperature, °C	S1	S2	Average	CV (1s%)	Spec	d2s (%)	Spec
|G*|/sin(delta) Original, Kpa	**52**	2.752	2.814	2.783	1.1	2.3	2.2	6.4
	58	1.241	1.227	1.234	0.6	2.3	1.1	6.4
	64	0.591	0.587	0.589	0.3	2.3	0.7	6.4

Table 32. Emulsion Type D: Dynamic Shear Rheometer (PAV Residue).

Test	Temperature, °C	S1	S2	Average	CV (1s%)	Spec	d2s (%)	Spec
G*sinδ PAV, Kpa	**19**	5696	5924	5810	2.0	4.9	3.9	13.8
	22	3800	3980	3890	2.3	4.9	4.6	13.8
	25	2685	2666	2676	0.4	4.9	0.7	13.8

Table 33. Emulsion Type D: Bending Beam Rheometer (BBR).

Test	Temperature, °C	S1	S2	Average	CV (1s%)	Spec	d2s (%)	Spec
Stiffness BBR, MPa	**-18**	163	165	164.0	0.6	2.5	1.2	7.2
	-24	397	401	399.0	0.5	2.5	1.0	7.2
Test	**Temperature, °C**	**S1**	**S2**	**Average**	**CV (1s%)**	**Spec**	**d2s (%)**	**Spec**
m-value BBR	**-18**	0.343	0.340	0.342	0.4	1.0	0.9	2.9
	-24	0.264	0.261	0.263	0.6	1.0	1.1	2.9

9.2. Reflective Cracking Test Results

9.2.1. Non-graded , 6% Lime Slurry

Table 34. Reflective Cracking Test Results: Non-graded, 6% Lime Slurry.

Sample	Air Voids (%)	No Cycles	Critical Fracture Energy (in-lbs./in^2)	Crack Propagation Rate	Crack Resistance Index (β)
A-1	13.2	519	0.305	0.439	74.8
A-2	14	474	0.346	0.440	74.7
B-1	13.7	114	0.376	0.491	67.9
B-2	13.8	151	0.353	0.519	64.1
C-1	13.5	244	0.193	0.481	69.2
C-2	12.6	316	0.198	0.346	87.2
D-1	13.4	1414	0.252	0.351	86.5
D-2	13.7	1094	0.235	0.358	85.6

Table 35. Reflective Cracking Test Statistics: Non-graded, 6% Lime Slurry.

Sample	Number of Cycles			Critical Fracture Energy (in-lbs./in^2)			Crack Propagation Rate		
	Average	Std. Dev.	COV	Average	Std. Dev.	COV	Average	Std. Dev.	COV
A-1	497	31.82	6%	0.33	0.00	1%	0.44	0.0007	1%
A-2									
B-1	133	26.16	20%	0.36	0.02	4%	0.51	0.0198	4%
B-2									
C-1	280	50.91	18%	0.20	0.00	2%	0.41	0.0955	23%
C-2									
D-1	1254	226.27	18%	0.24	0.01	5%	0.35	0.0049	1%
D-2									

9.2.2. Non-graded, 4.5% Lime Slurry

Table 36. Reflective Cracking Test Results: Non-graded, 4.5% Lime Slurry.

Sample	Air Voids (%)	No Cycles	Critical Fracture Energy (in-lbs./in^2)	Crack Propagation Rate	Crack Resistance Index (β)
A-1	14.1	242	0.297	0.462	71.7
A-2	13.2	322	0.289	0.470	70.7
B-1	13.4	89	0.343	0.525	63.3
B-2	13.7	62	0.325	0.519	64.1
C-1	13.5	138	0.189	0.482	69.1
C-2	12.9	171	0.192	0.494	67.5
D-1	12.8	349	0.200	0.411	78.5
D-2	12.6	432	0.197	0.424	76.8

Table 37. Reflective Cracking Test Statistics: Non-graded, 6% Lime Slurry.

Sample	Number of Cycles			Critical Fracture Energy (in-lbs./in^2)			Crack Propagation Rate		
	Average	Std. Dev.	COV	Average	Std. Dev.	COV	Average	Std. Dev.	COV
A-1	497	31.82	6%	0.33	0.00	1%	0.44	0.0007	1%
A-2									
B-1	133	26.16	20%	0.36	0.02	4%	0.51	0.0198	4%
B-2									
C-1	280	50.91	18%	0.20	0.00	2%	0.41	0.0955	23%
C-2									
D-1	1254	226.27	18%	0.24	0.01	5%	0.35	0.0049	1%
D-2									

9.3. Flexural Beam Fatigue Test Results

9.3.1. Type A / 52 -34 / CMS2S / NG / 6.0%LS

Table 38. CIR Beam Fatigue Test Results: Type A / 52 -34 / CMS2S / NG / 6.0%LS.

CIR BEAM FATIGUE RESULTS						
Type A / 52 -34 / CMS2S / NG / 6.0%LS						
Temperature [°F]	**Sample ID**	**Air Voids Level (%)**	**Dynamic Modulus E* (psi)**	**Initial Flexural Stiffness (psi)**	**Flexural Strain [microstrain]**	**Number of Cycles to Failure 50% SR**
55	S1	13.4	679,808	647,623	254.4	84,366
	S2	13.2	679,808	615,714	390.8	15,936
	S3	13.7	679,808	417,288	550.5	3,507
	S4	13.5	679,808	448,254	758.1	309
70	S5	13.9	512,326	221,342	414.1	25,909
	S6	13.1	512,326	220,921	653.8	3,353
	S7	13.6	512,326	155,974	830.4	1,214
	S8	14.1	512,326	178,048	826.4	2,158
85	S9	13.6	366,009	289,205	405.1	91,774
	S10	13.8	366,009	280,300	398.1	87,460
	S11	13.0	366,009	285,724	551.5	32,203
	S12	13.2	366,009	285,826	555.3	41,032
	S13	12.8	366,009	249,262	711.2	8,767
	S14	12.9	366,009	244,432	690.1	6,800

9.3.2. Type B / 64 -28 / Latex / NG / 6.0% LS

Table 39. CIR Beam Fatigue Test Results: Type B / 64 -28 / Latex / NG / 6.0% LS.

Type B / 64 -28 / Latex / NG / 6.0% LS						
Temperature [°F]	**Sample ID**	**Air Voids Level (%)**	**Dynamic Modulus E* (psi)**	**Initial Flexural Stiffness (psi)**	**Flexural Strain [microstrain]**	**Number of Cycles to Failure 50% SR**
55	S1	13.9	877,519	748,076	249.9	94,019
	S2	13.6	877,519	784,030	401.3	41,942
	S3	13.5	877,519	782,576	402.5	36,654
	S4	13.8	877,519	540,309	555.4	2,860
	S5	13.2	877,519	540,701	551.2	3,258
70	S6	13.4	684,468	602,936	409.7	46,687
	S7	13.7	684,468	232,699	611.2	5,218
	S8	13.5	684,468	138,351	803.4	1,215
	S9	13.7	684,468	138,439	826	2,154
85	S10	13.1	506,754	264,433	400.1	143,737
	S11	13.5	506,754	277,022	547.2	44,204
	S12	13.2	506,754	267,435	552.9	34,365
	S13	14.2	506,754	254,179	713.9	11,168
	S14	13.6	506,754	252,409	703.2	9,946

9.3.3. Type C / 64 -28 / Polymer / NG / 6.0%LS

Table 40. CIR Beam Fatigue Test Results: Type C / 64 -28 / Polymer / NG / 6.0%LS.

Type C / 64 -28 / Polymer / NG / 6.0%LS						
Temperature [°F]	**Sample ID**	**Air Voids Level (%)**	**Dynamic Modulus E* (psi)**	**Initial Flexural Stiffness (psi)**	**Flexural Strain [microstrain]**	**Number of Cycles to Failure 50% SR**
55	**S1**	13.7	856,531	748,076	254.5	161,910
	S2	13.4	856,531	774,879	406.4	47,588
	S3	13.3	856,531	787,932	399.6	33,058
	S4	13.6	856,531	644,736	550.4	6,211
70	**S5**	13.0	686,271	615,714	423.15	59,068
	S6	13.2	686,271	676,717	601.8	6,722
	S7	13.5	686,271	505,094	823.5	4,523
	S8	14.0	686,271	505,877	723.4	3,644
85	**S9**	12.9	523,861	277,138	400.5	250,051
	S10	13.5	523,861	272,830	398.4	201,639
	S11	13.3	523,861	196,845	552.8	51,828
	S12	13.0	523,861	271,772	708.8	20,886
	S13	14.0	523,861	269,654	698.3	15,319

9.3.4. Type D / 58 -28 / Rubber / NG / 6.0%LS

Table 41. CIR Beam Fatigue Test Results: Type D / 58 -28 / Rubber / NG / 6.0%LS.

Type D / 58 -28 / Rubber / NG / 6.0%LS						
Temperature [°F]	**Sample ID**	**Air Voids Level (%)**	**Dynamic Modulus E* (psi)**	**Initial Flexural Stiffness (psi)**	**Flexural Strain [microstrain]**	**Number of Cycles to Failure 50% SR**
55	**S1**	12.5	749,452	691,772	252.1	80,905
	S2	13.6	749,452	658,761	404.3	20,839
	S3	13.9	749,452	683,708	397.5	24,531
	S4	12.9	749,452	494,738	552.3	5,617
	S5	13.2	749,452	673,570	547.7	4,257
70	**S6**	13.1	586,196	603,444	399.6	31,411
	S7	13.8	586,196	668,885	617.7	4,067
	S8	13.3	586,196	702,998	603.3	3,621
	S9	13.5	586,196	286,740	801.3	1,759
85	**S10**	13.4	436,763	285,724	397.5	67,787
	S11	13.5	436,763	274,861	402.3	58,770
	S12	13.2	436,763	287,900	556.1	19,786
	S13	13.6	436,763	287,711	548.0	24,762
	S14	13.3	436,763	248,276	721.2	7,280
	S15	13.1	436,763	250,669	708.7	4,830

9.3.5. Type A / CMS2S / 52 -34 / NG / 4.5%LS

Table 42. CIR Beam Fatigue Test Results: Type A / 52 -34 / CMS2S / NG / 4.5%LS.

CIR BEAM FATIGUE RESULTS						
Type A / 52 -34 / CMS2S / NG / 4.5%LS						
Temperature [°F]	**Sample ID**	**Air Voids Level (%)**	**Dynamic Modulus E* (psi)**	**Initial Flexural Stiffness (psi)**	**Flexural Strain [microstrain]**	**Number of Cycles to Failure**
						50% SR
55	**S1**	13.4	846,114	688,929	252.5	54,712
	S2	13.2	846,114	694,432	399.87	8,735
	S3	13.7	846,114	681,432	404.3	6,928
	S4	13.5	846,114	754,232	551.55	1,001
	S5	13.9	846,114	693,218	557.6	327
70	**S6**	13.1	646,146	542,318	249.9	198,200
	S7	13.6	646,146	552,369	412.2	21,218
	S8	14.1	646,146	589,941	405.3	17,000
	S9	13.6	646,146	601,318	539.1	7,800
	S10	13.8	646,146	568,974	548.1	6,200
85	**S11**	13.0	466,500	352,218	407.8	57,714
	S12	13.2	466,500	343,569	553.4	18,735
	S13	12.8	466,500	301,759	551.2	16,424
	S14	12.9	466,500	299,768	723.9	5,924
	S15	13.1	466,500	318,967	718.9	7,218

9.3.6. Type B / 64 -28 / Latex / NG / 4.5% LS

Table 43. CIR Beam Fatigue Test Results : Type B / 64 -28 / Latex / NG / 4.5% LS.

Type B / 64 -28 / Latex / NG / 4.5% LS						
Temperature [°F]	**Sample ID**	**Air Voids Level (%)**	**Dynamic Modulus E* (psi)**	**Initial Flexural Stiffness (psi)**	**Flexural Strain [microstrain]**	**Number of Cycles to Failure 50% SR**
55	**S1**	13.9	790,743	758,312	253.1	47,715
	S2	13.6	790,743	924,732	412.1	11,224
	S3	13.5	790,743	832,423	408.9	13,225
	S4	13.8	790,743	718,625	561.3	1,414
70	**S5**	13.2	637,138	501,732	255.3	119,314
	S6	13.4	637,138	514,635	398.9	35,812
	S7	13.7	637,138	511,625	421.4	24,318
	S8	13.5	637,138	501,316	559.9	5,200
	S9	13.7	637,138	499,768	562.3	4,300
85	**S10**	13.1	482,141	399,418	399.8	72,414
	S11	13.5	482,141	342,716	552.6	28,918
	S12	13.2	482,141	353,756	547.9	31,411
	S13	14.2	482,141	348,961	719.5	6,450
	S14	13.6	482,141	355,716	711.4	7,211

9.3.7. Type C / 64 -28 / Polymer / NG / 4.5%LS

Table 44. CIR Beam Fatigue Test Results: Type C / 64 -28 / Polymer / NG / 4.5%LS.

Type C / 64 -28 / Polymer / NG / 4.5%LS						
Temperature [°F]	**Sample ID**	**Air Voids Level (%)**	**Dynamic Modulus E* (psi)**	**Initial Flexural Stiffness (psi)**	**Flexural Strain [microstrain]**	**Number of Cycles to Failure 50% SR**
55	**S1**	13.7	937,335	824732	259.8	101,218
	S2	13.4	937,335	754894	424.3	39,918
	S3	13.3	937,335	801732	418.5	27,511
	S4	13.6	937,335	899728	553.6	3,414
	S5	13.0	937,335	918742	565.1	5120
70	**S6**	13.2	748,852	711322	258.9	211,321
	S7	13.5	748,852	699568	418.5	42,715
	S8	14.0	748,852	724345	407.3	16,221
	S9	12.9	748,852	683751	556.3	11,200
	S10	13.5	748,852	701456	552.4	8,900
85	**S11**	13.3	579,339	401328	400.1	142,525
	S12	13.0	579,339	513618	547.2	41,218
	S13	14.0	579,339	418676	551.3	34,365
	S14	13.4	579,339	399221	703.2	9,211
	S15	12.0	579,339	476578	713.9	11,418

9.3.8. Type D / 58 -28 / Rubber / NG / 4.5%LS

Table 45. CIR Beam Fatigue Test Results: Type D / 58 -28 / Rubber / NG / 4.5%LS.

Type D / 58 -28 / Rubber / NG / 4.5%LS						
Temperature [°F]	**Sample ID**	**Air Voids Level (%)**	**Dynamic Modulus E* (psi)**	**Initial Flexural Stiffness (psi)**	**Flexural Strain [microstrain]**	**Number of Cycles to Failure**
						50% SR
55	**S1**	12.5	786,634	691,779	248.7	25,713
	S2	13.6	786,634	692,102	411.2	11,314
	S3	13.9	786,634	689,073	409.7	9,878
	S4	12.9	786,634	694,145	557.5	3,200
	S5	13.2	786,634	689,760	559.6	2,750
70	**S6**	13.1	623,357	549,406	249.9	41,315
	S7	13.8	623,357	551,076	423.2	11,218
	S8	13.3	623,357	548,243	407.4	16,414
	S9	13.5	623,357	550,716	552.5	4,100
	S10	13.4	623,357	546,091	548.1	3,124
85	**S11**	13.5	463,704	410,173	400.1	39,228
	S12	13.2	463,704	407,980	547.2	9,615
	S13	13.6	463,704	407,420	551.3	8,714
	S14	13.3	463,704	410,681	703.2	3,280
	S15	13.1	463,704	406,505	713.9	5,400
	S16	12.9	463,704	410,774	708.7	4830

9.4. Average Dynamic Modulus Values for non-graded CIR mixtures

Table 46. Average Dynamic Modulus Values for Non-Graded CIR Mixtures.

Average Modulus (psi)	**Frequency (Hz) →**					
Temperature (°F)	**0.1**	**0.5**	**1**	**5**	**10**	**25**
14	1,007,974	1,138,787	1,193,687	1,316,834	1,367,769	1,432,991
40	631,003	761,468	818,857	952,773	1,010,109	1,085,054
70	302,871	402,082	449,294	567,566	621,533	694,926
100	120,651	176,825	206,030	285,891	325,406	382,127
130	42,683	67,939	82,169	124,575	147,338	181,959

Table 47. Statistics for Dynamic Modulus Values for Non-Graded CIR Mixtures.

Standard Deviation	**Frequency (Hz) →**					
Temperature (°F)	**0.1**	**0.5**	**1**	**5**	**10**	**25**
14	61,500	99,414	118,620	169,248	193,366	227,064
40	6,063	17,627	25,141	49,254	62,638	83,117
70	1,859	1,029	1,108	3,671	6,283	11,594
100	2,346	3,363	3,430	2,811	2,365	1,876
130	1,888	184	1,126	3,035	3,605	4,025
Average +95% CI	**Frequency (Hz) →**					
Temperature (°F)	**0.1**	**0.5**	**1**	**5**	**10**	**25**
14	1,093,207	1,276,565	1,358,083	1,551,396	1,635,756	1,747,679
40	639,405	785,897	853,700	1,021,034	1,096,919	1,200,246
70	305,447	403,508	450,830	572,654	630,240	710,994
100	123,902	181,487	210,784	289,787	328,684	384,727
130	45,300	68,193	83,730	128,782	152,334	187,537
Average -95% CI	**Frequency (Hz) →**					
Temperature (°F)	**0.1**	**0.5**	**1**	**5**	**10**	**25**
14	922,742	1,001,008	1,029,292	1,082,272	1,099,782	1,118,302
40	622,601	737,039	784,015	884,512	923,299	969,862
70	300,295	400,657	447,757	562,479	612,825	678,858
100	117,399	172,164	201,276	281,995	322,129	379,526
130	40,067	67,684	80,608	120,368	142,342	176,380